NASA Technical Paper 1252

Aerodynamic Characteristics of a Hypersonic Research Airplane Concept Having a 70° Swept Double-Delta Wing at Mach Number 0.2

Jim A. Penland, Theodore R. Creel, Jr.,
and James L. Dillon

SEPTEMBER 1978

NASA

NASA Technical Paper 1252

Aerodynamic Characteristics of a Hypersonic Research Airplane Concept Having a 70° Swept Double-Delta Wing at Mach Number 0.2

Jim A. Penland, Theodore R. Creel, Jr.,
and James L. Dillon
Langley Research Center
Hampton, Virginia

NASA
National Aeronautics
and Space Administration

Scientific and Technical Information Office

1978

SUMMARY

A wind-tunnel investigation of the static longitudinal, lateral, and directional stability characteristics of a hypersonic research airplane concept having a 70° swept double-delta wing was conducted in the Langley low-turbulence pressure tunnel. The configuration variables included wing planform, tip fins, center fin, and scramjet engine modules. The investigation was conducted at a Mach number of 0.2 over a Reynolds number (based on fuselage length) range of 2.26×10^{6} to 19.75×10^{6} (with a majority of tests at 10.0×10^{6}). Tests were conducted through an angle-of-attack range from about -2° to 34°, at angles of sideslip of 0° and 5°, and at elevon deflections of 0°, -5°, -10°, -15°, and -20°.

The drag coefficient of the integrated scramjet engine appears relatively constant with Reynolds number at the test Mach number of 0.2. Mild pitch-up was exhibited by the models equipped with tip fins. The forward delta, a highly swept forward portion of the wing, was destabilizing. The center fin model had a higher trimmed maximum lift-drag ratio and a wider trim lift and angle-of-attack range than the tip fin model. Both the tip fin models and center fin models exhibited positive dihedral effect and positive directional stability. Roll control was positive for the tip fin model, but yaw due to roll control was unfavorable.

INTRODUCTION

Present jet airplanes are cruising at speeds of Mach 2 to 3 (refs. 1 to 3), and it appears that the Mach number limit for aircraft utilizing conventional petroleum-based fuels is about 5 (ref. 4). Some unique problems associated with Mach numbers of 5 and above include the development of new propulsion systems which use nonpetroleum-derived fuels such as liquid hydrogen (ref. 5). Some of these new propulsion systems include cryogenic-fueled turbojets for low speeds, ramjets (subsonic combustion) for moderate supersonic speeds, and scramjets (supersonic combustion ramjets) for high supersonic and hypersonic speeds. New structural concepts must be developed which can provide cooled airframes and engine surfaces for protection from high aerodynamic heating as well as insulated tankage for cryogenic fuels such as liquid hydrogen.

One industry study (refs. 6 to 9) concluded that only through the use of both ground facilities and flight vehicles could these major required advancements in technology be made. These findings were in accord with previous NACA-NASA experience with the various research airplane projects from the X-1 to the X-15, each of which resulted in an extensive technology advancement at a minimum expenditure of cost and time. A need thus exists for comprehensive flight research in the range of Mach numbers from 3 to 5 and for detailed exploration to Mach 8.

The present configuration is one of several research airplane concepts under study at the Langley Research Center (refs. 10 to 12) that meets the requirements envisioned as necessary to provide a technology base for future high-speed aircraft. Such a research airplane would be air launched from a B-52 or C-5 and would have a length of 15.24 to 24.38 m (50 to 80 ft), a flight time of up to 800 sec with a nominal 40-sec cruise at a Mach number of about 7 on the scramjet engine, and a return to base for a dead-stick landing. In-flight tests would include powerless glides, rocket-boosted flights, and combined rocket-scramjet boost-cruise experiments.

The purpose of the present study was to investigate experimentally the longitudinal, lateral, and directional stability and control of this large-fuselage, double-delta wing configuration at subsonic landing speeds. Studies of this same design concept at subsonic, supersonic, and hypersonic speeds (refs. 13 to 15) have also been completed. The tests were parametric in nature and included configuration buildup, variations in wing planform, longitudinal control, and roll control. This study was conducted at a Mach number of 0.2 over a Reynolds number (based on fuselage length) range of 2.26×10^6 to 19.75×10^6 (with the majority of tests at 10.0×10^6). The angle-of-attack range was from about -2° to 34° with angles of sideslip of 0° and 5°.

SYMBOLS

The longitudinal characteristics are presented about the stability axes, and the lateral directional characteristics are presented about the body axes. The body and stability axis systems are illustrated in figure 1. The moment reference point was at the design center-of-gravity location which was at a longitudinal station 64.5 percent of the fuselage length and at a vertical station 1.3 percent of the fuselage length below the vehicle reference line. Values are given in both SI and U.S. Customary Units. The measurements and calculations were made in U.S. Customary Units.

A — reference area, area of 70° delta wing including fuselage intercept, 0.043 m^2 (67.2 in^2)

b — wing span, 0.217 m (8.542 in.)

$C_{A,b}$ — base axial force coefficient, $\frac{\text{Base axial force}}{q_\infty A}$

C_D — drag coefficient, $\frac{D}{q_\infty A}$

C_L — lift coefficient, $\frac{L}{q_\infty A}$

C_{L_α} — rate of change of C_L with angle of attack, per degree

C_l rolling-moment coefficient, $\frac{M_X}{q_\infty Ab}$

C_{l_β} rate of change of C_l with angle of sideslip, per degree

$C_{l_{\delta_H}}$ rolling-moment coefficient due to roll control, per degree

C_m pitching-moment coefficient, $\frac{M_Y}{q_\infty A\ell}$

C_{m_α} rate of change of C_m with angle of attack, per degree

$\partial C_m/\partial C_L$ rate of change of C_m with lift coefficient, longitudinal stability parameter

C_n yawing-moment coefficient, $\frac{M_Z}{q_\infty Ab}$

C_{n_β} rate of change of C_n with angle of sideslip, per degree

$C_{n_{\delta_H}}$ yawing-moment coefficient due to roll control, per degree

C_Y side-force coefficient, $\frac{F_Y}{q_\infty A}$

C_{Y_β} rate of change of C_Y with angle of sideslip, per degree

$C_{Y_{\delta_H}}$ side-force coefficient due to roll control, per degree

D drag, $F_N \sin \alpha + F_A \cos \alpha$

F_A axial force along X-axis (positive direction is -X)

F_N normal force along Z-axis (positive direction is -Z)

F_Y side force along Y-axis (positive direction is +Y)

L lift, $F_N \cos \alpha - F_A \sin \alpha$

L/D lift-drag ratio

ℓ length of model fuselage, 0.508 m (20.0 in.)

M Mach number

M_X, M_Y, M_Z moments about X-, Y-, and Z-axes

q_∞ free-stream dynamic pressure

R Reynolds number based on fuselage length

X,Y,Z reference axes

α angle of attack, degrees

β angle of sideslip, degrees

δ_e elevon deflection angle, positive when trailing edge is down, degrees

δ_H differential elevon deflection, positive to provide positive roll, $\delta_{H,left} - \delta_{H,right}$, degrees

Subscripts:

o condition at zero lift

E model scramjet engine

S stability axis system

t trim condition, $C_m = 0$

Model nomenclature:

B_1 body with high profile nose

B_2 body with low profile nose

E model scramjet engine

F_D forward delta wing

V_C center fin, vertical

V_T tip fins, vertical

W_{1f} wing, positive camber, forward position (fig. 4(a))

W_{1a} wing, positive camber, aft position, 0.0254 m (1.0 in.) aft of W_{1f}

W_{2f} wing, negative camber, forward position

MODEL

A photograph of a model of the winged hypersonic airplane configuration is shown in figure 2. The test model was of modular design, as shown in figure 3, to allow the buildup of variations of the basic model (fig. 4(a)) from components consisting of the body, a forward delta wing, a 70° swept clipped-delta wing, tip fins, a center fin, and an engine. The model design rationale was primarily based on the stability and control requirements at the design hypersonic cruise Mach number range of 8 to 10. The forward delta wing was included in the design to help decrease the rearward shift of the aerodynamic center with increasing Mach number. The tip fins were designed with 7.5° toe-in and were located outboard of the fuselage flow field to enhance the directional stability at hypersonic speeds. A center fin having the same total planform area as the sum of the tip fins was also tested. The wedge-shaped center fin (fig. 4(b)) was tested to assess the difference in directional stability between it and the tip fins. Elevons could be deflected from -20° to 5° in 5° increments. A model scramjet engine was used to complete the configuration buildup (fig. 4(c)). The engine consisted of six clustered modules of the concept described in reference 16, each having scale outside dimensions, angles, and areas, but without scale inside fuel struts and contraction ratio. The design internal contraction ratio of the model scramjet was approximately 2 (compared with about 4 for the flight engine) in order to partly account for the relatively low Reynolds number and the resulting thick boundary layer of this test. The wing was also tested inverted in the forward position and in the aft position upright. Geometric details of the model are shown in figure 4 and are given in table I.

APPARATUS AND TESTS

The tests were conducted in the Langley low-turbulence pressure tunnel at a Mach number of 0.2 over a Reynolds number range of 2.26×10^6 to 19.75×10^6, with dynamic pressure varying from 2777 to 25 089 Pa. A six-component strain-gage balance was installed inside the model fuselage and was attached to the tunnel sting-support system. Force and moment data were measured through an angle-of-attack range of -2° to 34° and at angles of sideslip of 0° and 5°. All screw holes and joints were filled with wax before each test run. Tunnel blockage corrections were made for all tests by utilizing the method of reference 17 to determine the solid blockage of the body and wing and the method of reference 18 to determine the lift interference. With the exception of a series of variable Reynolds numbers tests, all runs were made with fixed transition by the method presented in reference 19. The transition strips used consisted of 0.0025-m (0.1-in.) wide strips of 0.0254 to 0.0508 mm (0.001 to 0.002 in.) diameter grit (No. 220 grit). The transition strips were placed on the fuselage 0.025 m (1 in.) downstream of station 0 and 5 percent of the local chord downstream of all leading edges on both the top and bottom surfaces of the wing and the left and right sides of the vertical tails. No grit was applied to the engine module.

The results are presented without base pressure correction except where noted. Typical variations of base axial force measured during the test are presented in figure 5 for various configurations at a Reynolds number of about 10.0×10^6.

RESULTS AND DISCUSSION

All the basic data presented in this paper were machine plotted from the computational tape output, and the data points were machine faired using the cubic spline method. Because of the preliminary nature of this study, individual curves such as L/D plotted against α were not given detailed cross-checks against polar plots of C_L plotted against C_D.

Static Longitudinal Aerodynamics

Reynolds number variations, component buildup.- A buildup of configurations from the wing-body to the complete configuration was tested over a wide Reynolds number range with free transition, and the longitudinal characteristics are presented in figures 6 to 9. The sensitivity of the various configurations from B_1W_{1f} to $B_1W_{1f}V_TF_DE$ to changes in Reynolds number was minimal above a Reynolds number of about 10.0×10^6, which indicated that the boundary layer was becoming transitional and that the skin-friction drag was ceasing to diminish with increasing Reynolds number, as would be expected with a boundary layer that was predominantly all laminar or all turbulent. As a result of this observation, all remaining tests were made at a Reynolds number of approximately 10.0×10^6, and transition strips were applied as described in the section entitled "Apparatus and Tests" to minimize the possibility of local regions of separation and to assure turbulent flow over the model.

The small variations of pitching moment and drag coefficients with varying Reynolds numbers are considered to be within the accuracy of the data.

Reynolds number variation, scramjet engine model drag.- The variation of the scramjet engine drag with Reynolds number at zero lift of the model and at a Mach number of 0.2 is presented in figure 10. The test results are presented for both uncorrected fuselage base pressure and with the fuselage base pressure corrected to free-stream static pressure. The width-to-height ratio for the model test engine was approximately 5. The drag coefficients are referenced to the engine inlet (frontal) area and were obtained from the difference between tests with the engine on and the engine off at zero lift. It can be seen that the drag coefficients of the engine were high and approach that of a flat plate with an aspect ratio of 5 at an angle of attack of 90° to the flow (ref. 20). Additional engine drag data may be seen in reference 21 for similar model designs. It appears that, within the scatter of the data, the drag penalty of adding this integrated scramjet engine concept is relatively constant with Reynolds number at subsonic speeds.

Component buildup.- The variations of the longitudinal characteristics with component buildup are presented in figure 11 for the tip fin configuration. The addition of tip fins had a decided linearizing effect on the lift curves, which was due in part to decreased tip losses. The addition of the forward delta improved the lift from an angle of attack of about 5° to the onset of stall at about 26° and increased the drag of all configurations at all angles of attack because of increased vortex lift. The maximum lift coefficient was reduced by the installation of the model scramjet engine. The lift-drag ratio was decreased by the addition of either the tip fins and/or the forward delta to the basic body-wing. As expected, the addition of the engine greatly decreased the lift-drag ratio. All configurations were longitudinally stable except the body alone. The addition of the tip fins to the body-wing caused all configurations to mildly pitch-up at lift coefficients of 0.6 to 0.7 ($\alpha \approx 16°$) with the present center-of-gravity location. The forward delta is destabilizing as expected.

The results of the component buildup of the center fin configuration are presented in figure 12. Lift curves for the winged configurations were non-linear with angle of attack. The addition of the forward delta increased the lift slightly at higher angles of attack, and the engine installation reduced it. The drag was generally orderly with component buildup. The incremental drag due to engine installation was greatest at low angles of attack and washed out at the higher angles. The untrimmed lift-drag ratios are somewhat lower with the center fin installed than with the twin tip fins on (fig. 11(c)); however, the present center fin did not have a subsonic airfoil section which would, if incorporated, make L/D more nearly the same. The longitudinal stability of the body-wing configuration was unaffected by the addition of the center vertical tail. The forward delta was highly destabilizing but no pitch-up occurred before angles of attack of about 30°. The linearity of the pitching-moment curves with lift coefficient of the body-wing configuration was unaffected by the addition of the center fin whereas pitch-up was induced by the addition of the tip fins (fig. 11(e)).

Wing location and camber.- The results of tests on the tip fin model with the upright wing located at the aft fuselage station and with the wing inverted (negative camber) in the forward location are presented in figure 13 and are compared with the model having the forward located upright wing. The aft location of the wing decreased the lift significantly at angles of attack greater than 16° whereas the inverted wing showed about the same lift-curve slope but an increase in α_o. All lift curves were relatively linear until the high angle-of-attack separation region was reached, but both the aft wing relocation and the wing inversion reduced the lift. Drag was reduced at high angles of attack when the wing was inverted. The curves of lift-drag ratio reflect these lift and drag trends, with the aft wing showing a slight loss in lift-drag ratio and the inverted wing losing more than a unit in maximum lift-drag ratio. The longitudinal stability was improved with the wing in the aft location for the fixed center-of-gravity location, but this increased stability would be decreased if the center of gravity were shifted aft to account for the aft wing movement. The inverted wing test showed a slight decrease in longitudinal stability and a large positive increase in C_{m_o} and was self-trimming at a positive lift coefficient of about 0.5.

Nose contour.- The low profile nose was originated to provide additional directional stability at hypersonic speeds, and tests of reference 15 substantiate this design. The effect of nose contour was therefore investigated at $M = 0.2$, and the results are presented in figure 14. Essentially no difference was noted between the original and the low profile nose.

Drag Due to Lift

The drag polar, C_D plotted against C_L^2, is presented in figure 15 for the component buildup of the major configurations tested. The slopes of the curves are a measure of the drag due to lift and are relatively linear up to lift coefficients of about 1.0 whereas the models with the forward delta and/or the engine installed showed the earliest stalling tendencies.

Trim Characteristics

The basic trim data taken for various elevon deflection angles are presented in figure 16 for the body—wing—tip-fin model, in figure 17 for the body—wing—center-fin model, in figure 18 for the body—wing—tip-fin—forward delta wing model, and in figure 19 for the body—wing—tip-fin—forward delta wing engine model. Interpolation was required to determine some trim points and is shown as dashed lines on the basic data plots.

Trim of tip fin and center fin models.- A comparison of the trim characteristics of the model equipped with tip fins and the model with a center vertical tail is presented in figure 20. The model equipped with the center vertical tail shows not only the highest trimmed maximum lift-drag ratio but more importantly the widest trim lift and trim angle-of-attack range. The tip fins act as end plates on the wings and increase the local lift, but this aft-located lift produces a nose-down pitching moment and thus requires larger elevon deflections for trim. For a given lift coefficient, the center vertical tail model requires about 4° to 5° less elevon deflection to trim than does the tip fin model. The center fin model exhibits an increasing trimmed lift-curve slope with trimmed lift coefficient compared with the tip fin model which had a nearly constant lift-curve slope. The level of trimmed longitudinal stability increases with trim lift coefficient to about $C_{L_t} = 0.35$ for the center tail model but decreases for the tip fin model. It might be expected that, with the addition of the engine, the center tail configuration would retain its wide trim lift quality and exhibit the greater trimmed L/D.

Trim of buildup of tip fin model.- The trim characteristics of the tip fin models are presented in figure 21 for the basic body—wing—tip-fin configuration and for the models with the forward delta and the scramjet engine installed. The trim lift and angle-of-attack range presented was limited for the body—wing—tip-fin model by the limited test range of elevon deflections, but mild pitch-up and the present center-of-gravity location limited the trim range for the models with the forward delta and engine. The trimmed maximum lift-drag ratio decreased a full unit of L/D, to a low value of 3.2, with scramjet engine installation. The trimmed lift-curve slope was nearly constant for all tip fin models and all trim angles of attack. The forward delta was destabilizing as expected at all trim angles of attack, and the engine was slightly stabilizing at lift coefficients up to about 0.1. The longitudinal stability decreased with trim lift coefficient for all tip fin models.

Static Lateral-Directional Stability

The variations of the static lateral-directional stability with component buildup of the tip fin configurations are presented in figure 22. All configurations tested with the tip fins installed exhibited positive dihedral effect at all angles of attack and positive or neutral directional stability up to angles of attack of about 21° to 27°, depending on the model. The configurations without the tip fins exhibited positive dihedral effect at positive angles of attack greater than 2° but were directionally unstable throughout the test angle-of-attack range. It is not known what effect the 7.5° toe-in of the tip fins (required at hypersonic speeds) had on the lateral-directional stability at $M = 0.2$.

A comparison of the lateral-directional stability for the center fin and tip fin configurations is presented in figure 23. The center fin model exhibited a high level of positive dihedral effect at all angles of attack and was directionally stable at all test angles of attack except that region between $\alpha = 22^{\circ}$ and 29°. At angles of attack up to 16°, the center fin model had superior lateral-directional characteristics compared with the tip fin model.

A comparison of the variations of the lateral-directional stability with forward and aft wing location and with the reduced profile nose is presented in figure 24. It should be noted that the tip fins moved aft with the aft movement of the wing. Within the scatter of the data, it may be concluded that neither the aft shift of the wing or the use of a nose having a reduced profile had any large effect on the lateral-directional stability at the subsonic test conditions.

Roll Control

The results of tests to determine the roll control characteristics of the complete tip fin configuration with forward delta and engine are presented in figure 25. This investigation was conducted with the left elevon deflected 5° (down) and the right elevon -5° (up). It may be seen that the configuration had positive roll control but some adverse cross coupling (i.e., adverse yaw due to roll control at all angles of attack).

CONCLUSIONS

An analysis of the experimental data for a hypersonic research airplane concept having a 70° swept double-delta wing at a Mach number of 0.2 and a range of Reynolds numbers (based on fuselage length) from about 2.3×10^{6} to 19.75×10^{6} (with the majority of tests at 10.0×10^{6}) leads to the following conclusions:

1. The drag coefficient of the integrated scramjet engine appears relatively constant with Reynolds number at the test Mach number of 0.2 and approaches the drag of a flat plate of similar aspect ratio normal to the flow.

2. The model with tip fins had an unstable break in the pitching-moment curve at lift coefficients of 0.6 to 0.7 (angle of attack of approximately 16°), a condition that was further aggravated by the addition of the forward delta.

3. The model with the center fin had a relatively linear pitching-moment curve and reduced stability with the forward delta installed.

4. The center fin model had a higher trimmed maximum lift-drag ratio and a wider trim lift and angle-of-attack range than the tip fin model.

5. The trimmed maximum lift-drag ratio of the tip fin model with scramjet engine was a low 3.2.

6. Both the tip fin models and the center fin models exhibited positive directional stability and positive dihedral effect up to an angle of attack of about 21°.

7. The complete tip fin model exhibited positive roll control but adverse yaw due to roll control.

Langley Research Center
National Aeronautics and Space Administration
Hampton, VA 23665
June 27, 1978

REFERENCES

1. Wetmore, Warren C.: Concorde Impressive in Flights. Aviat. Week & Space Technol., vol. 100, no. 25, June 24, 1974, pp. 25-28.

2. SR-71 Sets Record. Aviat. Week & Space Technol., vol. 101, no. 10, Sept. 9, 1974, p. 17.

3. SR-71 Sets Mark in New Speed Category: London-Los Angeles. Aviat. Week & Space Technol., vol. 101, no. 12, Sept. 23, 1974, p. 28.

4. Kirkham, Frank S.; Jackson, L. Robert; and Weidner, John P.: The Case for a High-Speed Research Airplane - Results From an In-House Study. AIAA Paper No. 74-988, Aug. 1974.

5. Small, W. J.; Fetterman, D. E.; and Bonner, T. F., Jr.: Potential of Hydrogen Fuel for Future Air Transportation Systems. [Preprint] 73-ICT-104, American Soc. Mech. Eng., Sept. 1973.

6. Hypersonic Research Facilities Study. Volume II, Part 1, Phase I: Preliminary Studies - Research Requirements and Ground Facility Synthesis. NASA CR-114323, 1970.

7. Hypersonic Research Facilities Study. Volume II, Part 2, Phase I: Preliminary Studies - Flight Vehicle Synthesis. NASA CR-114324, 1970.

8. Hypersonic Research Facilities Study. Volume III, Part 2, Phase II: Parametric Studies - Flight Vehicle Synthesis. NASA CR-114326, 1970.

9. Hypersonic Research Facilities Study. Volume IV, Part 1, Phase III - Final Studies Flight Research Facilities. NASA CR-114327, 1970.

10. Clark, Louis E.: Hypersonic Aerodynamic Characteristics of an All-Body Research Aircraft Configuration. NASA TN D-7358, 1973.

11. Penland, Jim A.; Creel, Theodore R., Jr.; and Howard, Floyd G.: Experimental Low-Speed and Calculated High-Speed Aerodynamic Characteristics of a Hypersonic Research Airplane Concept Having a 65° Swept Delta Wing. NASA TN D-7633, 1974.

12. Penland, Jim A.; and Creel, Theodore R., Jr.: Low-Speed Aerodynamic Characteristics of a Lifting-Body Hypersonic Research Aircraft Configuration. NASA TN D-7851, 1975.

13. Creel, Theodore R., Jr.; and Penland, Jim A.: Low-Speed Aerodynamic Characteristics of a Hypersonic Research Airplane Concept Having a 70° Swept Delta Wing. NASA TM X-71974, 1974.

14. Penland, Jim A.; Fournier, Roger H.; and Marcum, Don C., Jr.: Aerodynamic Characteristics of a Hypersonic Research Airplane Concept Having a 70° Swept Double-Delta Wing at Mach Numbers From 1.50 to 2.86. NASA TN D-8065, 1975.

15. Clark, Louis E.; and Richie, Christine B.: Aerodynamic Characteristics at Mach 6 of a Hypersonic Research Airplane Concept Having a 70° Swept Delta Wing. NASA TM X-3475, 1977.

16. Henry, John R.; and Anderson, Griffin Y.: Design Considerations for the Airframe-Integrated Scramjet. NASA TM X-2895, 1973.

17. Herriot, John G.: Blockage Corrections for Three-Dimensional-Flow Closed-Throat Wind Tunnels, With Consideration of the Effect of Compressibility. NACA Rep. 995, 1950.

18. Garner, H. C.; Rogers, E. W. E.; Acum, W. E. A.; and Maskell, E. C.: Subsonic Wind Tunnel Wall Corrections. AGARDograph 109, Oct. 1966.

19. Braslow, Albert L.; and Knox, Eugene C.: Simplified Method for Determination of Critical Height of Distributed Roughness Particles for Boundary-Layer Transition at Mach Numbers From 0 to 5. NACA TN 4363, 1958.

20. Hoerner, Sighard F.: Fluid-Dynamic Drag. Hoerner Fluid Dynamics (Brick Town, N.J.), c.1965.

21. Penland, Jim A.; Dillon, James L.; and Pittman, Jimmy L.: An Aerodynamic Analysis of Several Hypersonic Research Airplane Concepts From M = 0.2 to 6.0. [Paper] 78-150, American Inst. Aeronaut. & Astronaut., Jan. 1978.

TABLE I.- GEOMETRIC CHARACTERISTICS OF MODEL

Wing:	
Reference area (includes area projected to fuselage center line), m^2 (in^2)	0.043 (67.200)
Exposed area, m^2 (in^2)	0.023 (36.121)
Wetted area, m^2 (in^2)	0.047 (72.242)
Span, m (in.)	0.217 (8.542)
Aspect ratio	1.086
Root chord (on fuselage center line), m (in.)	0.353 (13.896)
Tip chord, m (in.)	0.085 (3.355)
Taper ratio	0.241
Mean aerodynamic chord, m (in.)	0.248 (9.779)
Sweepback angles, deg:	
Leading edge	70
25-percent chord line	64
Trailing edge	0
Dihedral angle (airfoil mean line), deg	-3.64
Incidence angle, deg	0
Airfoil section (see fig. 4(a)):	
Thickness ratio -	
Exposed root	0.05
Tip	0.06
Leading-edge radius, m (in.):	
Fuselage center-line chord	0.000508 (0.020)
Tip	0.000508 (0.020)
Elevon area (both), m^2 (in^2)	0.005 (7.161)
Forward delta wing:	
Area exposed (outside of fuselage, forward of wing leading edge), m^2 (in^2)	0.002 (3.394)
Leading-edge sweep, deg	80
Wetted area (both), m^2 (in^2)	0.0044 (6.788)
Tip fin:	
Area (each), m^2 (in^2)	0.0038 (5.848)
Span, m (in.)	0.069 (2.730)
Aspect ratio	1.274
Root chord, m (in.)	0.086 (3.383)
Tip chord, m (in.)	0.029 (1.135)
Taper ratio	0.336
Mean aerodynamic chord, m (in.)	0.062 (2.445)
Sweepback angles, deg:	
Leading edge, top	55.0
Leading edge, bottom	70.1
Trailing edge, top	21.3
Toe-in angle, deg	7.5
Airfoil section:	
Thickness ratio	0.07
Leading-edge radius, m (in.)	0.000508 (0.020)

TABLE I.- Concluded

Center fin:	
Area (exposed), m^2 (in^2)	0.007 (11.492)
Span (exposed), m (in.)	0.086 (3.380)
Aspect ratio of exposed area	0.994
Root chord (fuselage surface line), m (in.)	0.128 (5.040)
Tip chord, m (in.)	0.045 (1.760)
Taper ratio	0.349
Mean aerodynamic chord of exposed area, m (in.)	0.093 (3.664)
Sweepback angles, deg:	
Leading edge	55.0
Trailing edge	24.6
Airfoil section:	
Thickness ratio -	
Tip	0.106
Root	0.106
Leading-edge radius, m (in.)	0.000508 (0.020)
Fuselage:	
Length, m (in.)	0.508 (20.000)
Maximum height, m (in.)	0.071 (2.782)
Maximum width, m (in.)	0.073 (2.866)
Fineness ratio of equivalent round body	6.822
Planform area, m^2 (in^2)	0.026 (40.445)
Wetted area, m^2 (in^2)	0.083 (128.460)
Wetted area (with wing on), m^2 (in^2)	0.078 (120.695)
Wetted area (with wing and forward delta on), m^2 (in^2)	0.077 (118.747)
Base area, m^2 (in^2)	0.002 (3.726)
Complete model (wing and forward delta):	
Planform area, m^2 (in^2)	0.052 (79.960)
Aspect ratio of planform	0.913
Planform area (without forward delta), m^2 (in^2)	0.049 (76.566)
Aspect ratio (without forward delta)	0.953
Model scramjet engine:	
Frontal area, m^2 (in^2)	0.00084 (1.308)
Width-to-height ratio	5.23

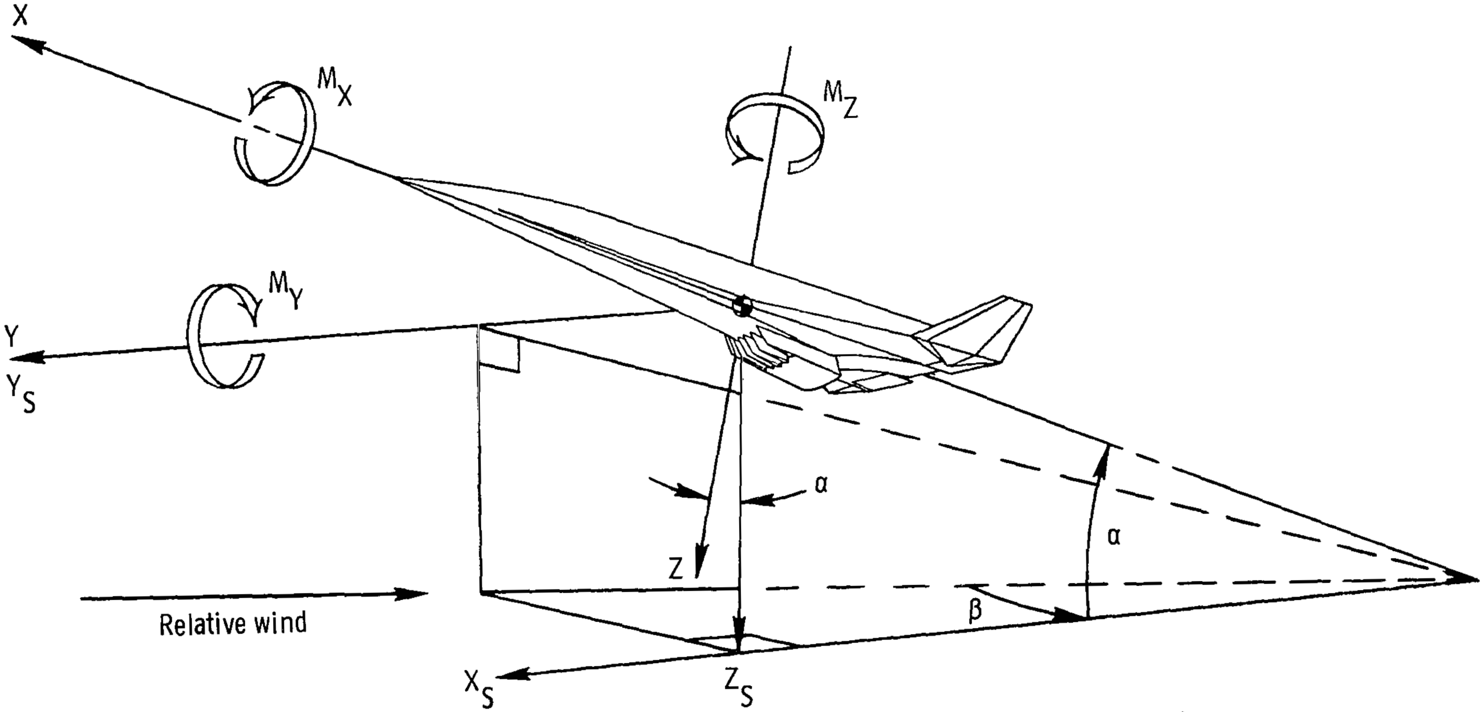

Figure 1.- Systems of reference axes; arrows indicate positive direction.

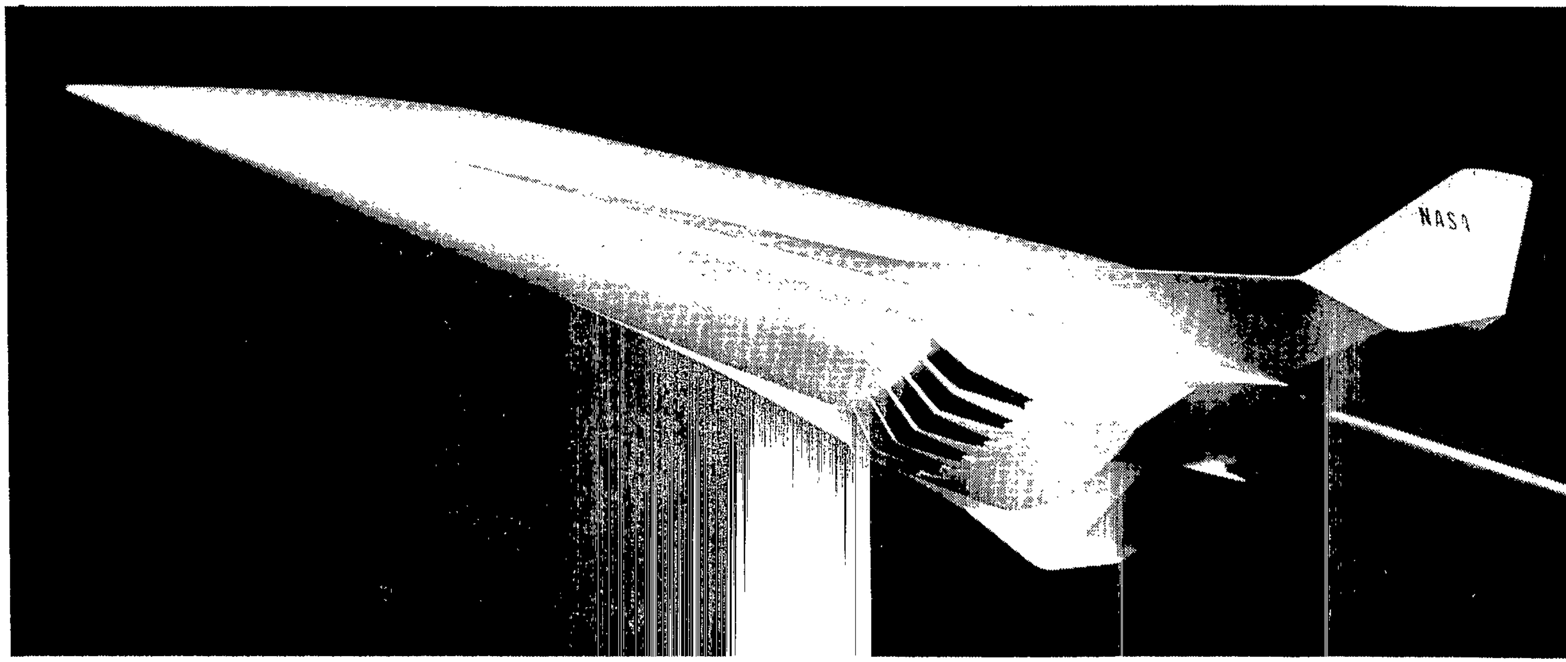

L-72-9146

Figure 2.- Photograph of configuration.

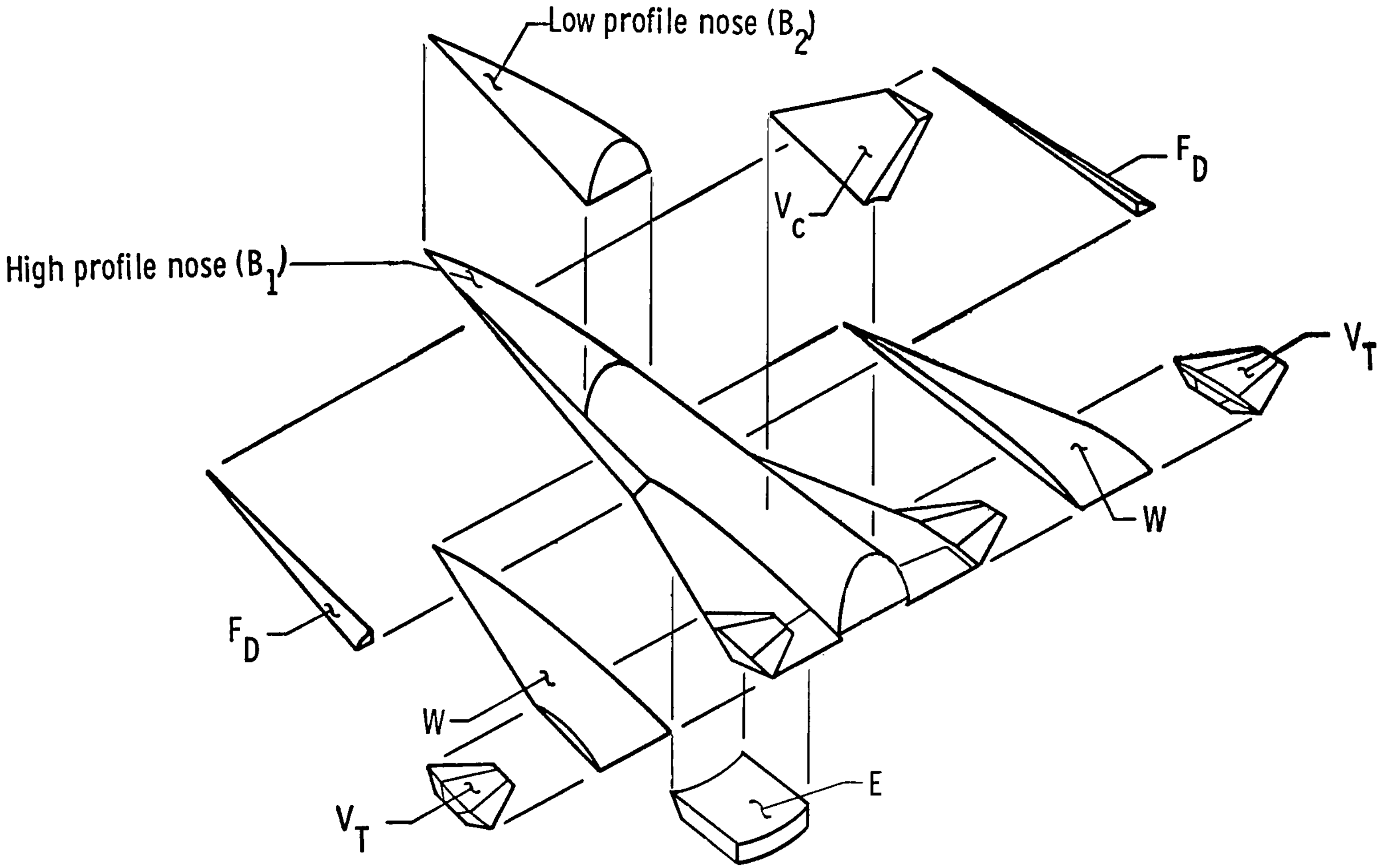

Figure 3.- Sketch of model showing interchangeable parts.

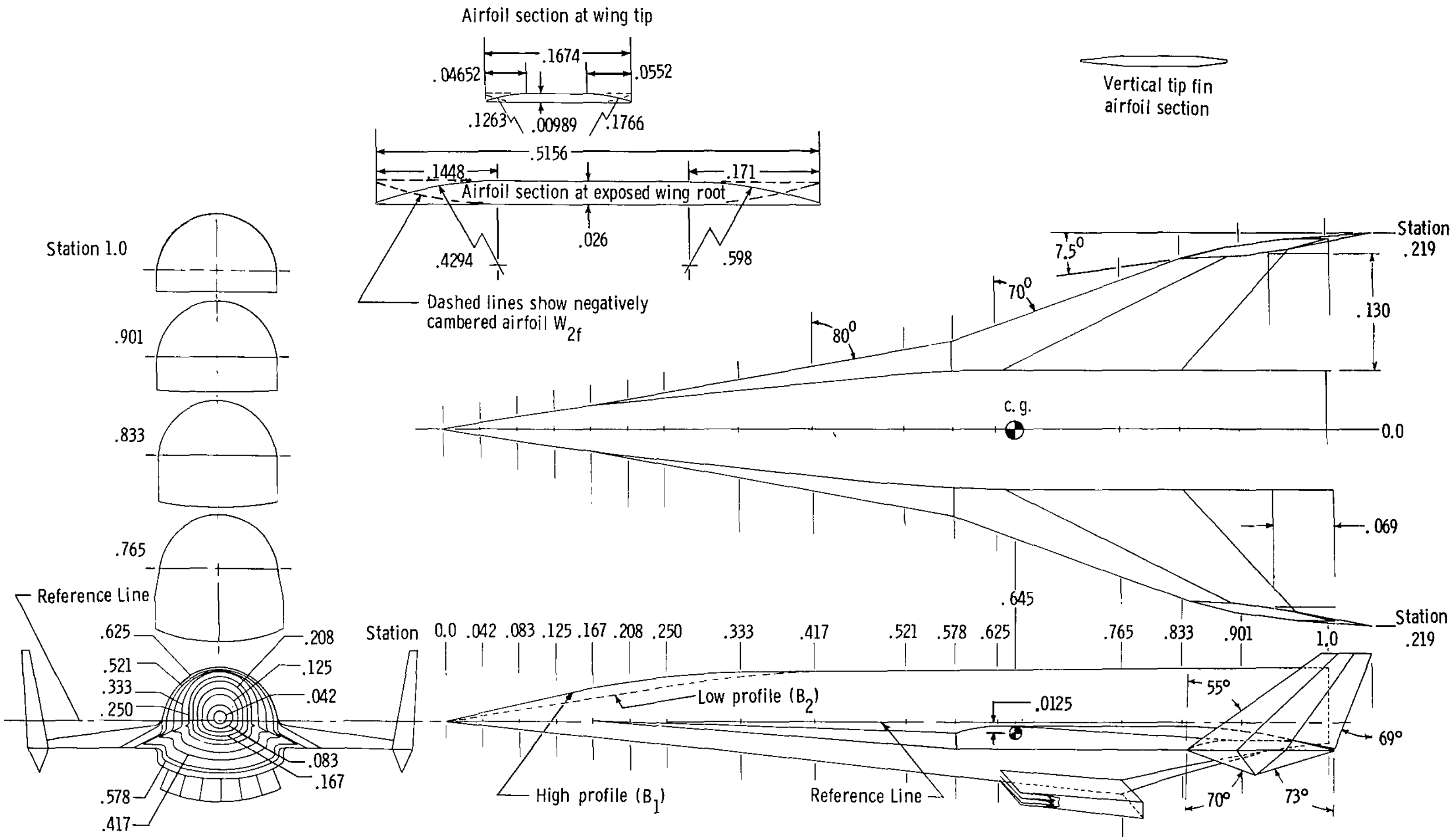

(a) Base-line configuration. All dimensions have been normalized by body length (ℓ = 50.8 cm). Wing drawn in forward location.

Figure 4.- Model general dimensions.

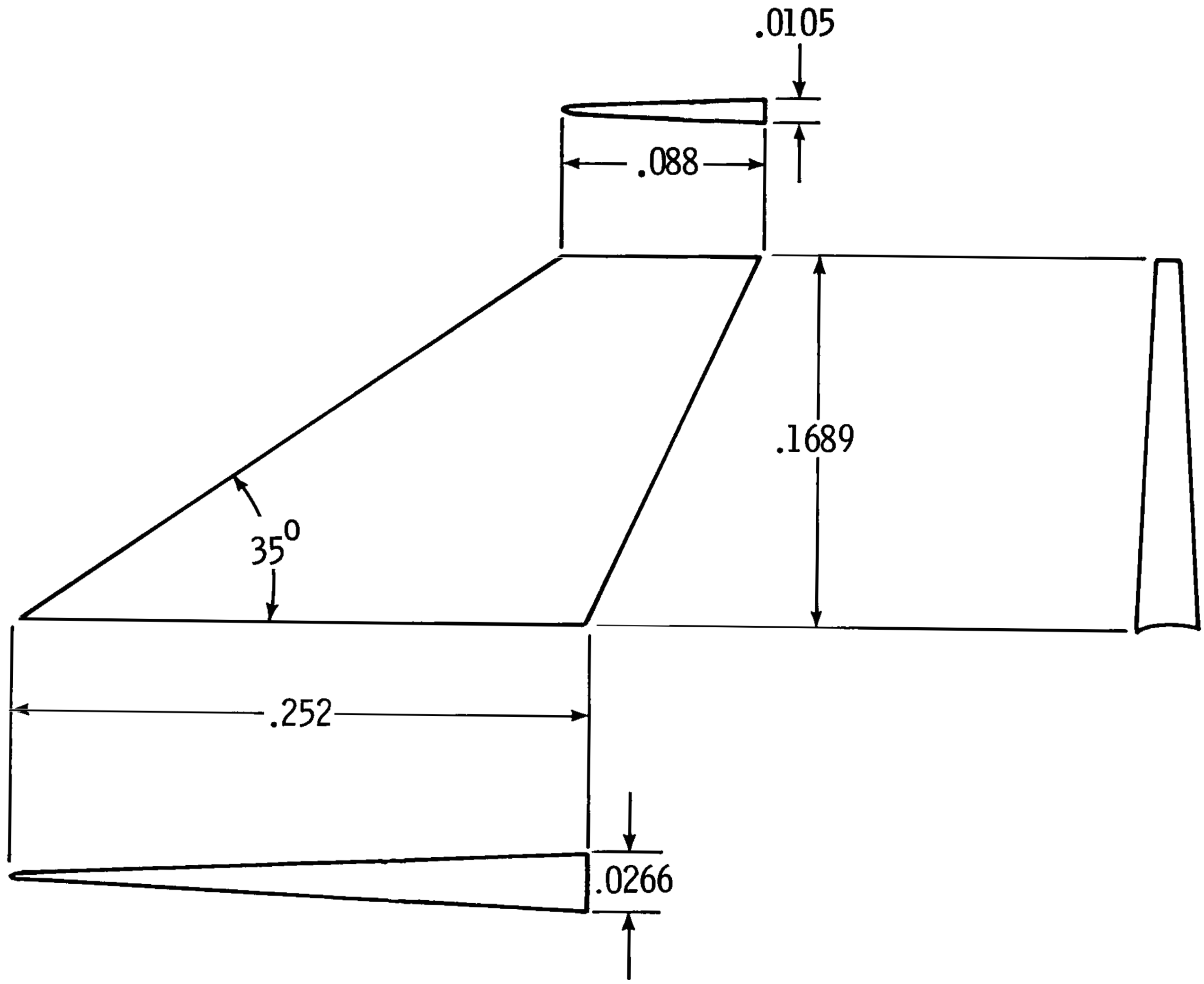

(b) Center fin.

Figure 4.- Continued.

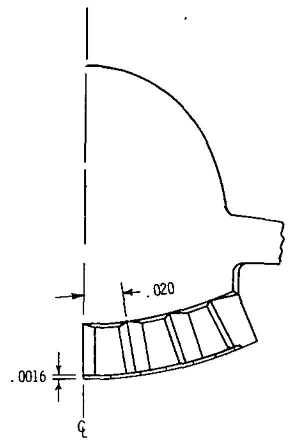

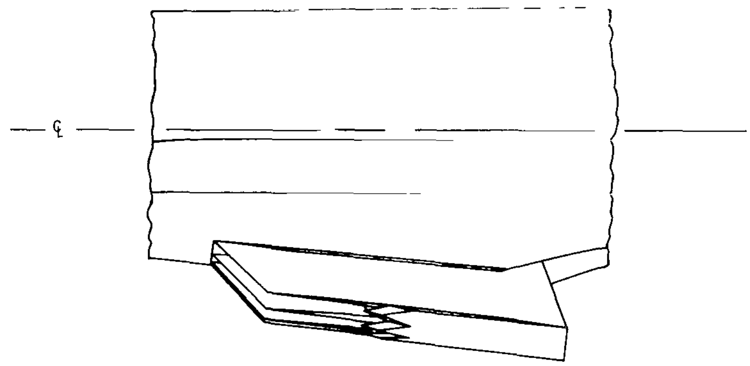

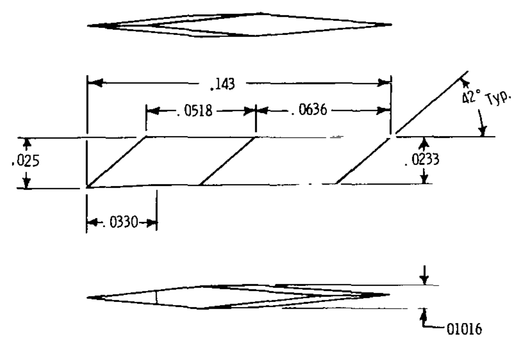

Inside splitter plate

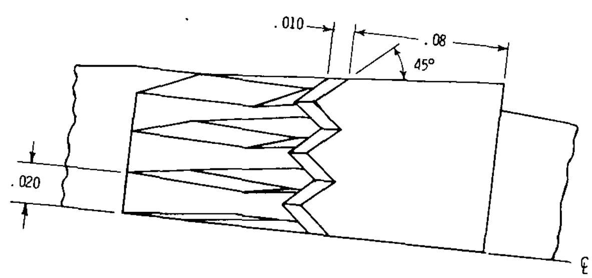

Bottom view of scramjet engine with cowl on

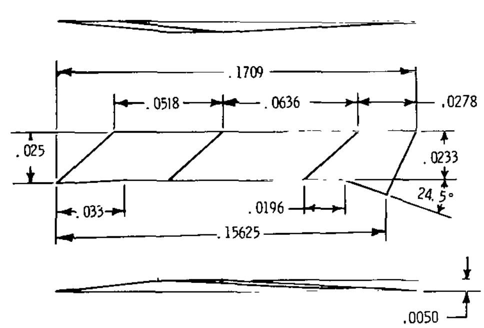

Left outside plate

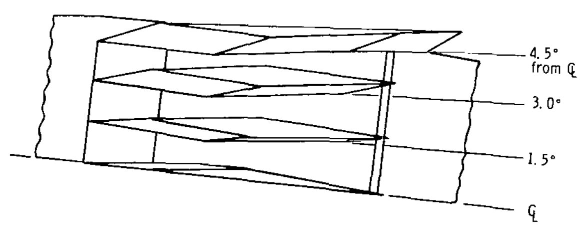

Bottom view of scramjet engine with cowl removed

(c) Scramjet engine. All dimensions have been normalized by body length (ℓ = 50.8 cm).

Figure 4.- Concluded.

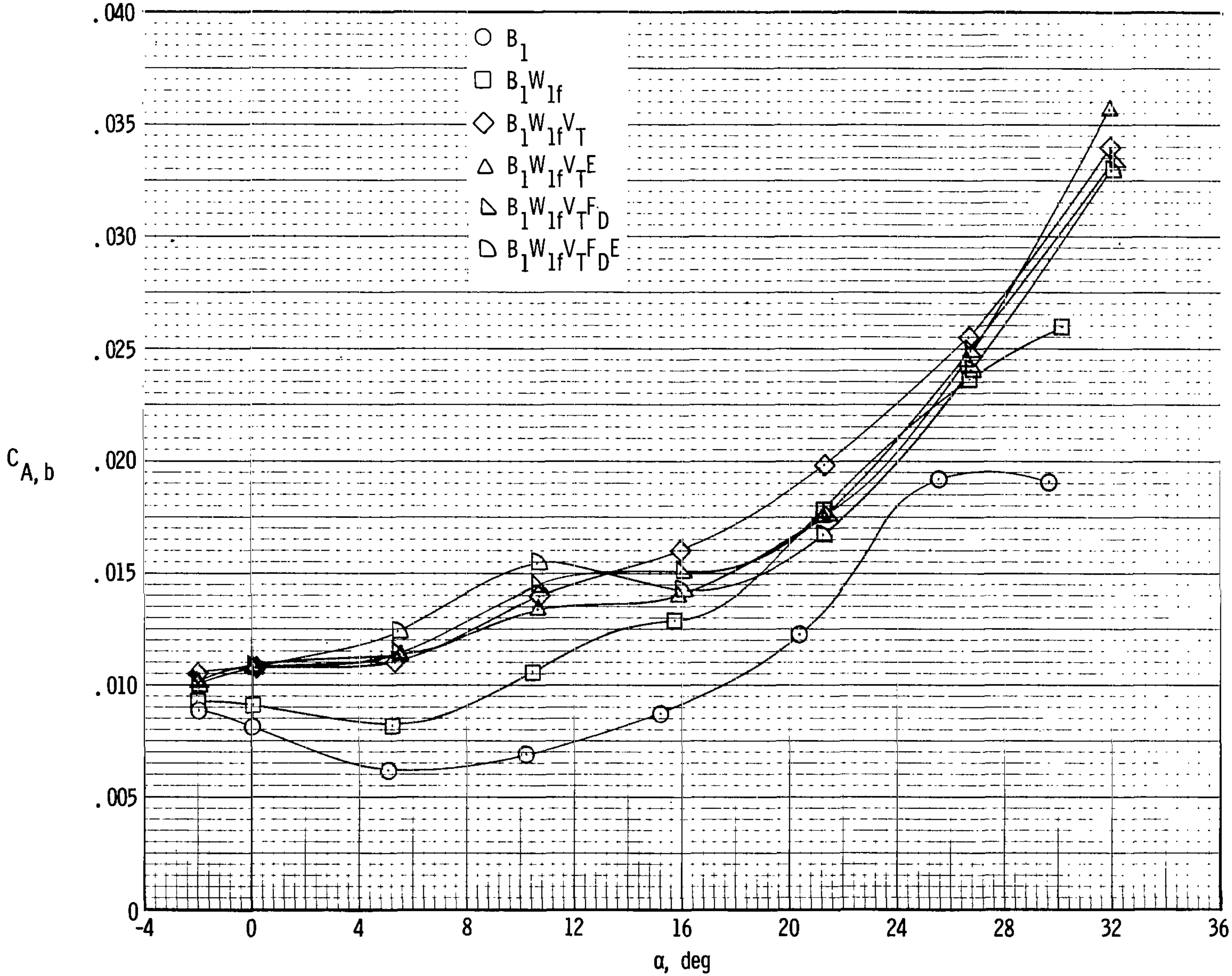

(a) Tip fin models.

Figure 5.- Variation of base axial force coefficient with angle of attack at $R = 10 \times 10^6$.

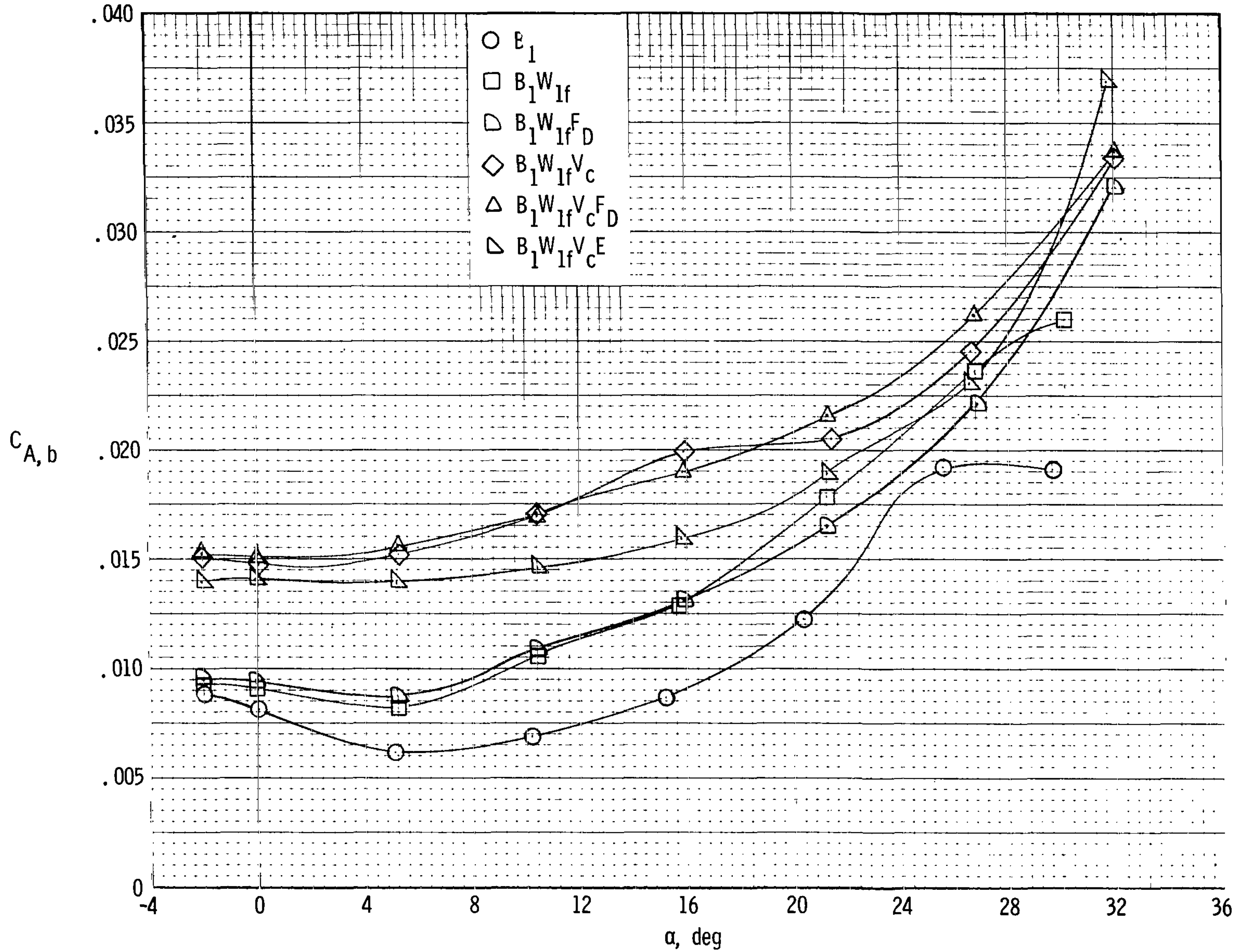

(b) Center fin models.

Figure 5.- Concluded.

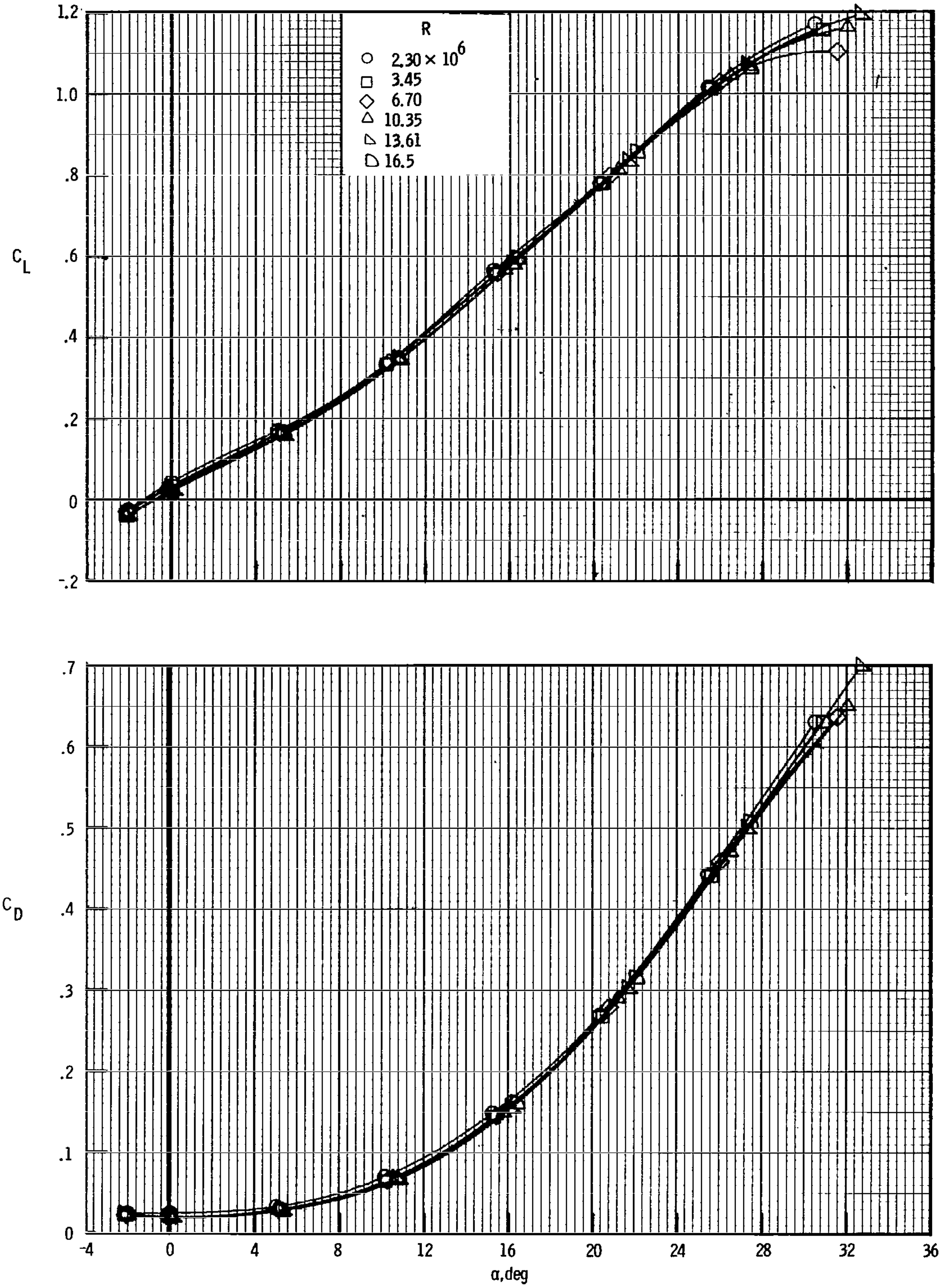

(a) Lift and drag.

Figure 6.- Reynolds number effects on longitudinal characteristics of B_1W_{1f} for $\delta_e = 0^\circ$.

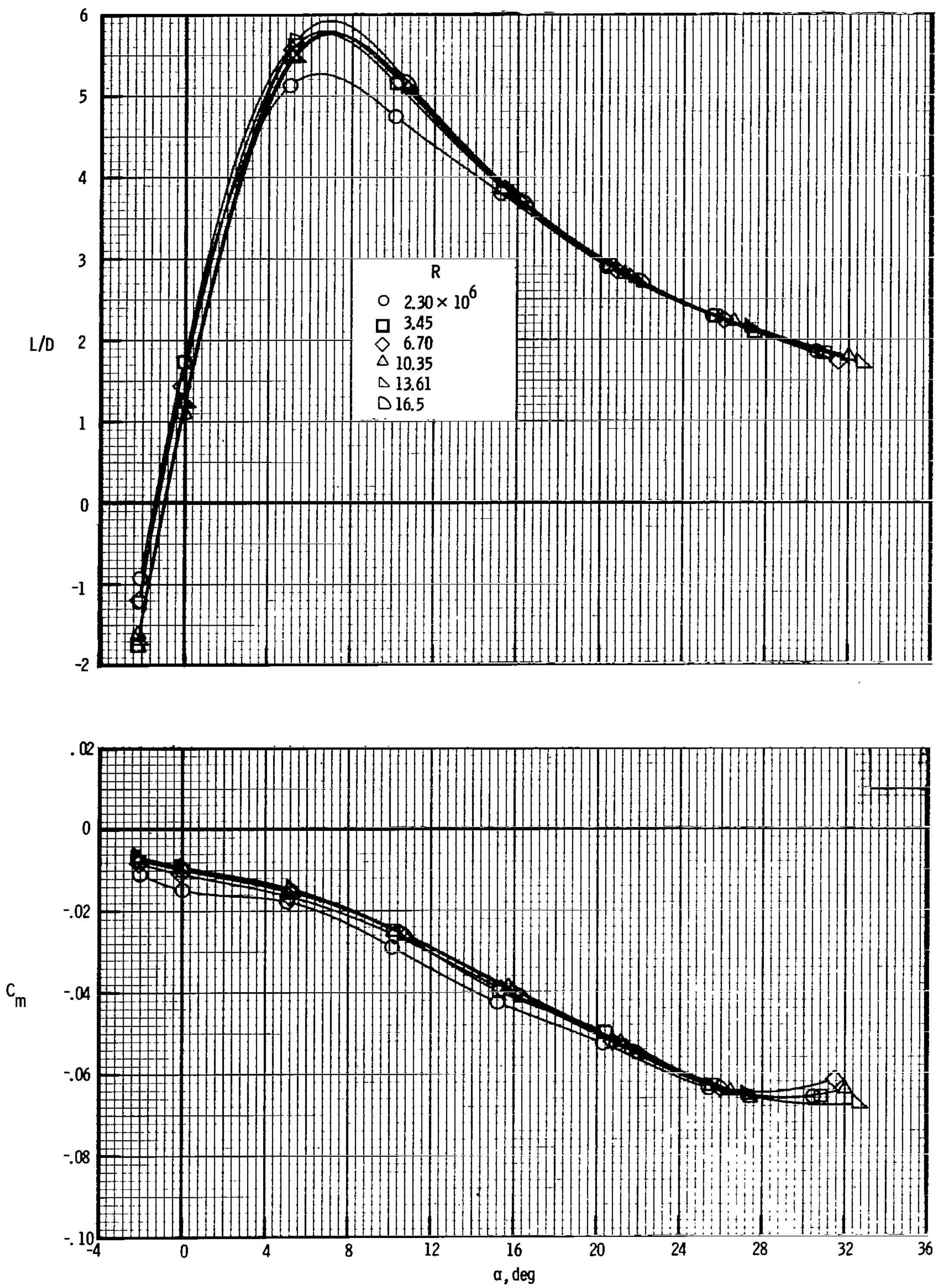

(b) Lift-drag ratio and pitch.

Figure 6.- Concluded.

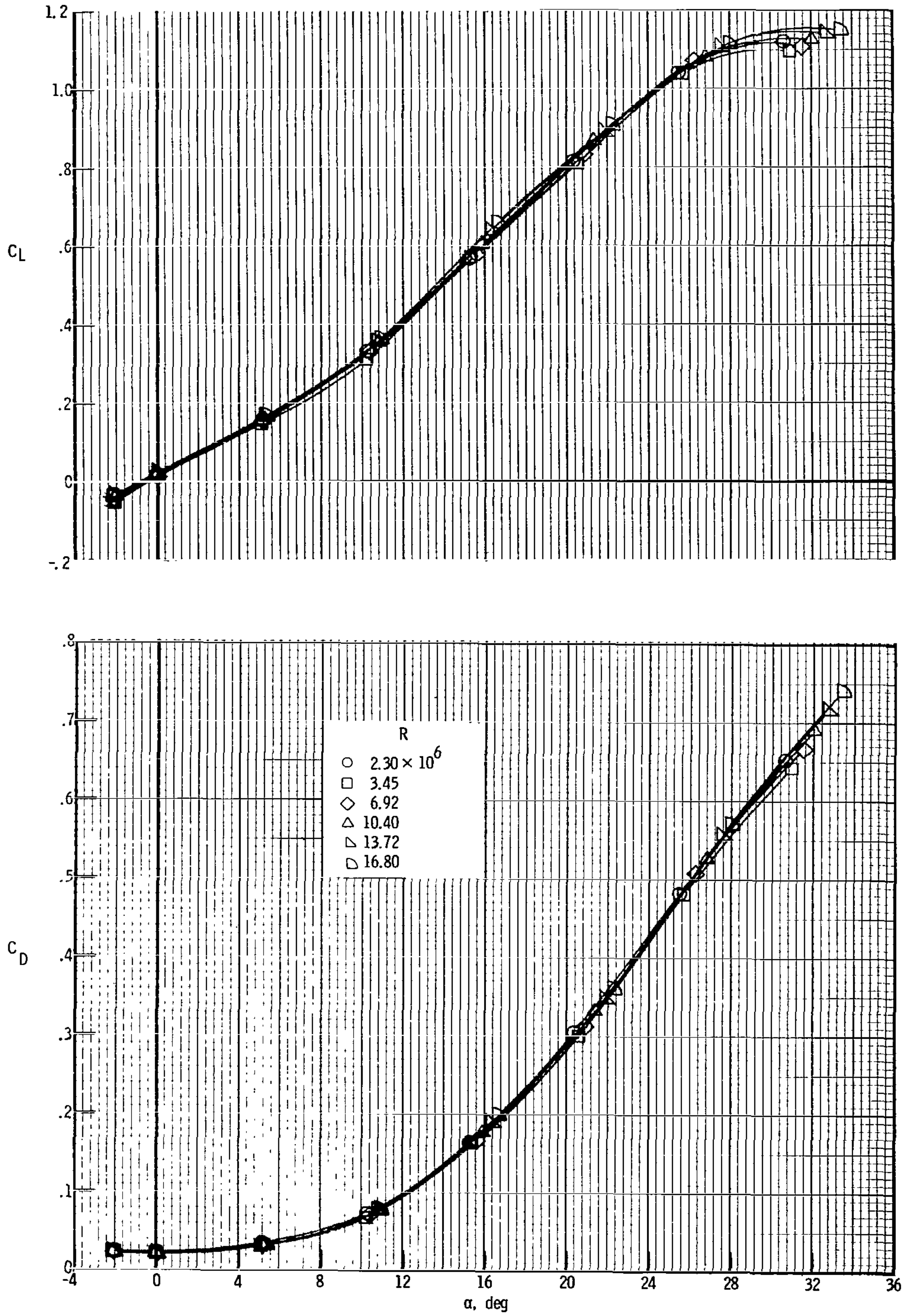

(a) Lift and drag.

Figure 7.- Reynolds number effects on longitudinal characteristics of $B_1W_{1f}F_D$ for $\delta_e = 0^{\circ}$.

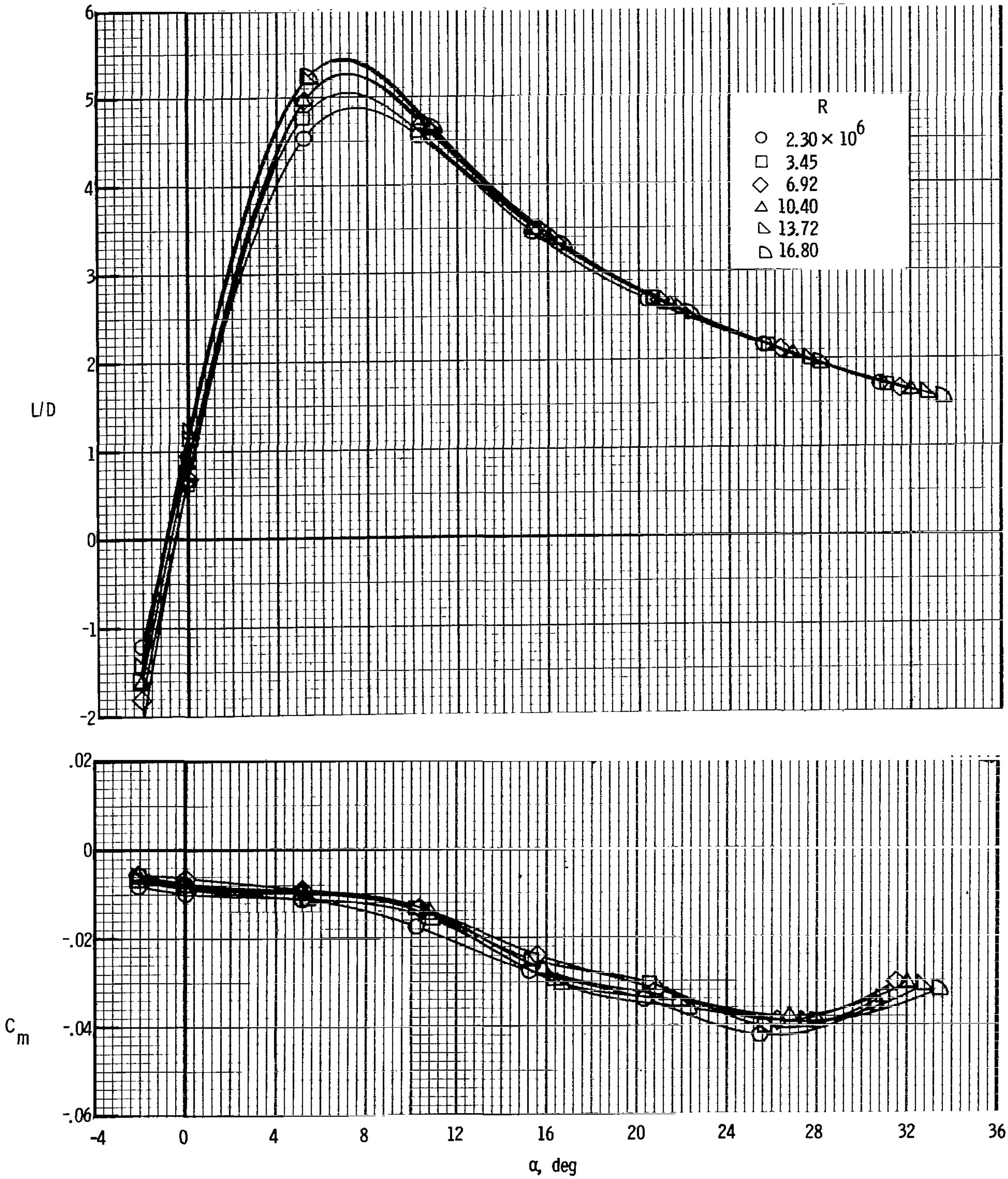

(b) Lift-drag ratio and pitch.

Figure 7.- Concluded.

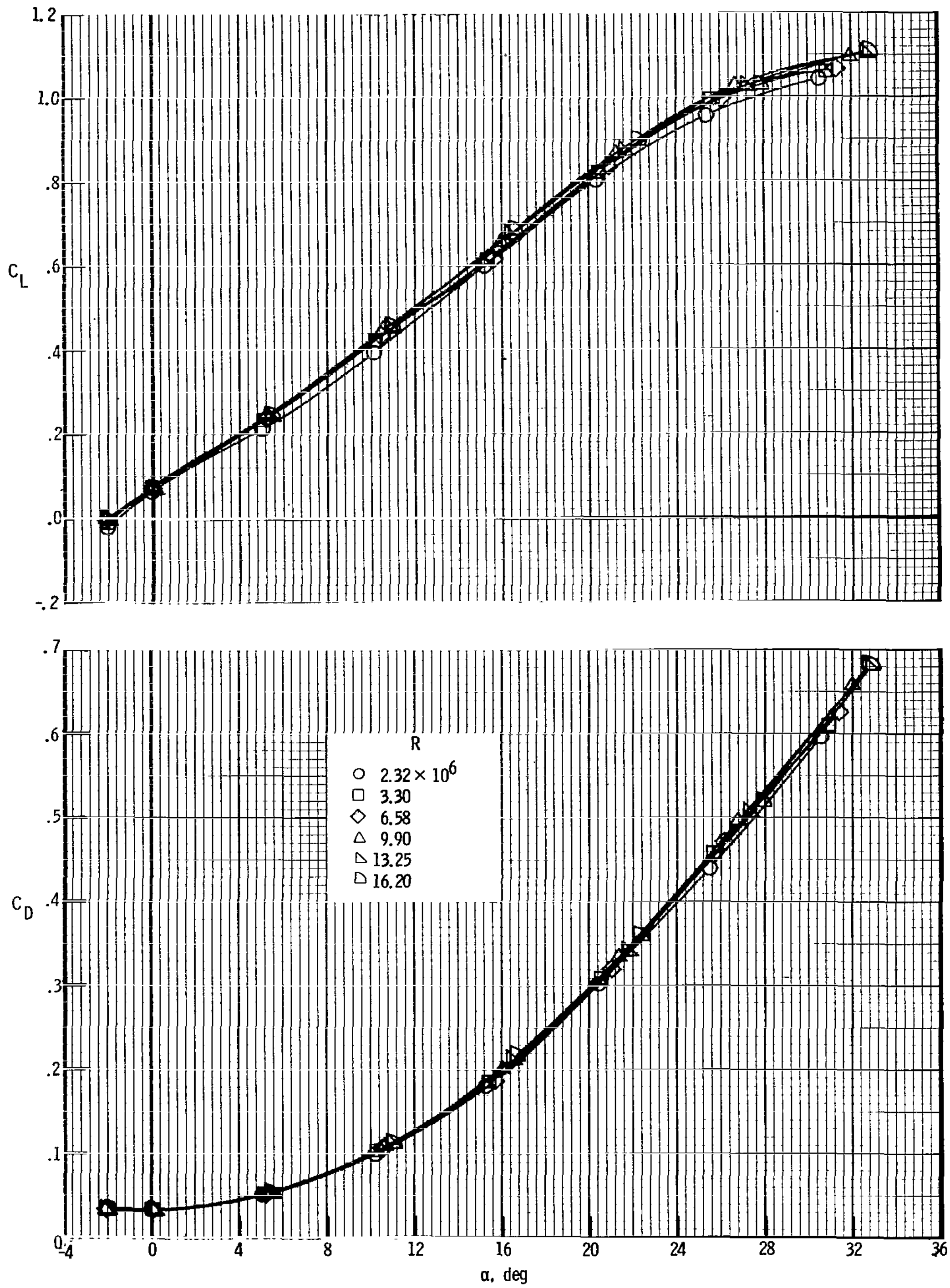

(a) Lift and drag.

Figure 8.- Reynolds number effects on longitudinal characteristics of $B_1W_{1f}F_DV_T$ for $\delta_e = 0^o$.

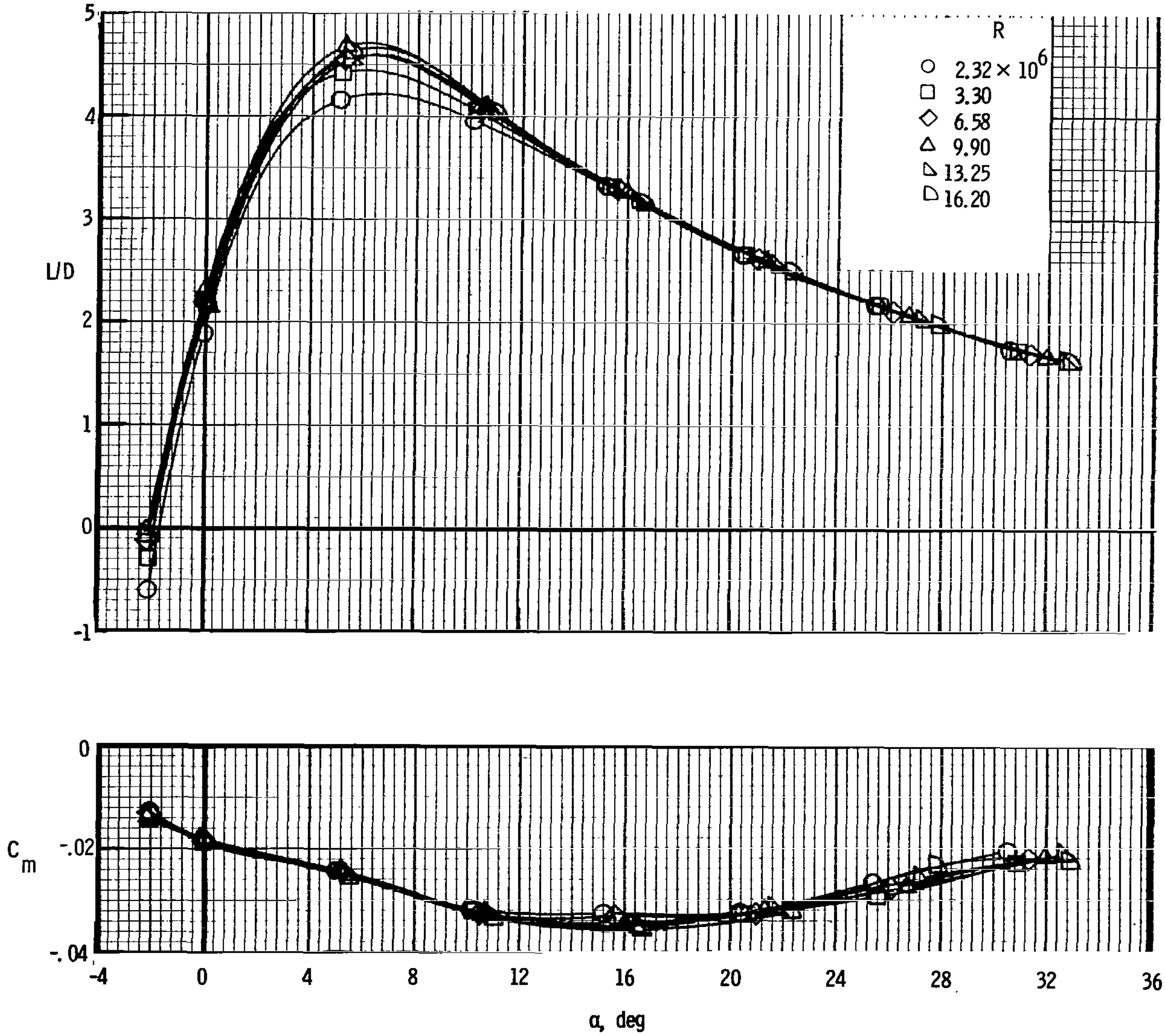

(b) Lift-drag ratio and pitch.

Figure 8.- Concluded.

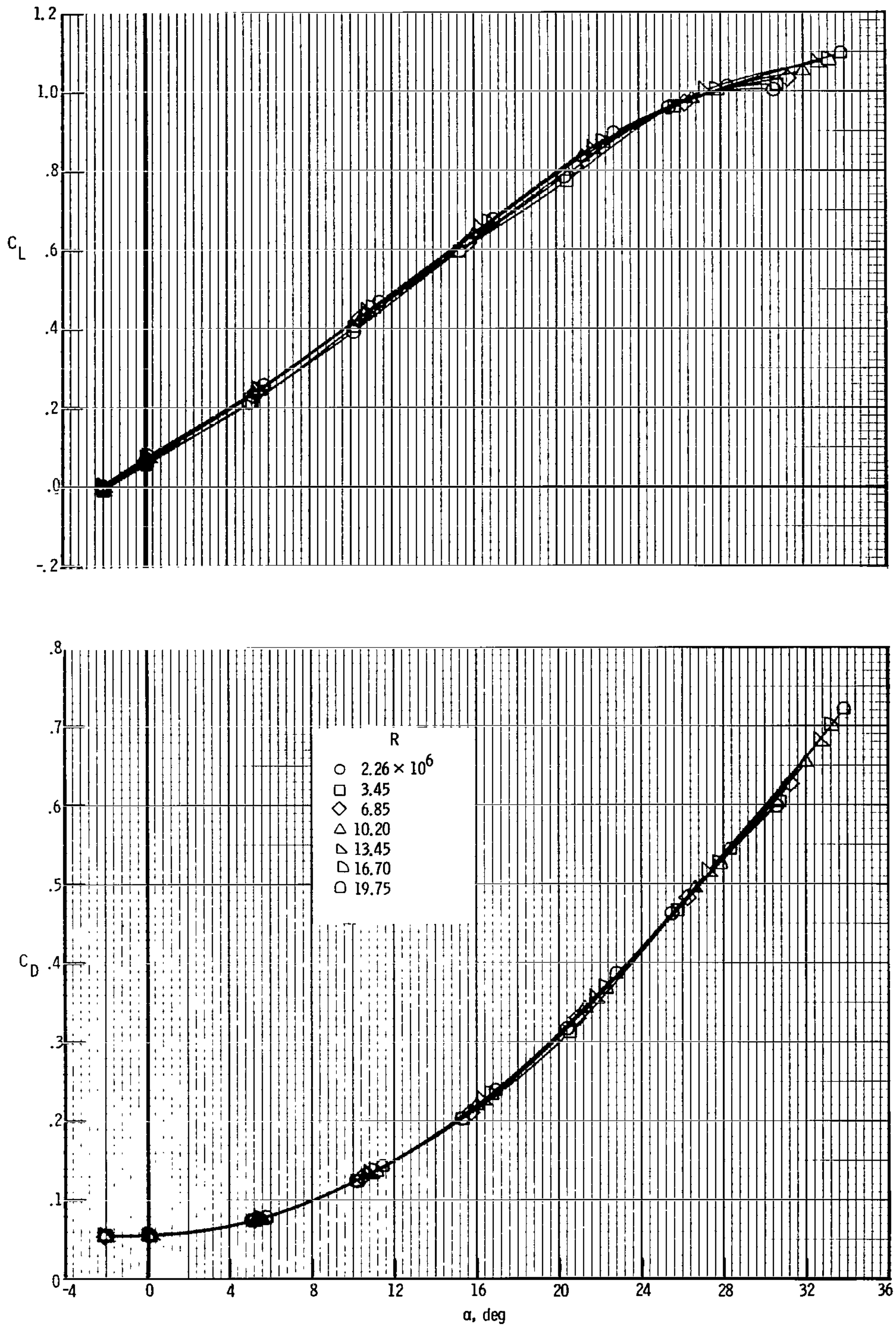

(a) Lift and drag.

Figure 9.- Effect of Reynolds number variation on longitudinal characteristics of $B_1W_{1f}V_TF_DE$ for $\delta_e = 0^\circ$.

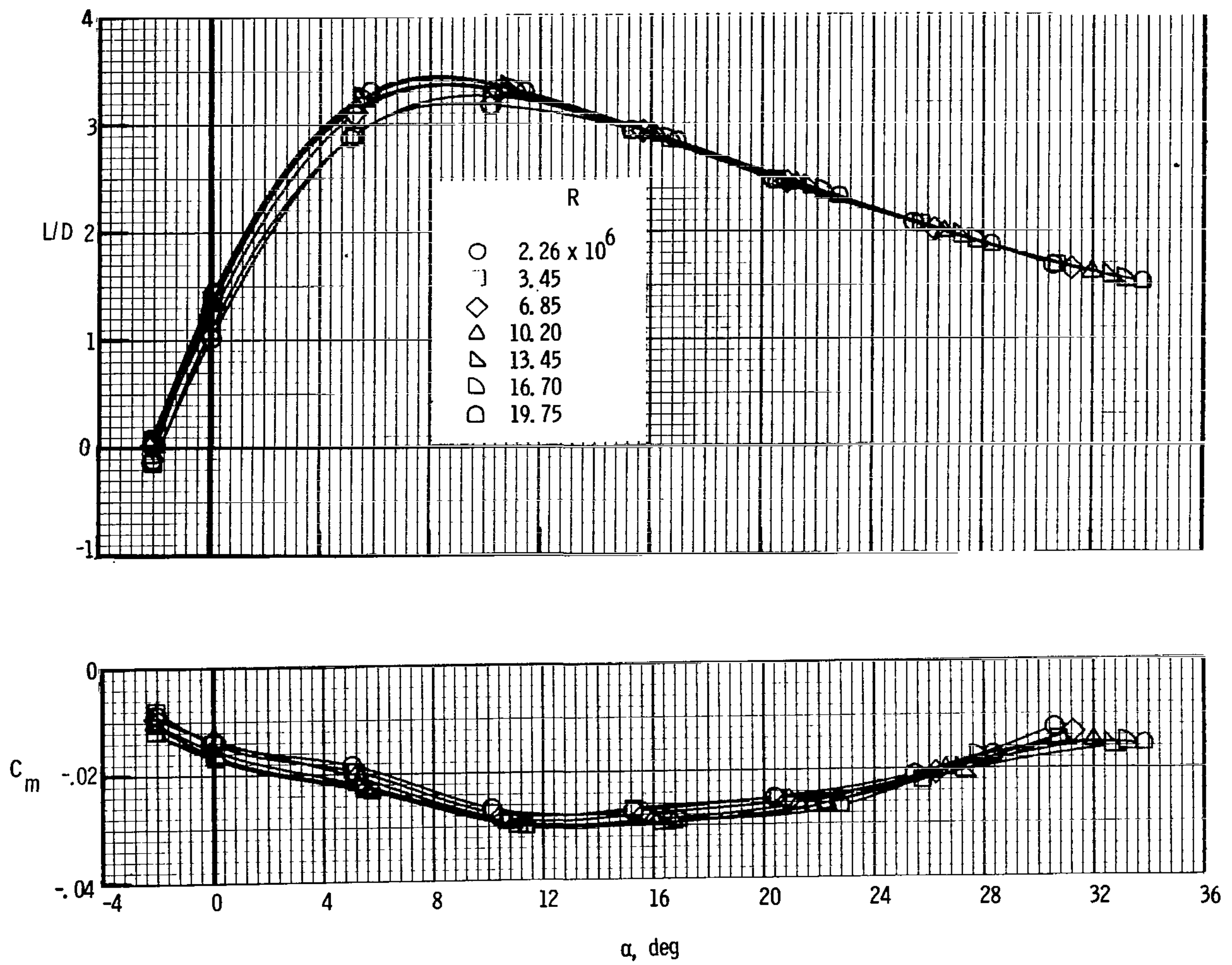

(b) Lift-drag ratio and pitch.

Figure 9.- Concluded.

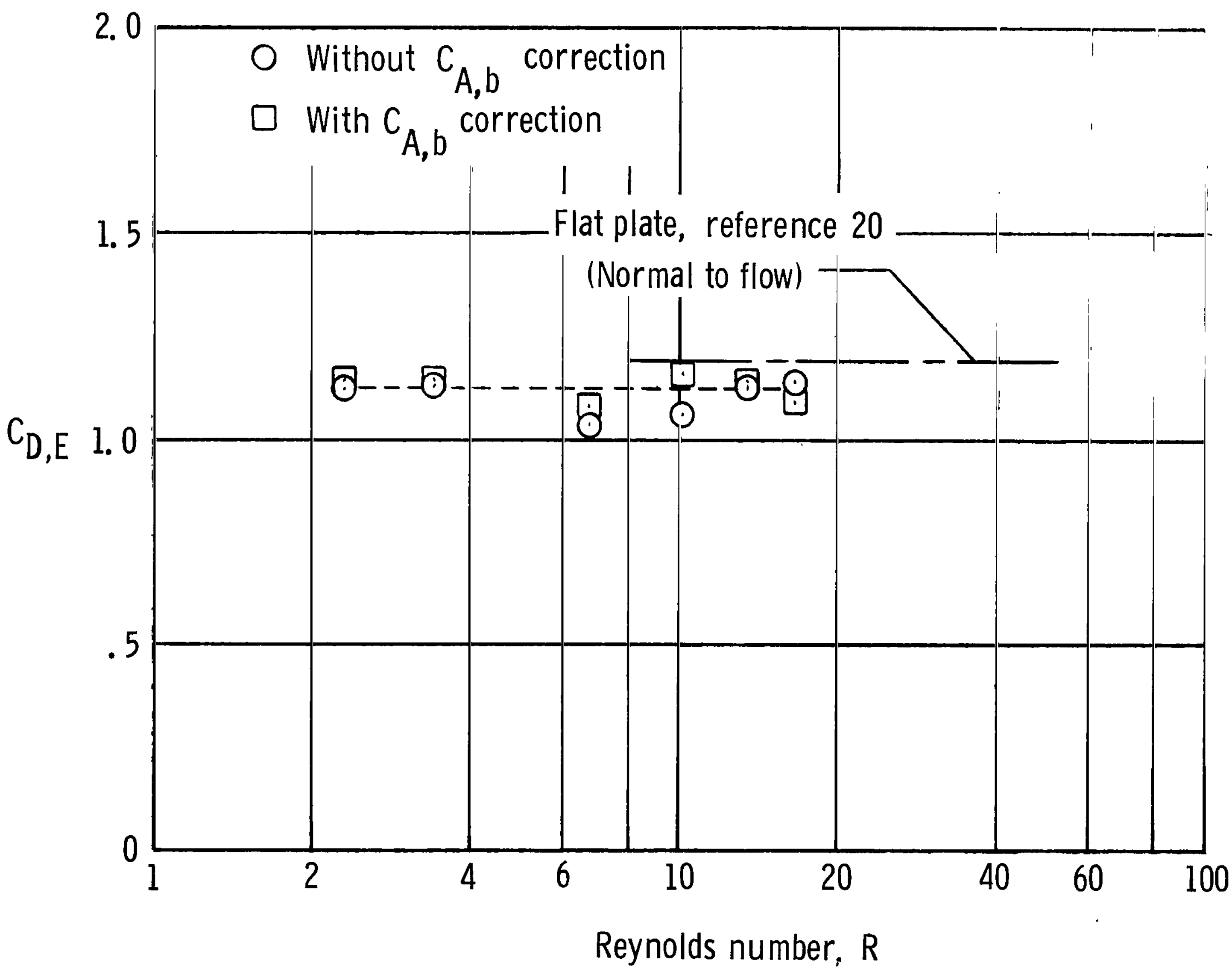

Figure 10.- Variation of scramjet engine drag with Reynolds number at $M = 0.2$.

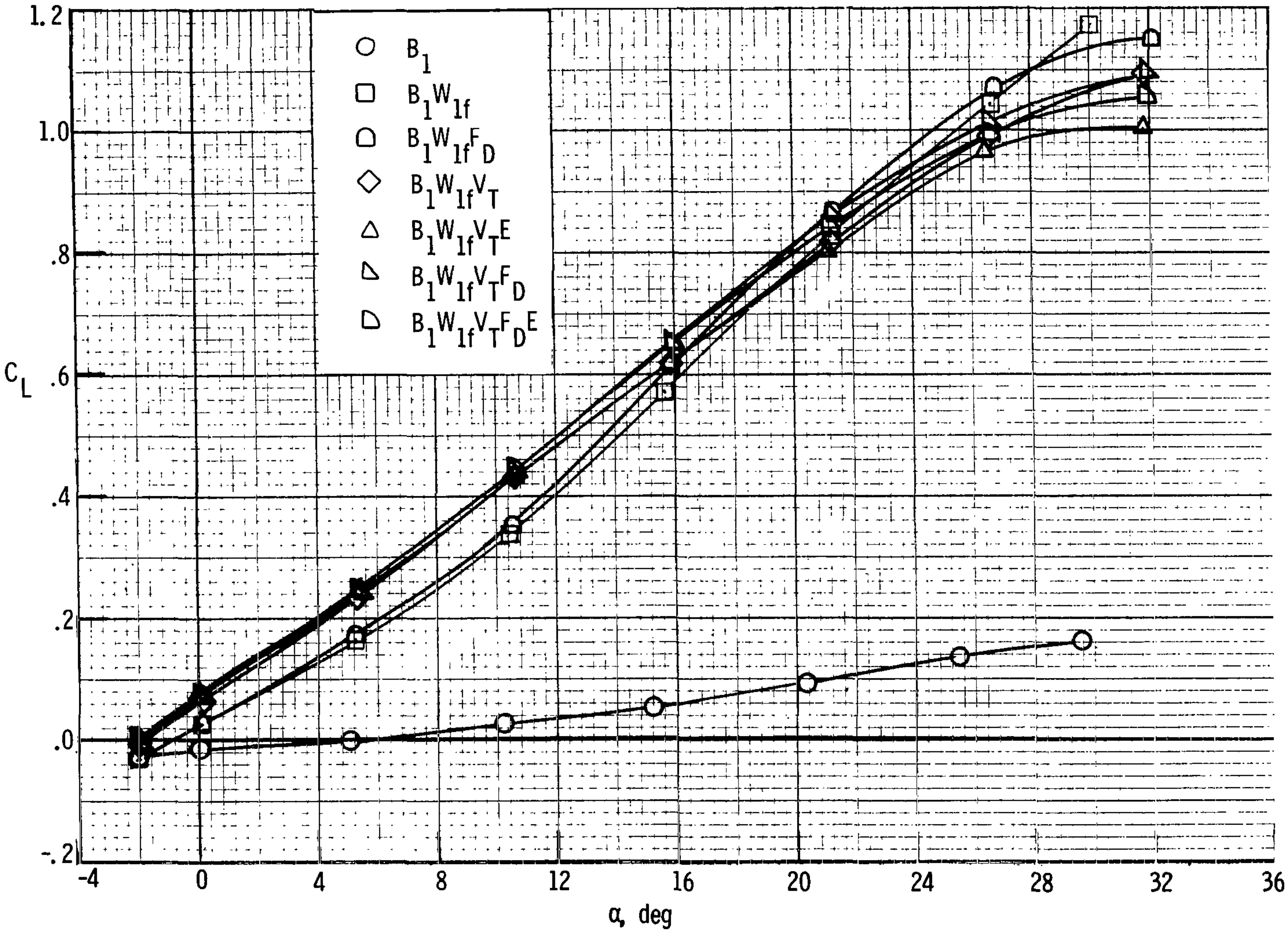

(a) Lift.

Figure 11.- Variation of longitudinal characteristics with component buildup of tip fin configuration for $\delta_e = 0^{\circ}$.

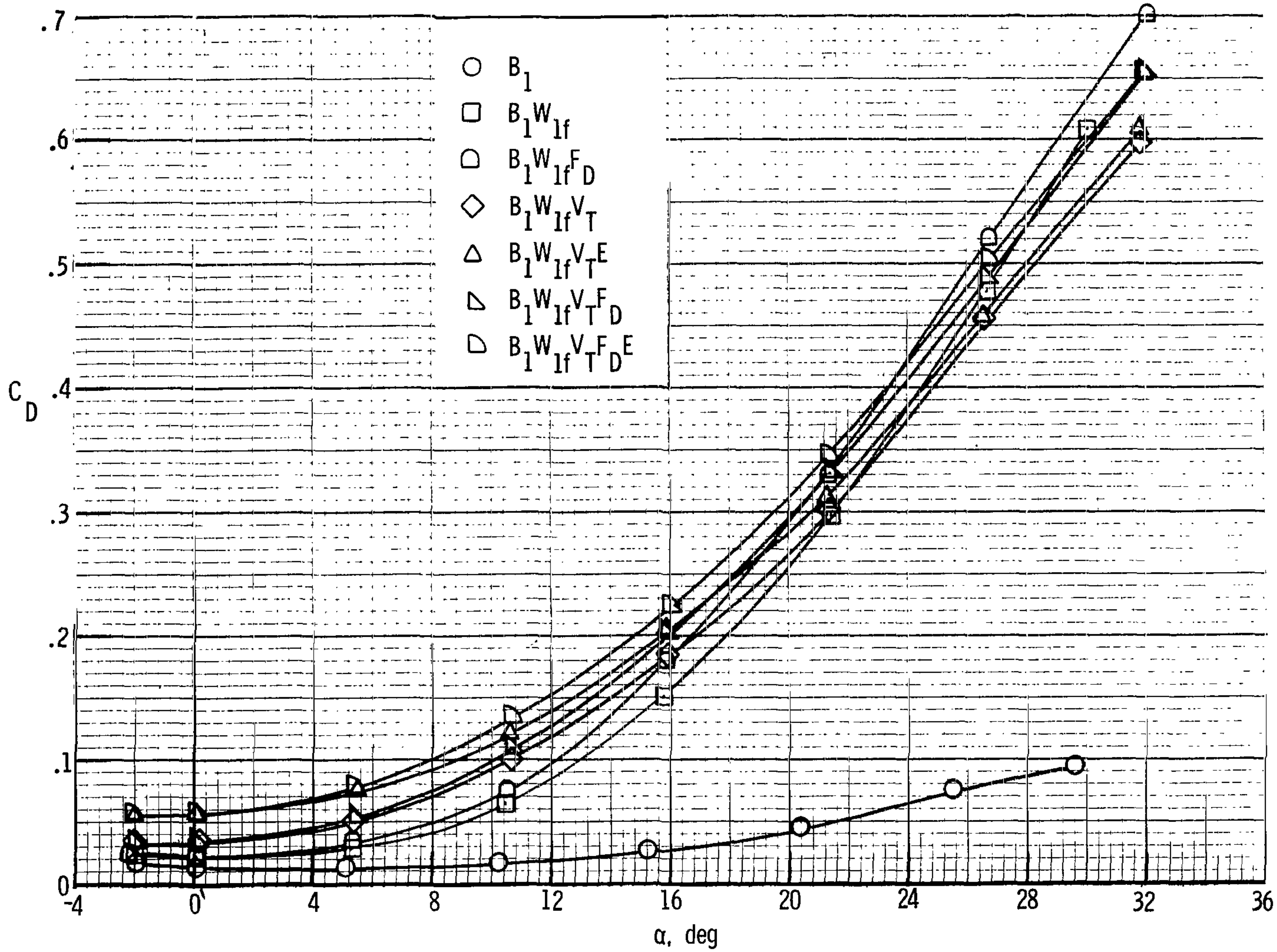

(b) Drag.

Figure 11.- Continued.

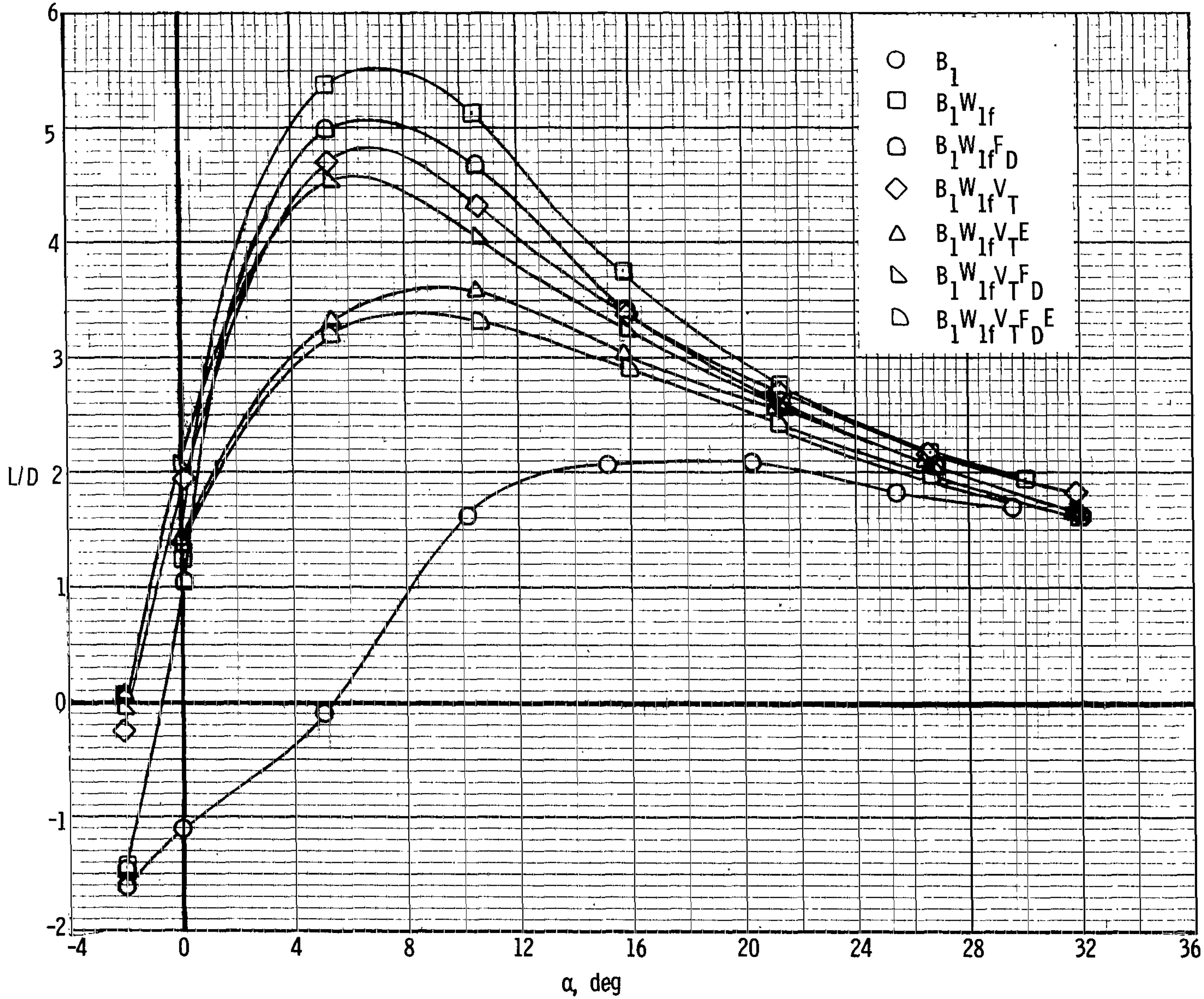

(c) Lift-drag ratio.

Figure 11.- Continued.

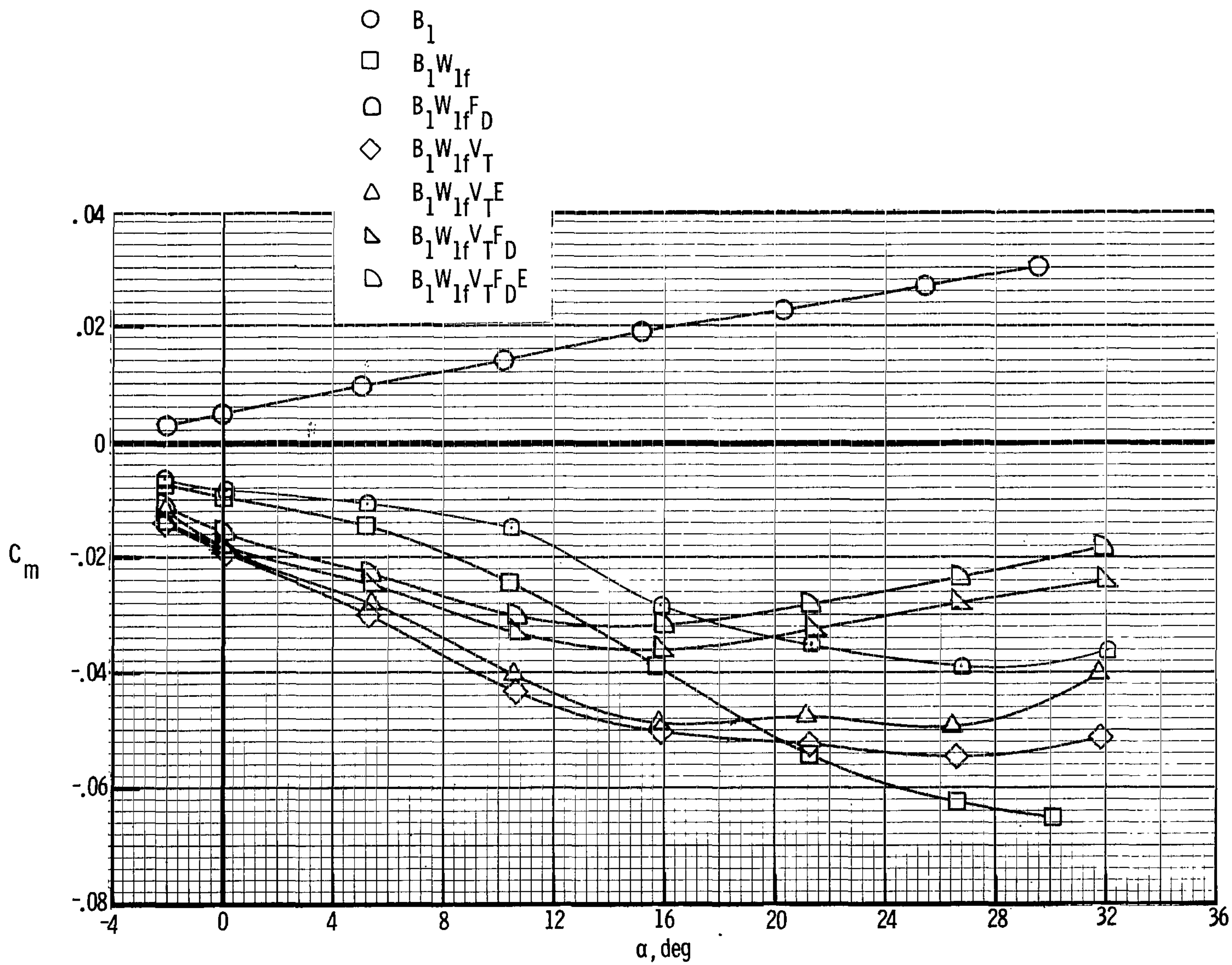

(d) Pitch.

Figure 11.- Continued.

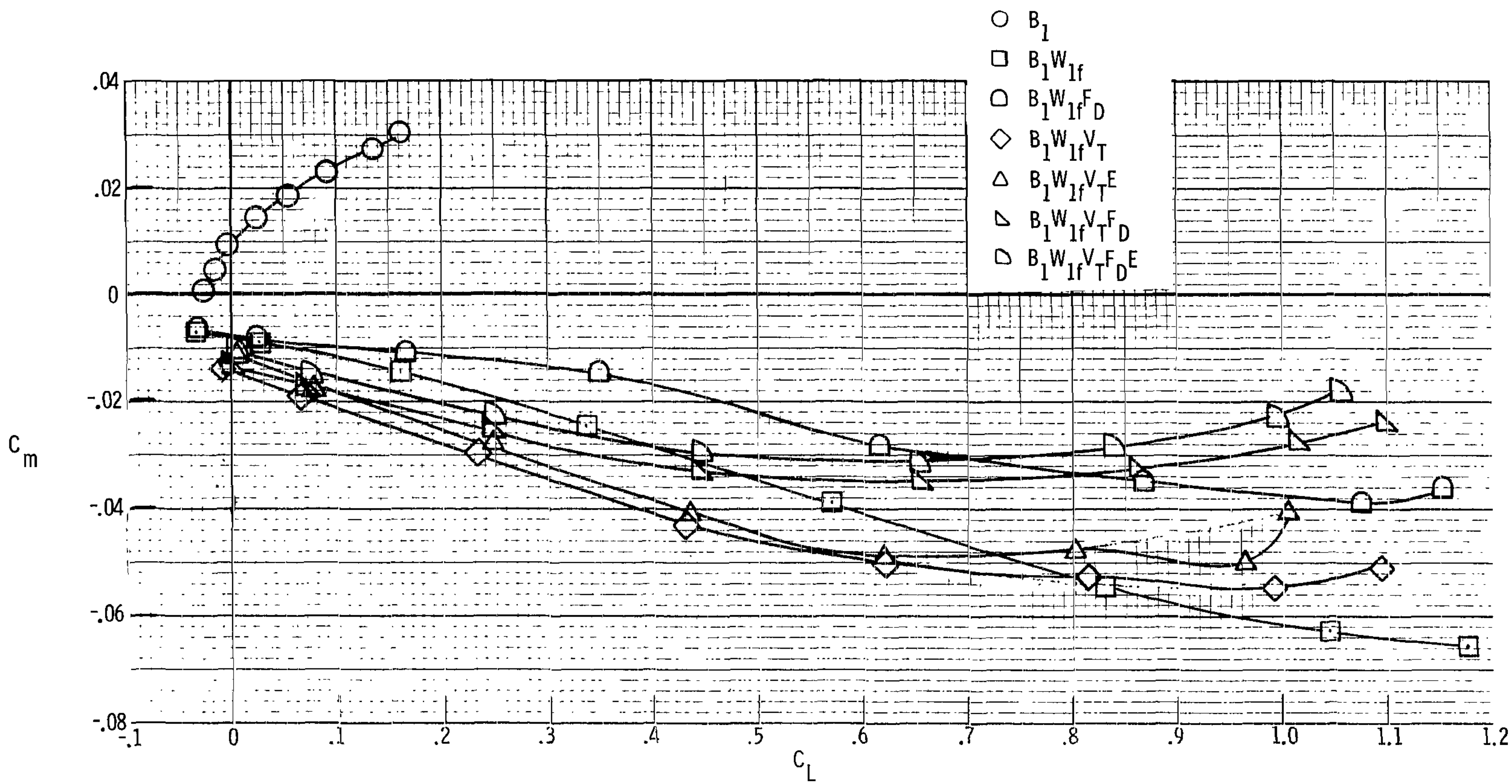

(e) Stability.

Figure 11.- Concluded.

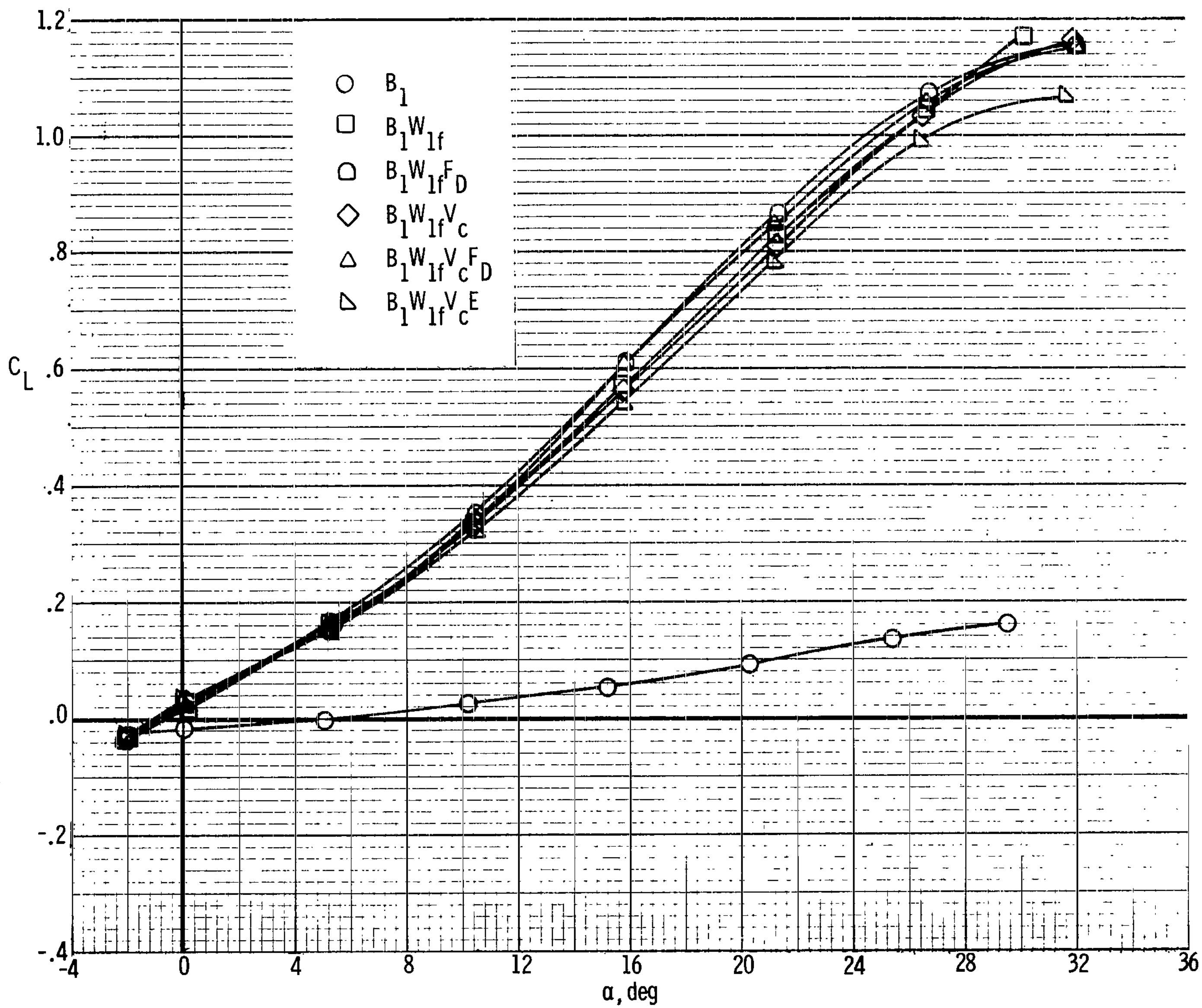

(a) Lift.

Figure 12.- Effect of engine on longitudinal characteristics with component buildup of center vertical tail configuration for $\delta_e = 0^{\circ}$.

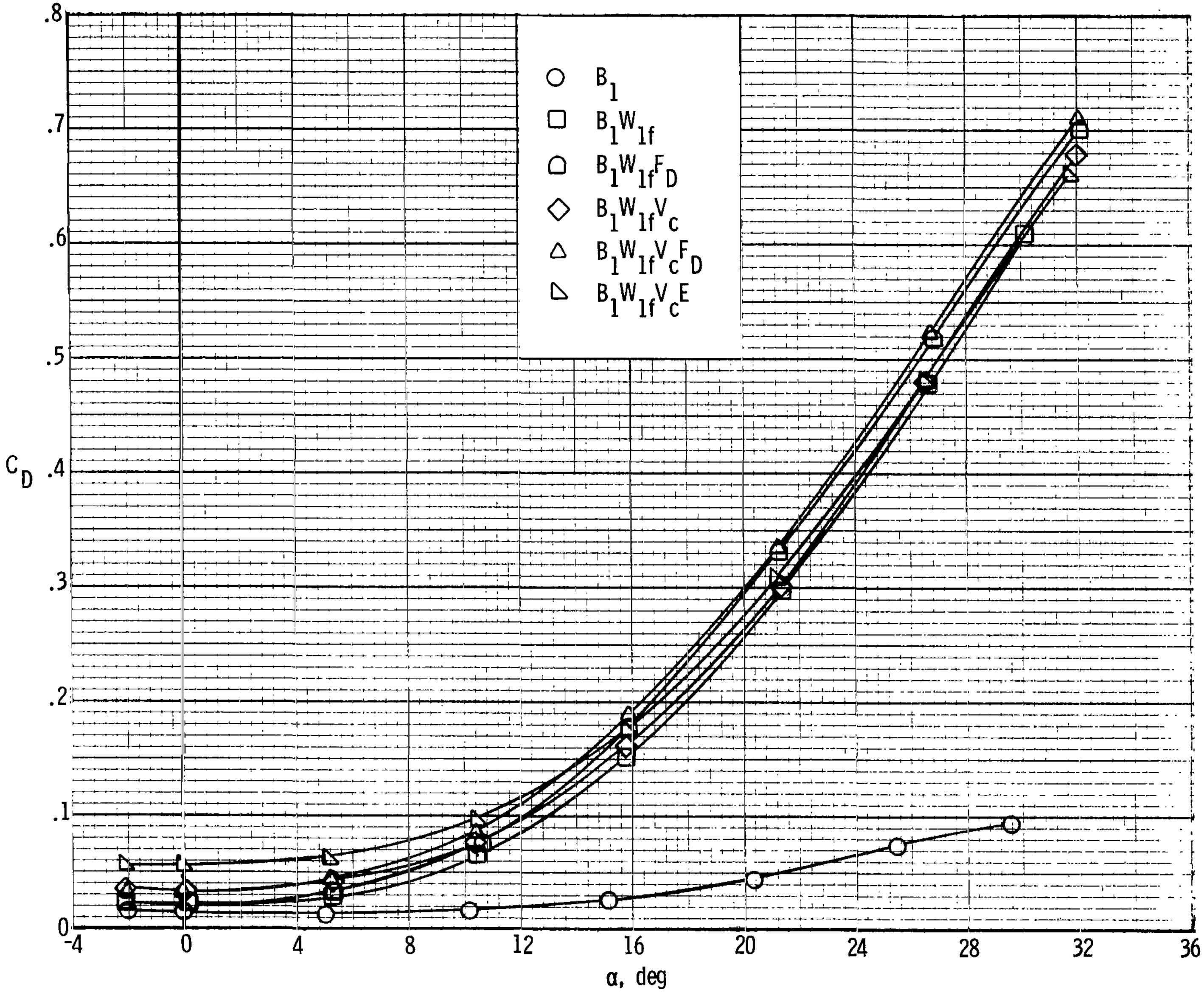

(b) Drag.

Figure 12.- Continued.

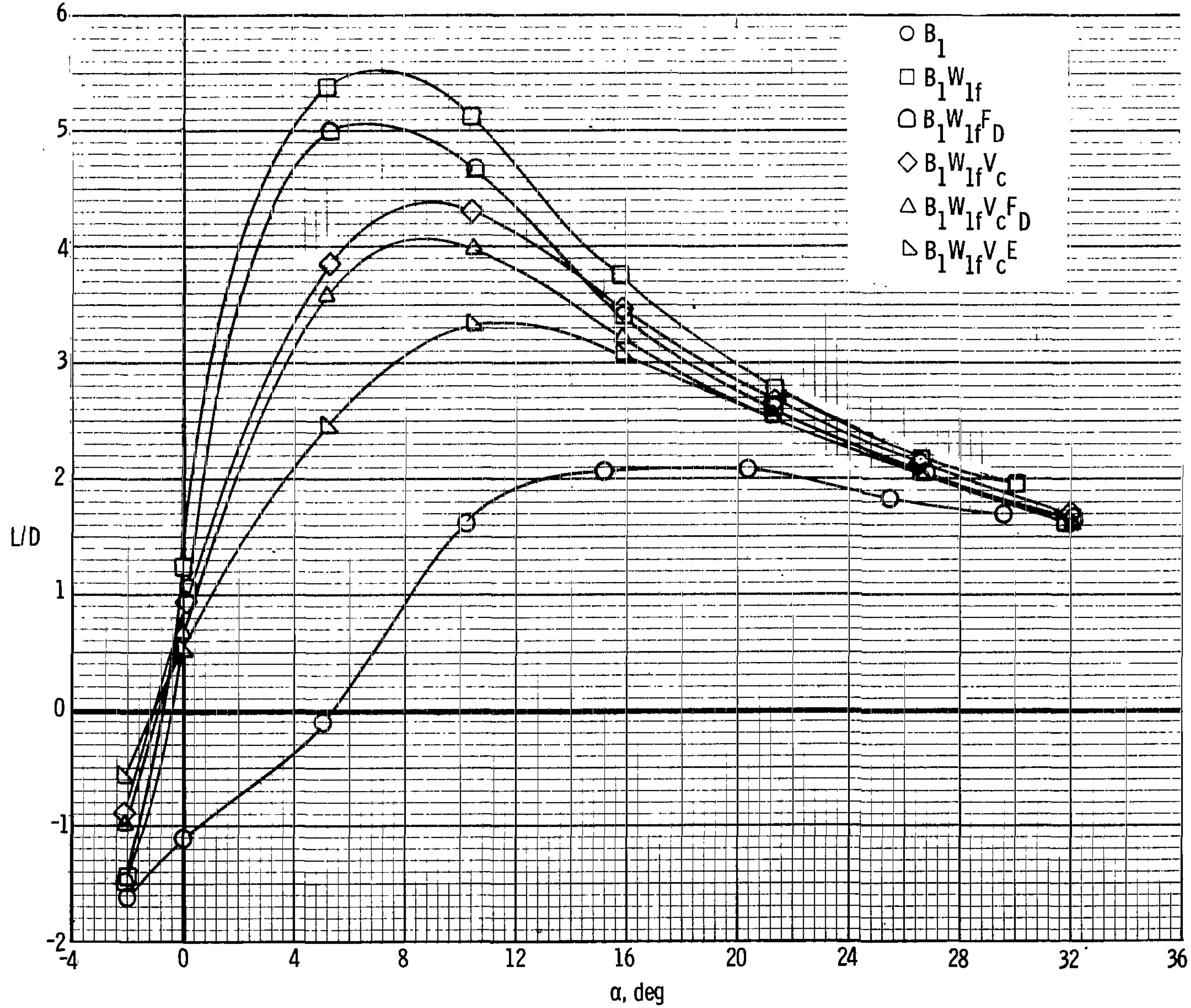

(c) Lift-drag ratio.

Figure 12.- Continued.

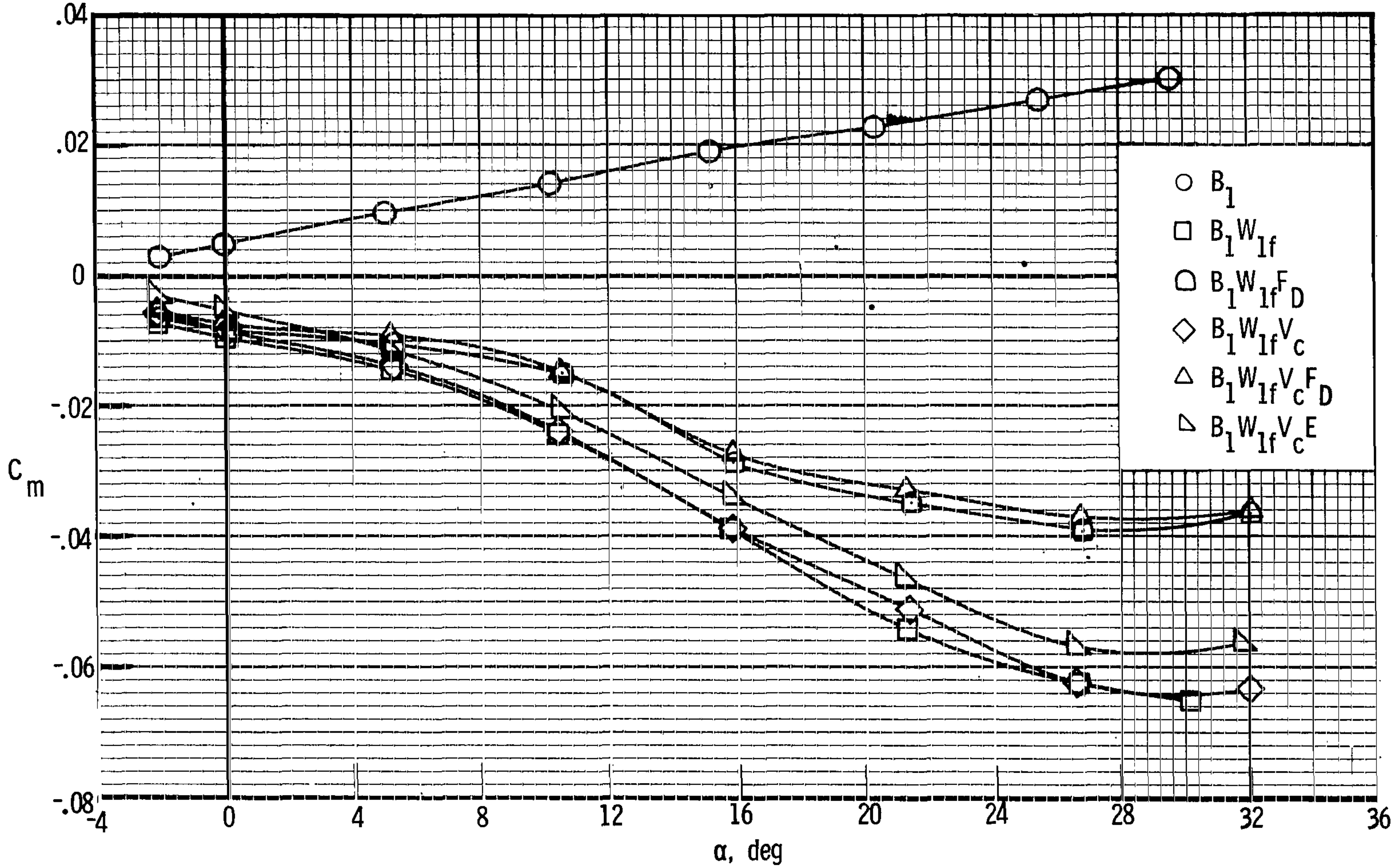

(d) Pitch.

Figure 12.- Continued.

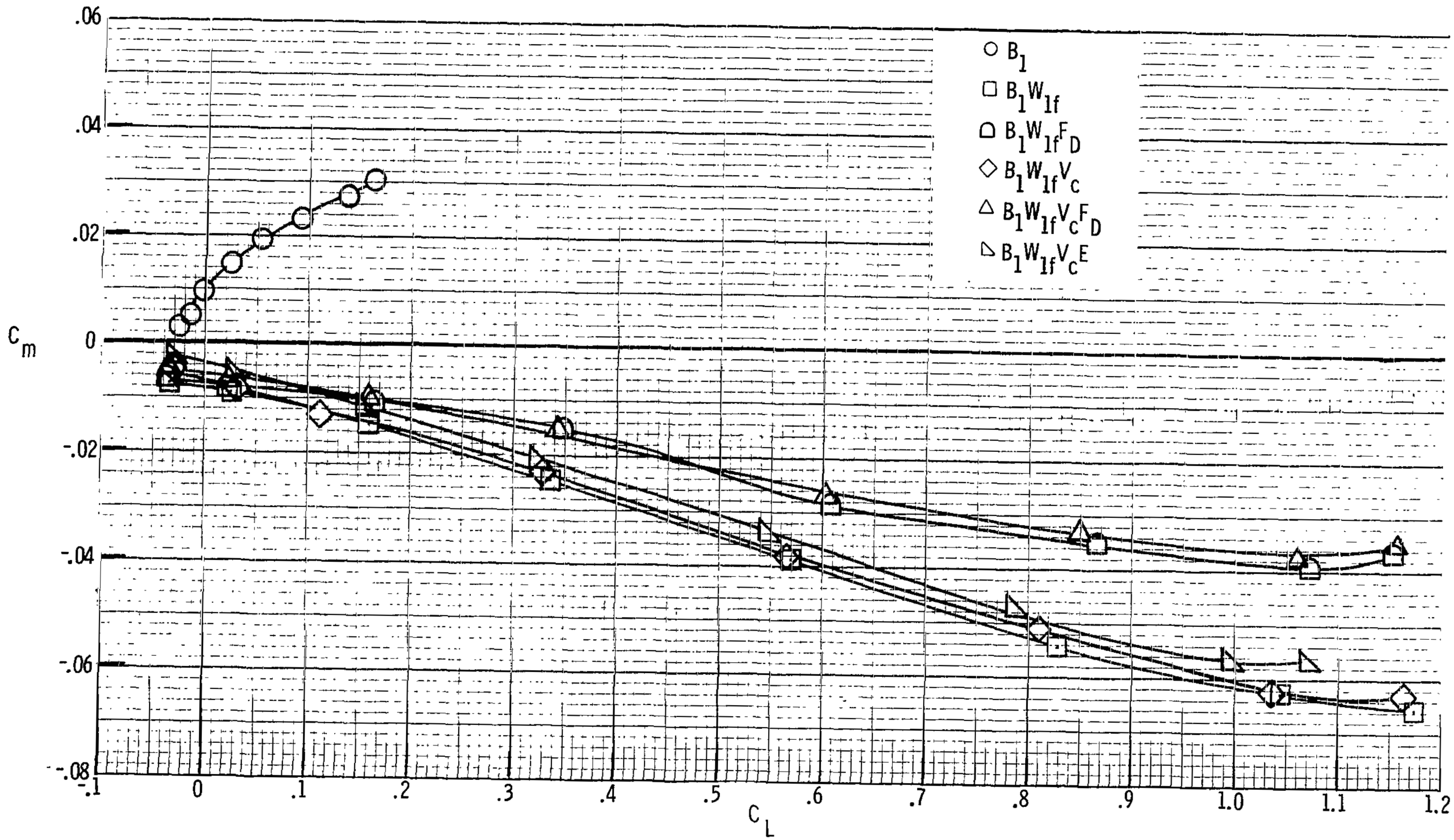

(e) Stability.

Figure 12.- Concluded.

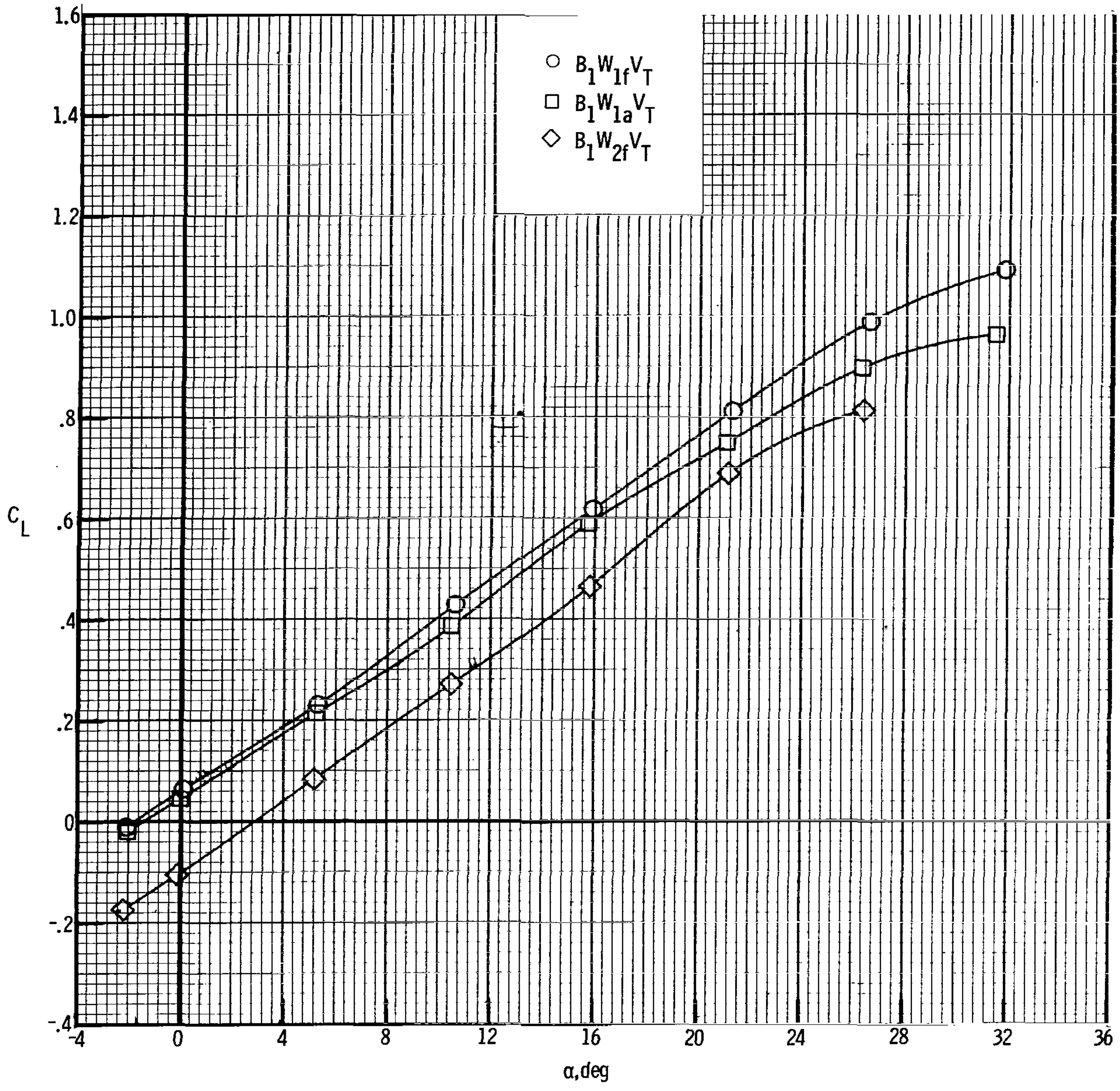

(a) Lift.

Figure 13.- Effect of wing location and camber on longitudinal characteristics of tip fin configuration for $\delta_e = 0^{\circ}$.

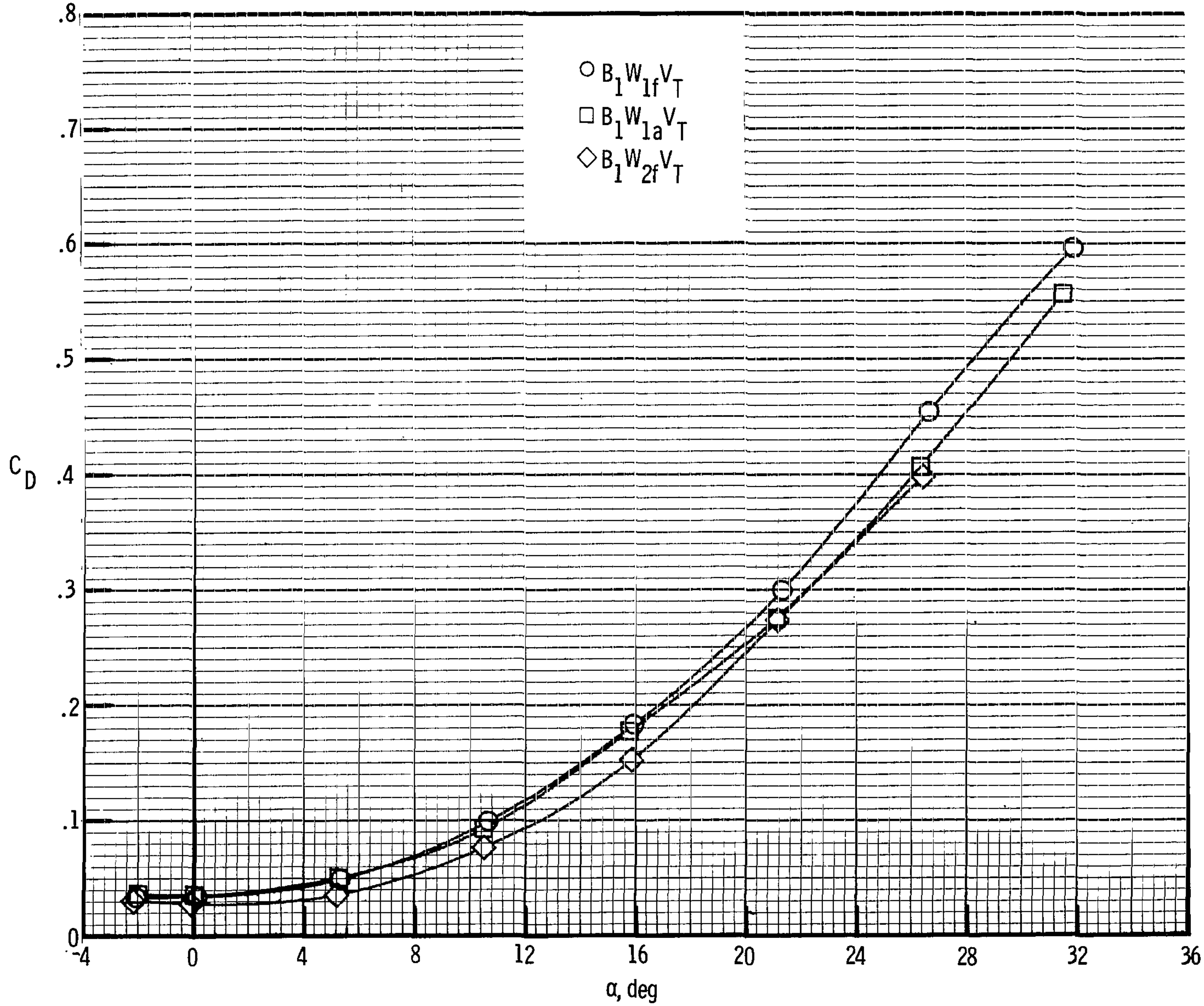

(b) Drag.

Figure 13.- Continued.

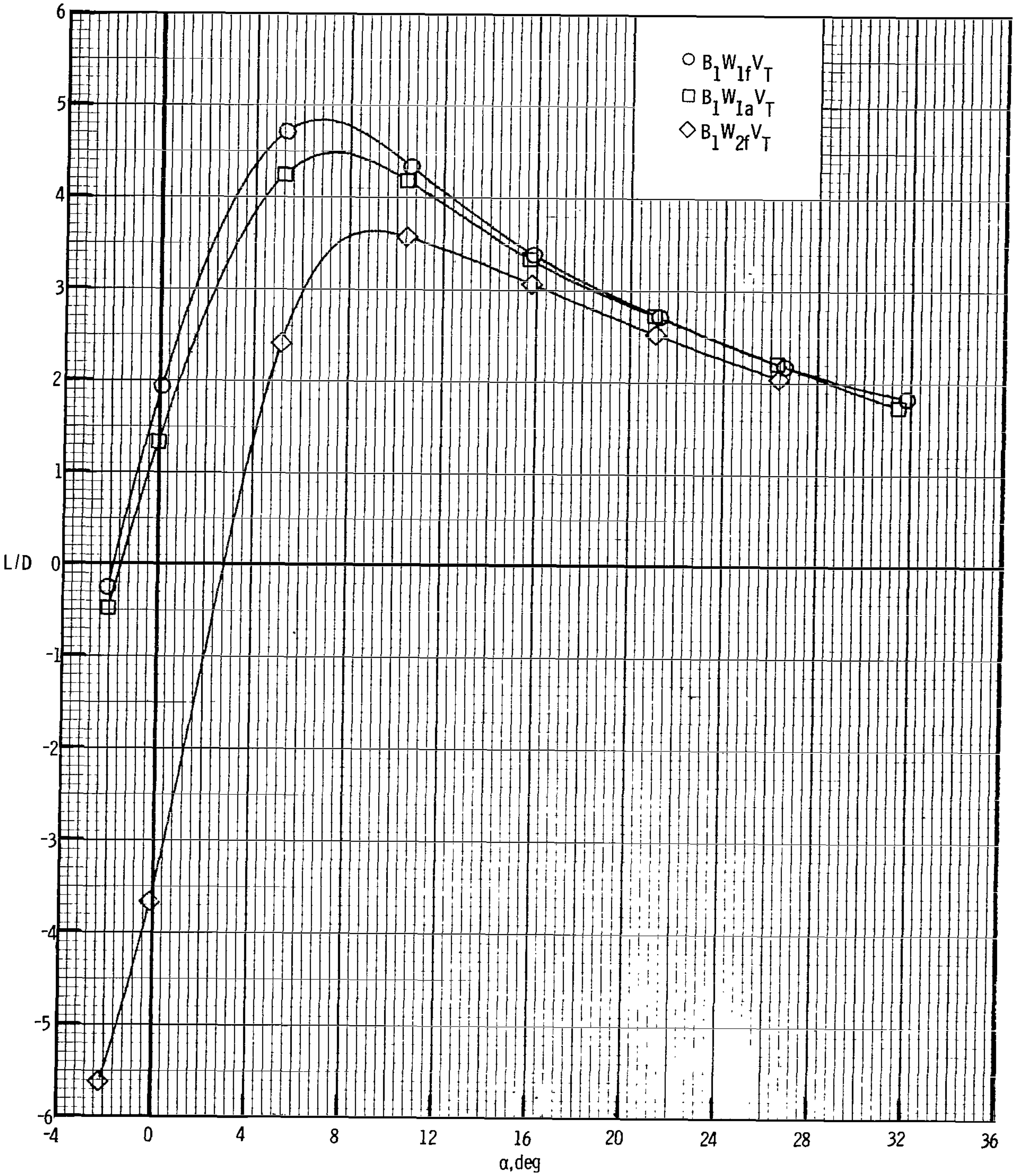

(c) Lift-drag ratio.

Figure 13.- Continued.

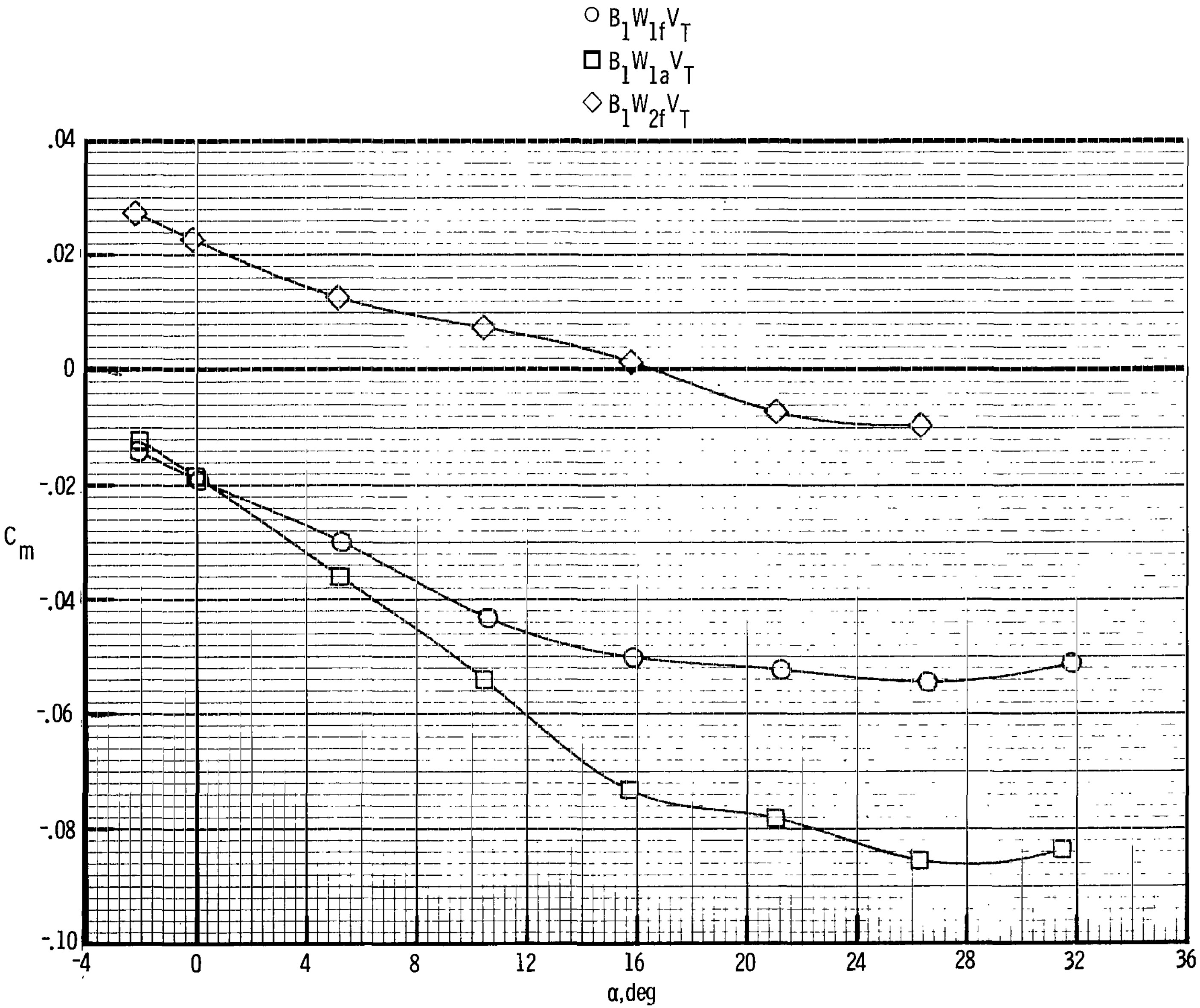

(d) Pitch.

Figure 13.- Continued.

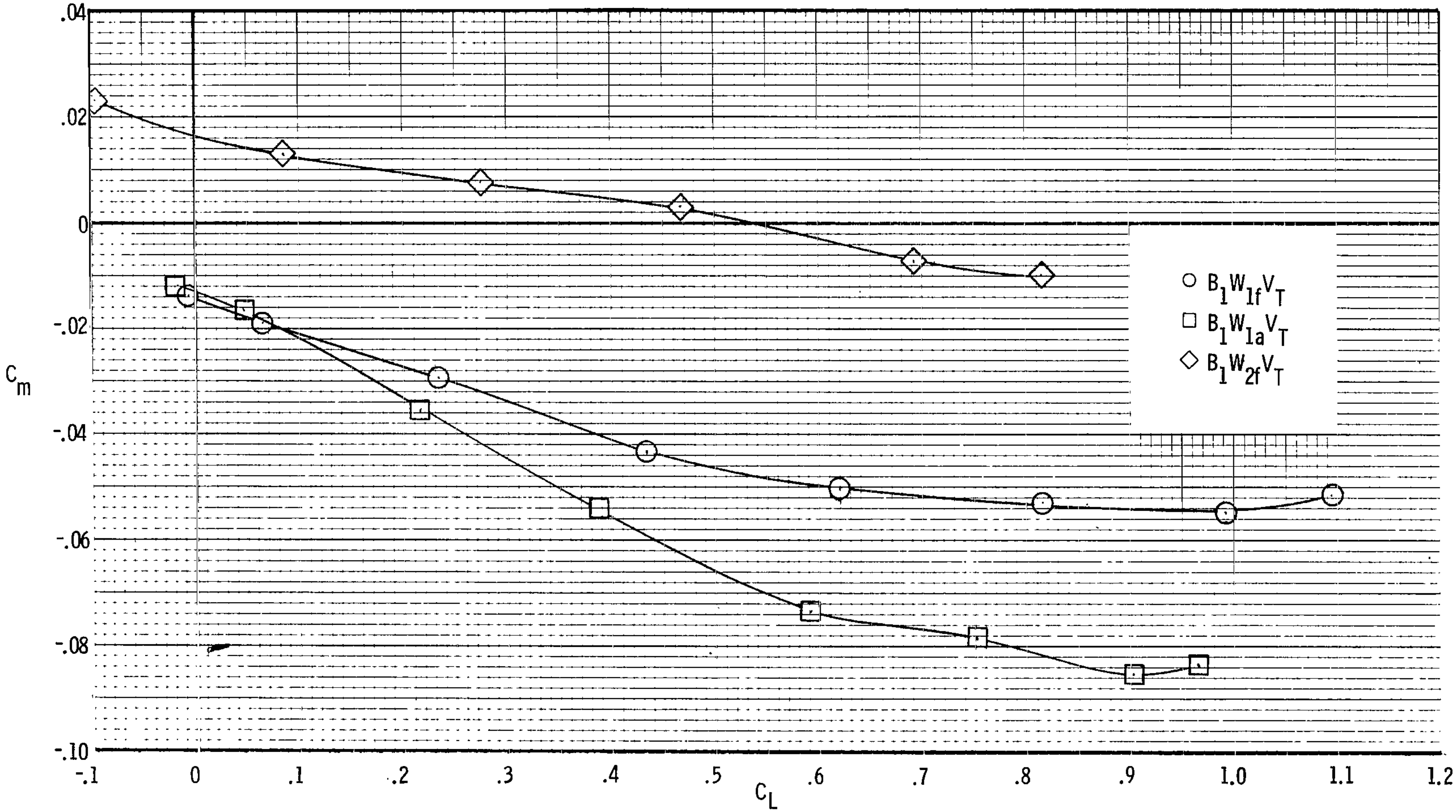

(e) Stability.

Figure 13.- Concluded.

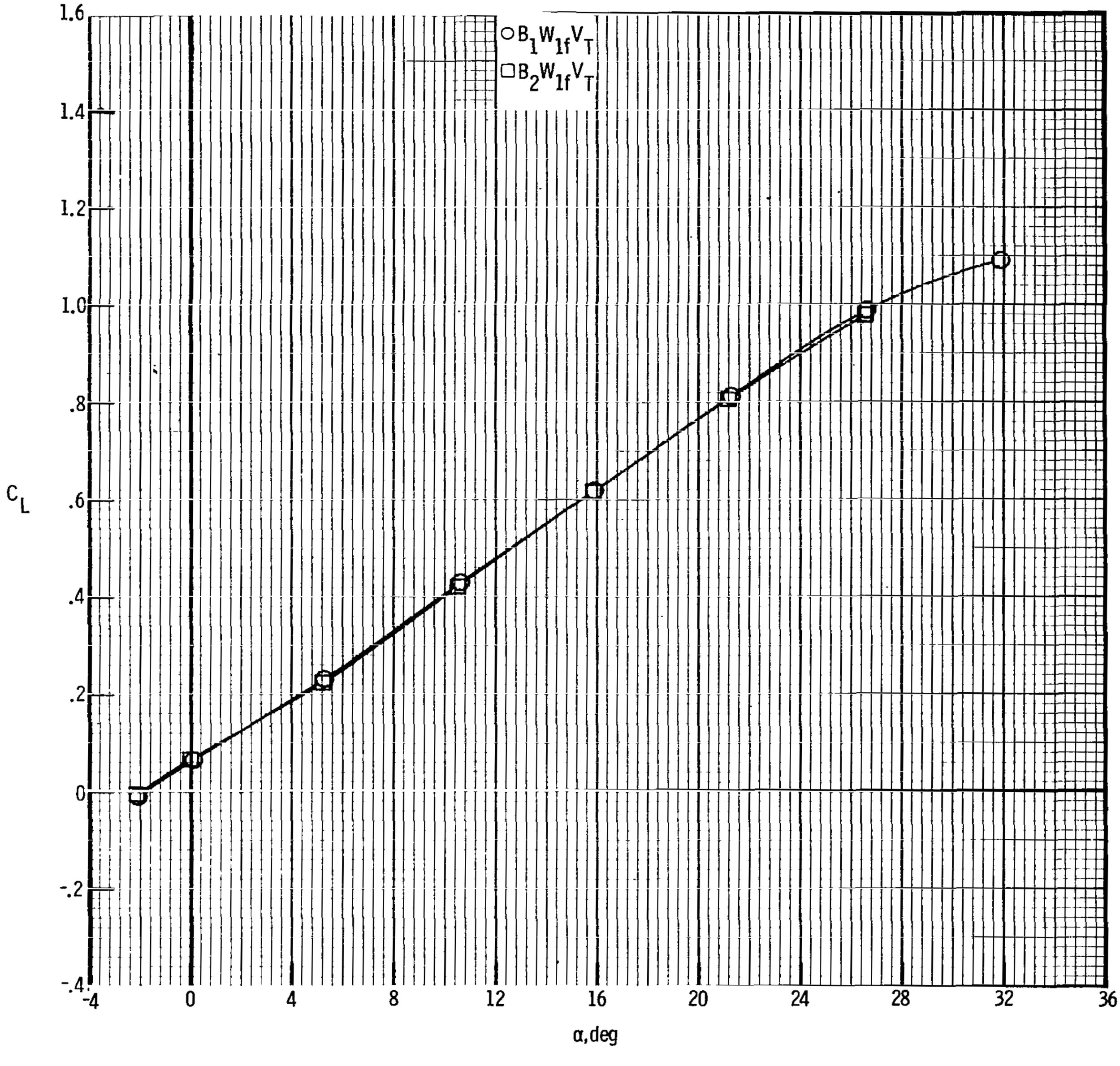

(a) Lift.

Figure 14.- Variation of longitudinal characteristics caused by difference in nose profile $\left(B_1W_{1f}V_T,\ B_2W_{1f}V_T\right)$ for $\delta_e = 0^{\circ}$.

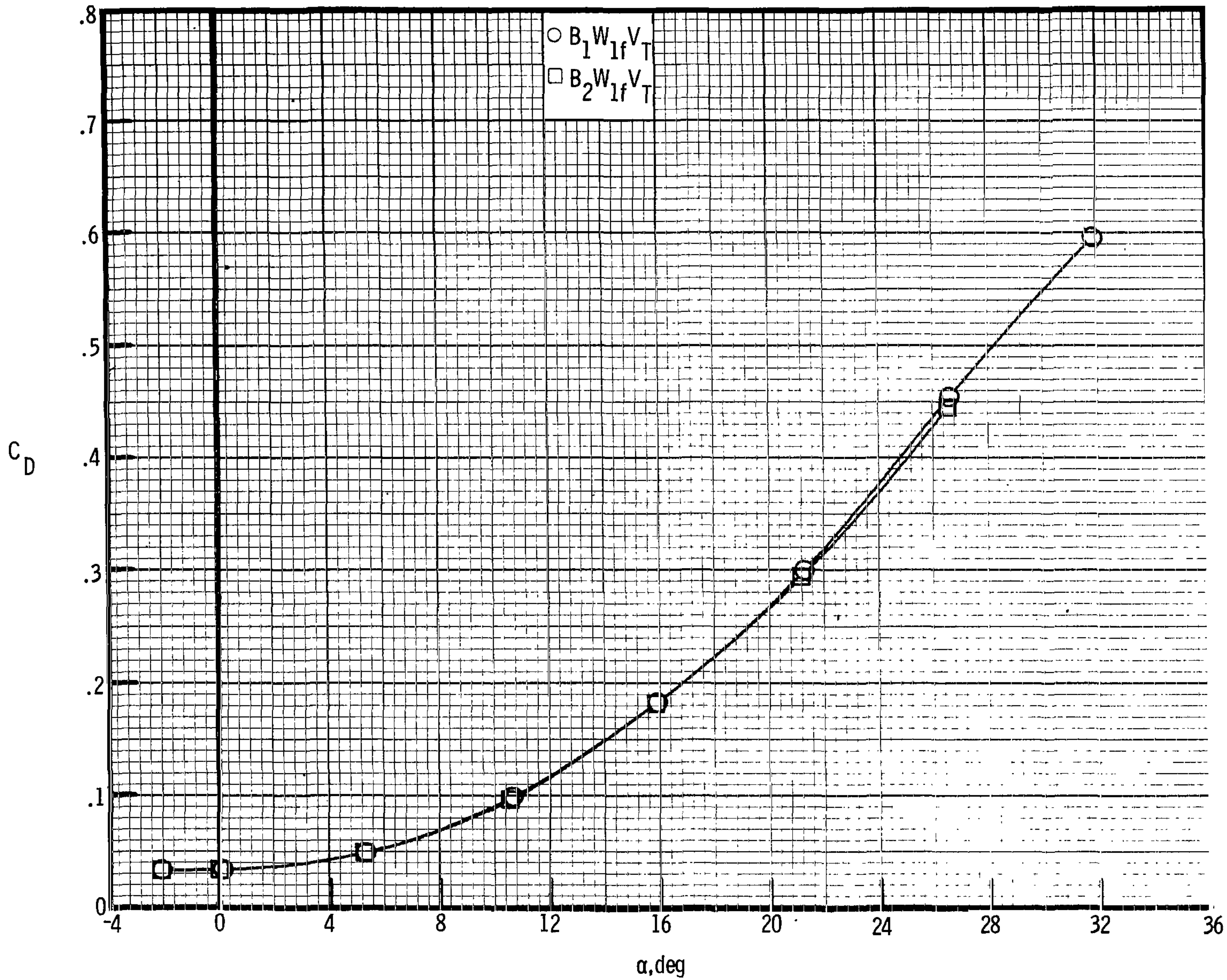

(b) Drag.

Figure 14.- Continued.

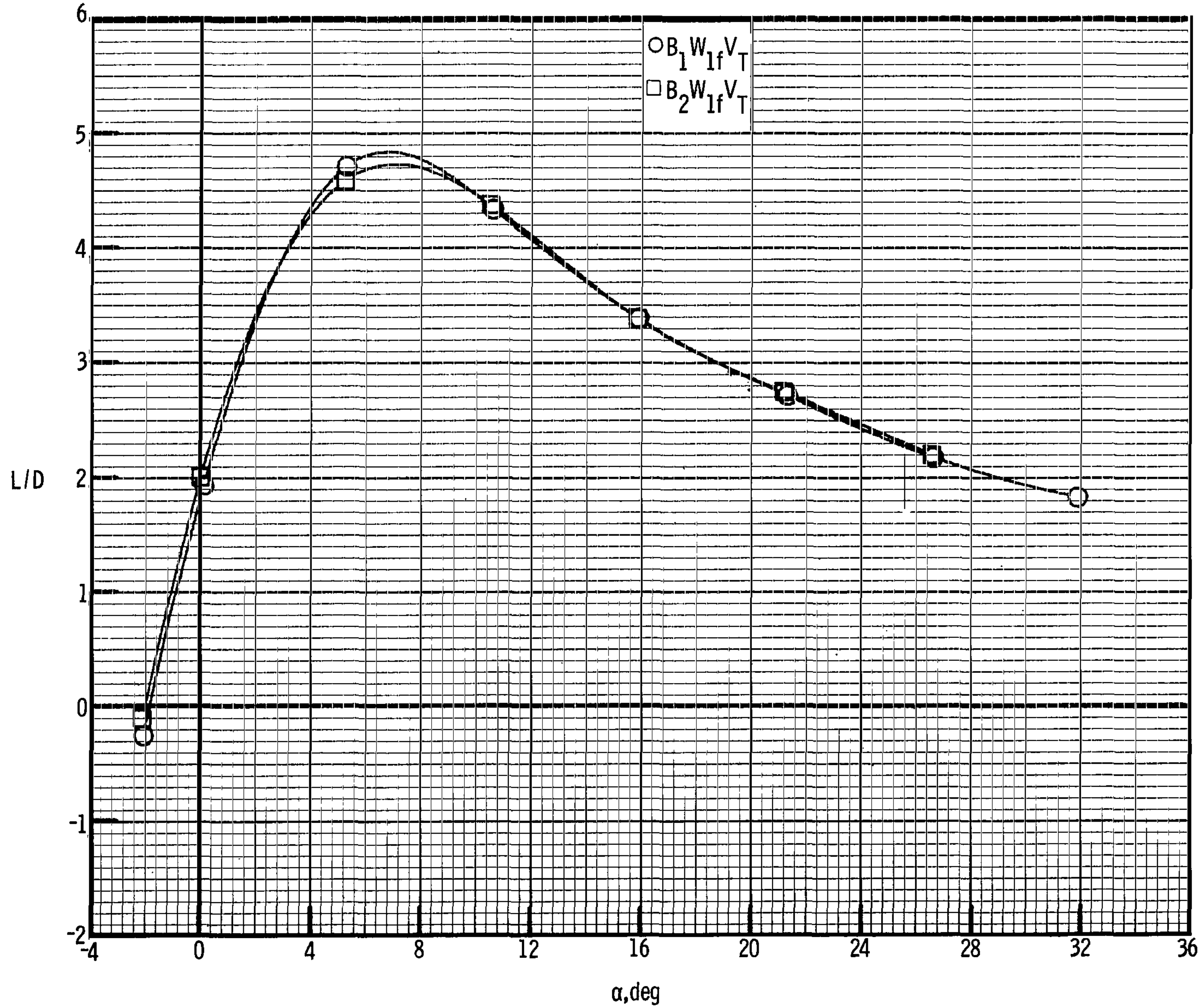

(c) Lift-drag ratio.

Figure 14.- Continued.

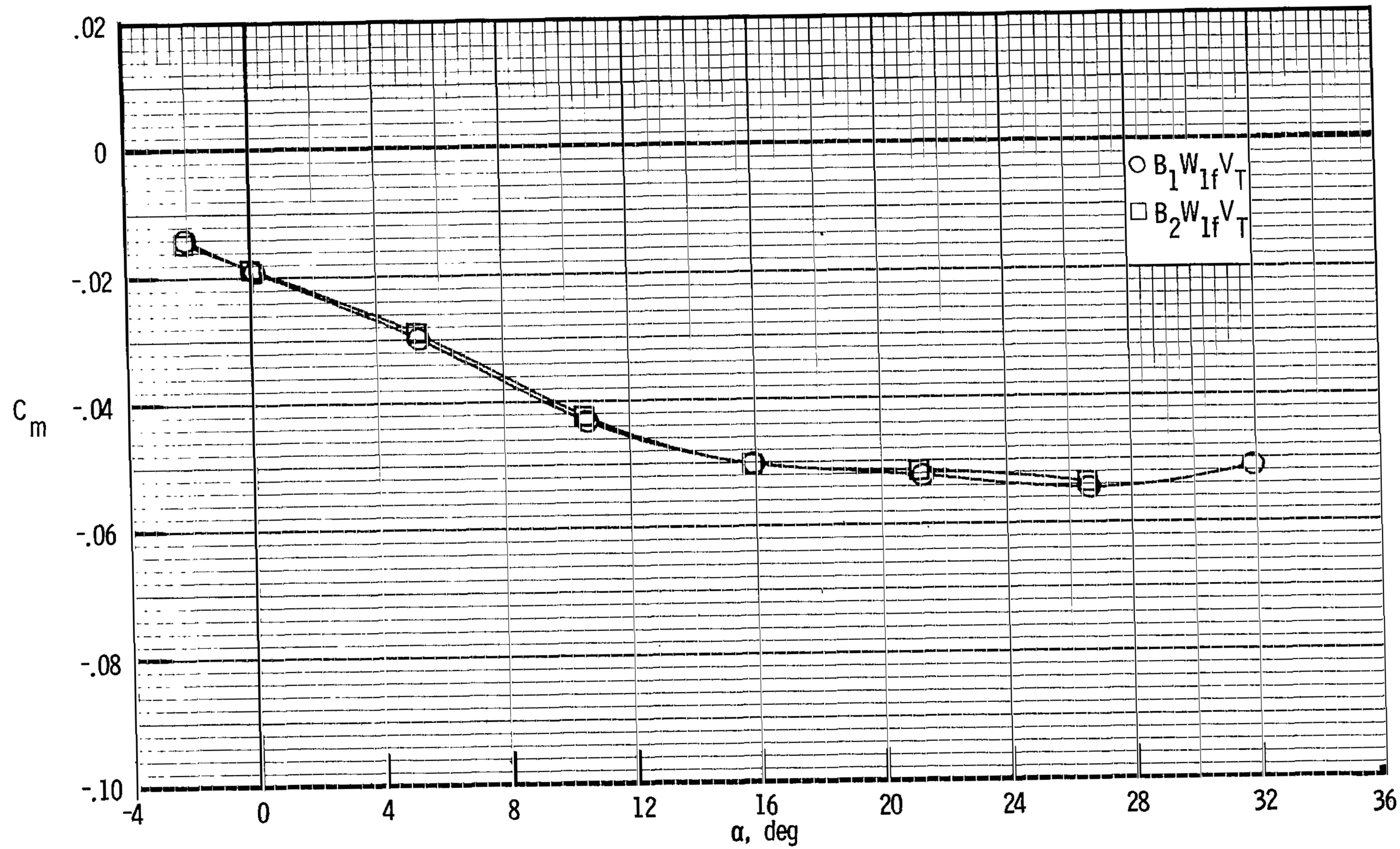

(d) Pitch.

Figure 14.- Continued.

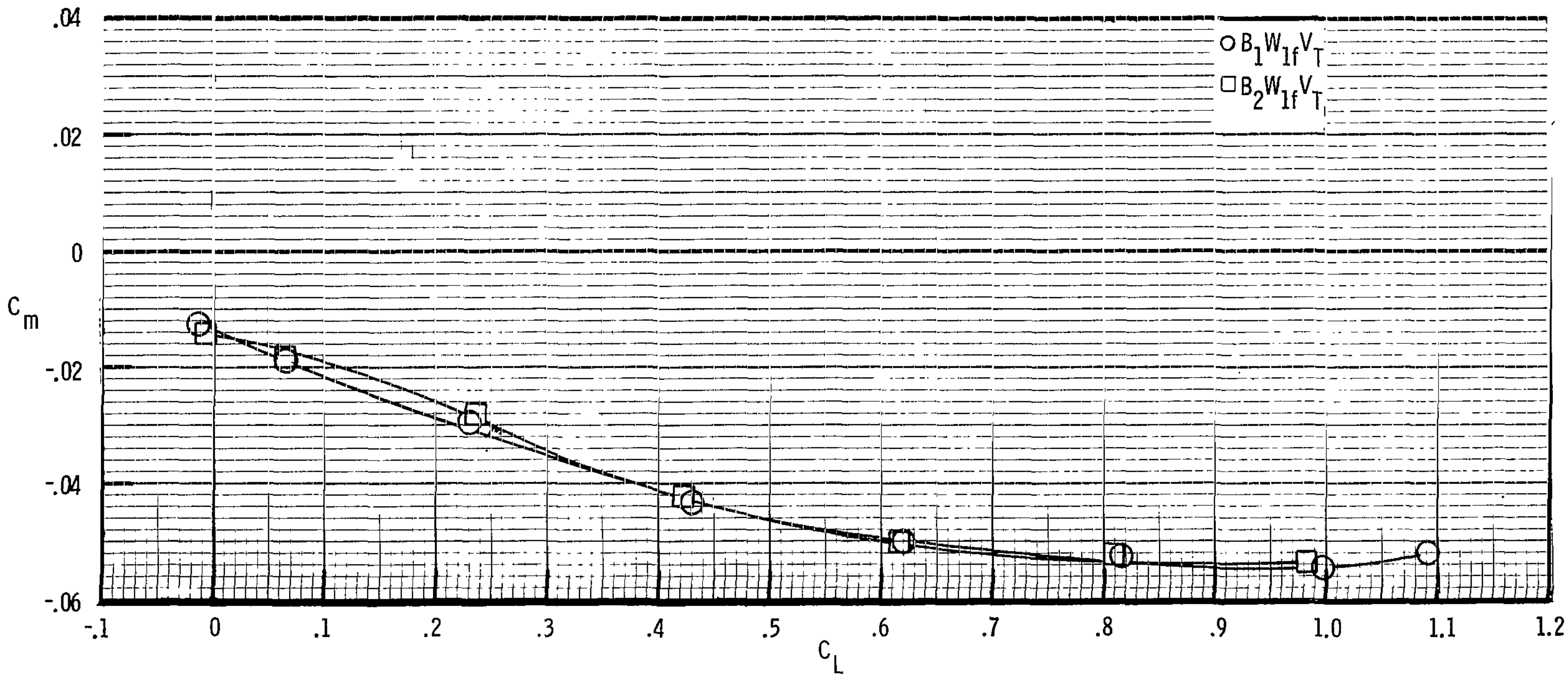

(e) Stability.

Figure 14.- Concluded.

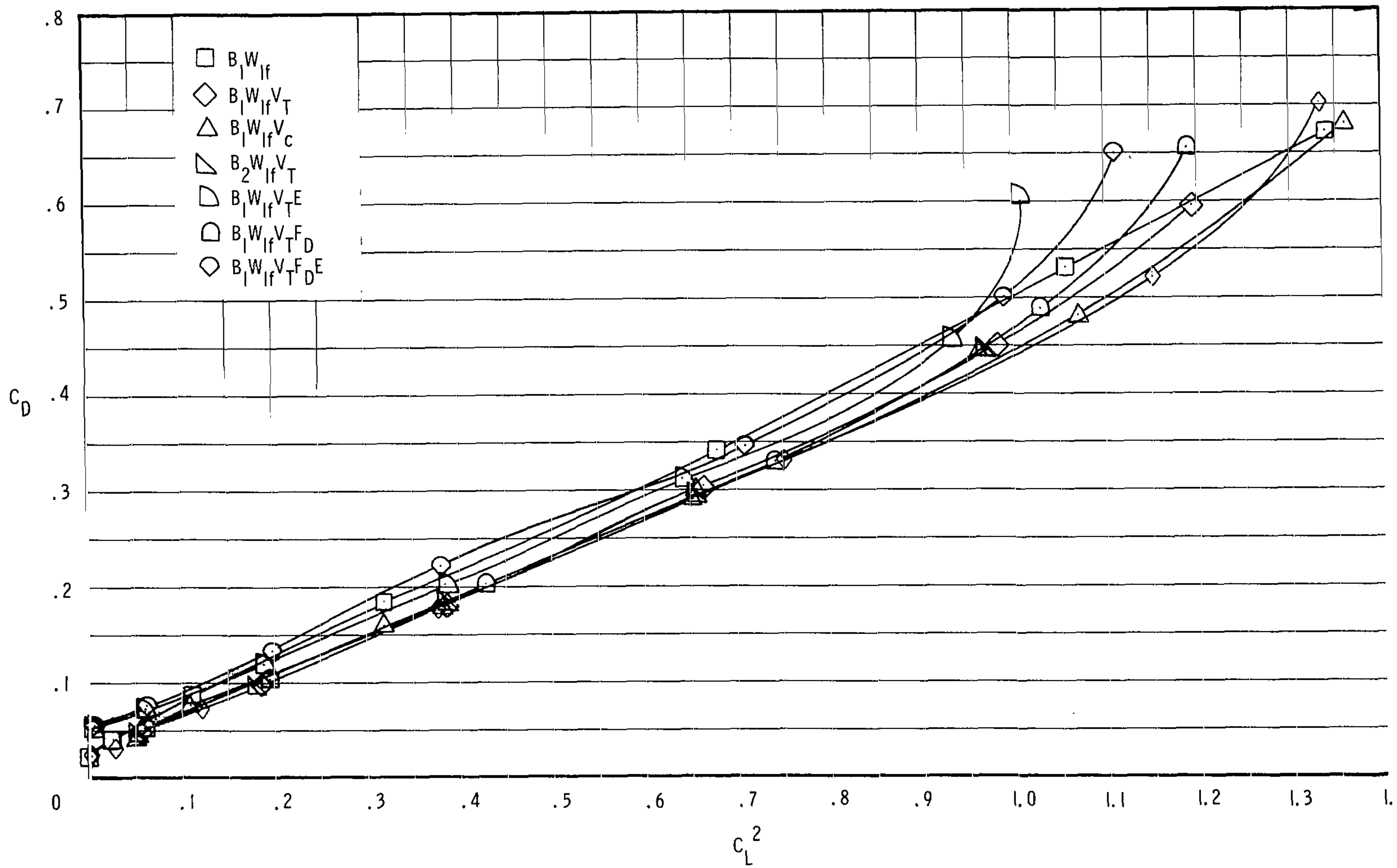

Figure 15.- Variation of drag due to lift of various winged configurations tested for $\delta_e = 0^\circ$.

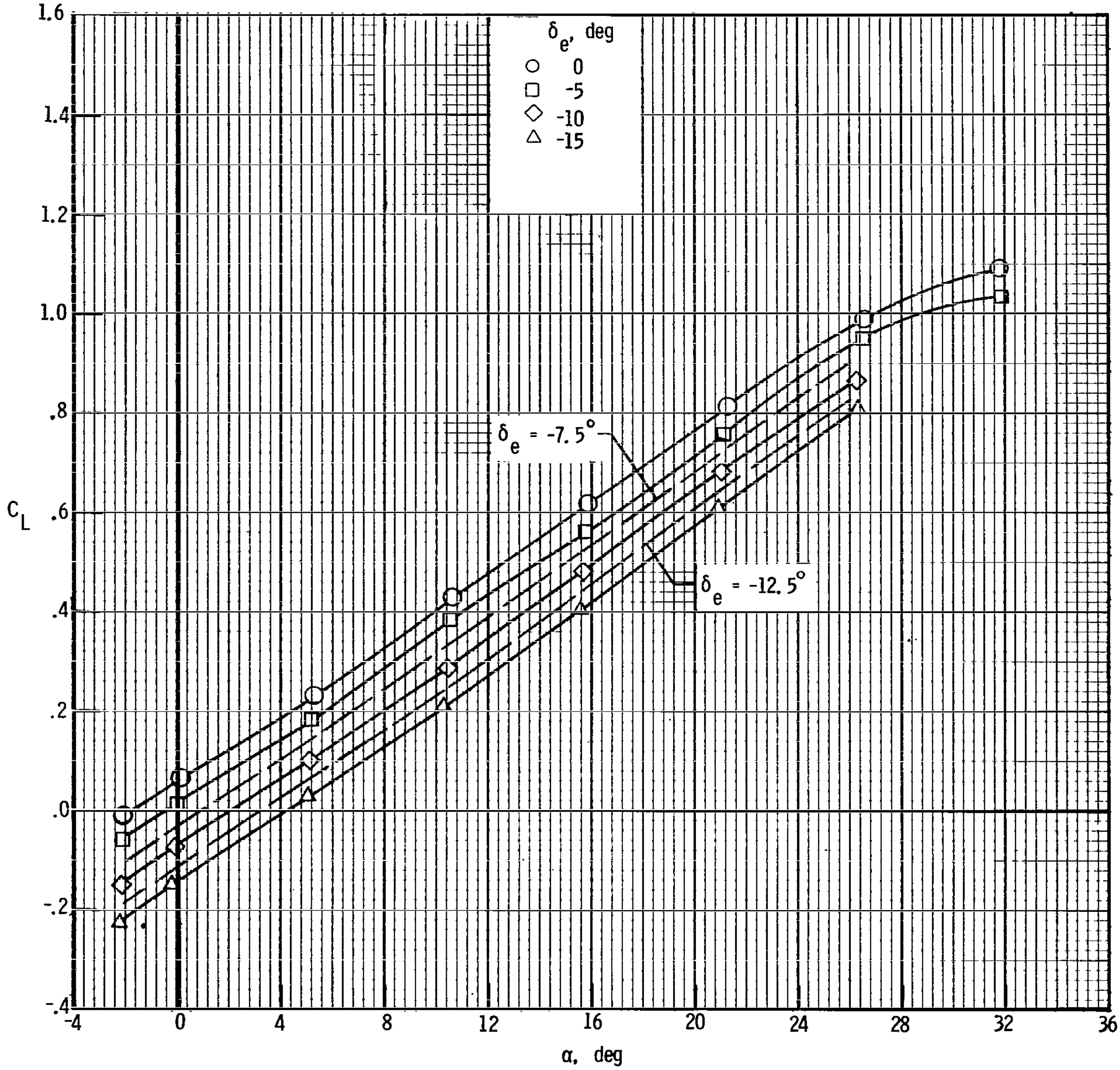

(a) Lift.

Figure 16.- Effect of elevon deflection on longitudinal characteristics of $B_1W_{1f}V_T$.

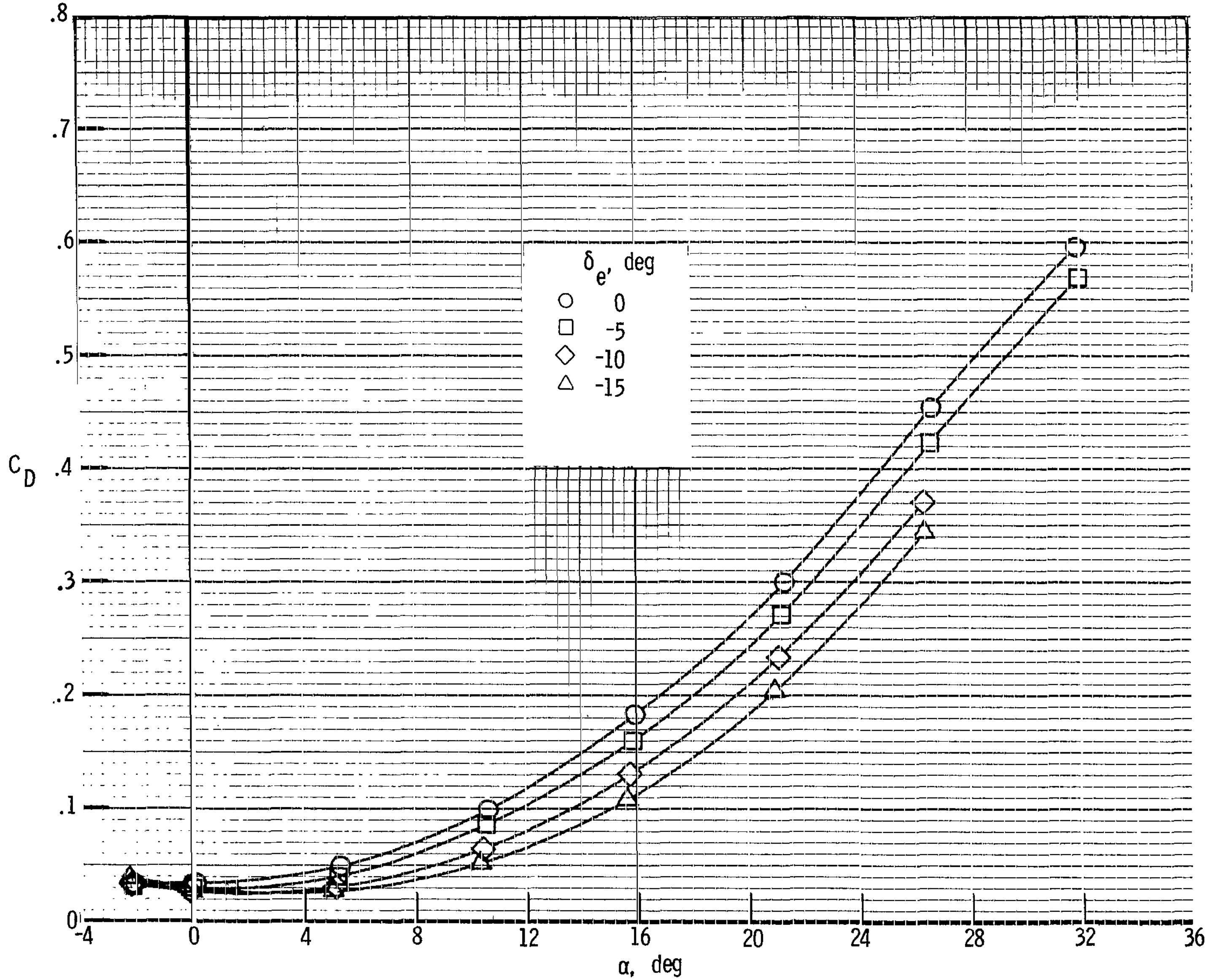

(b) Drag.

Figure 16.- Continued.

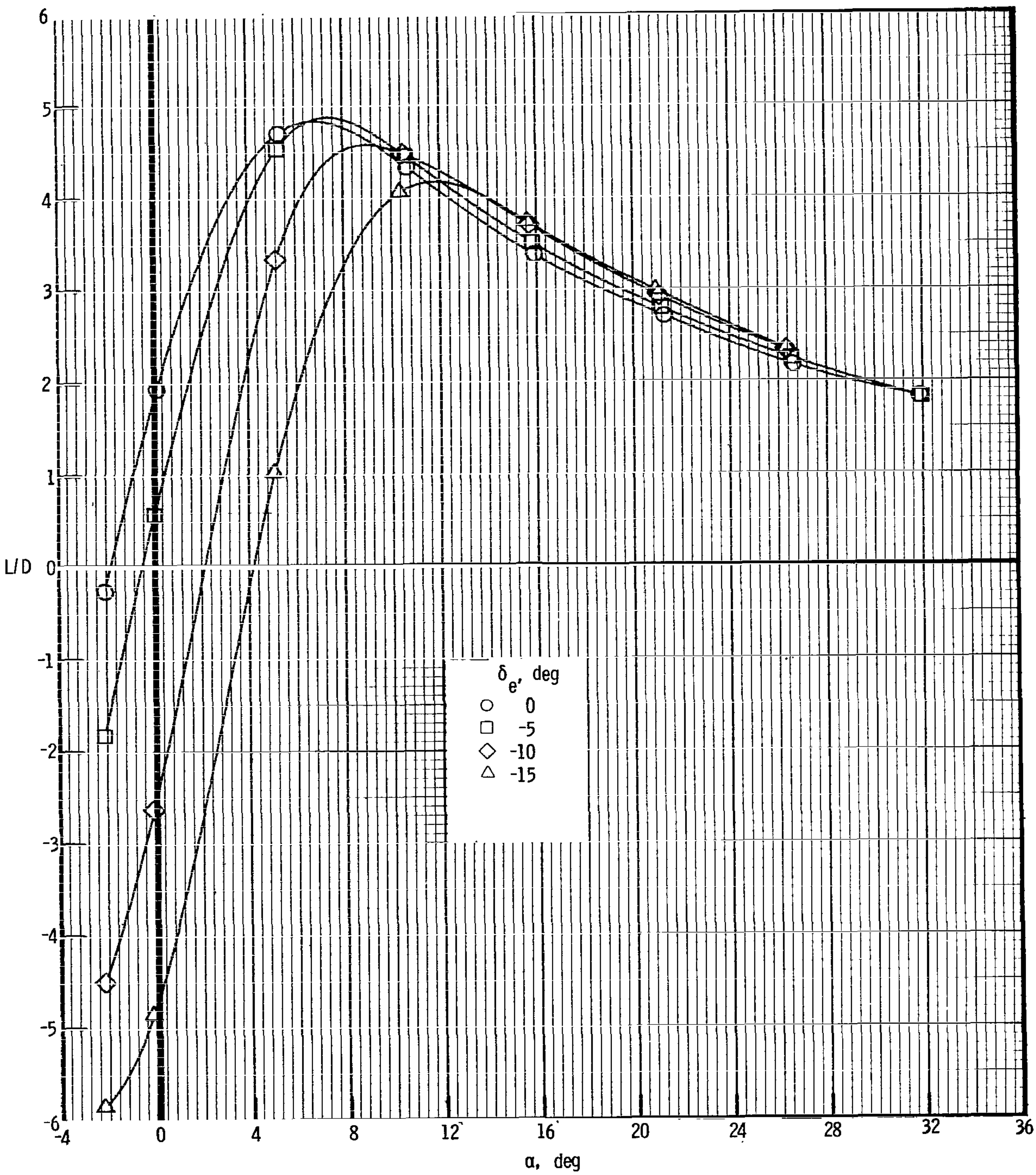

(c) Lift-drag ratio.

Figure 16.- Continued.

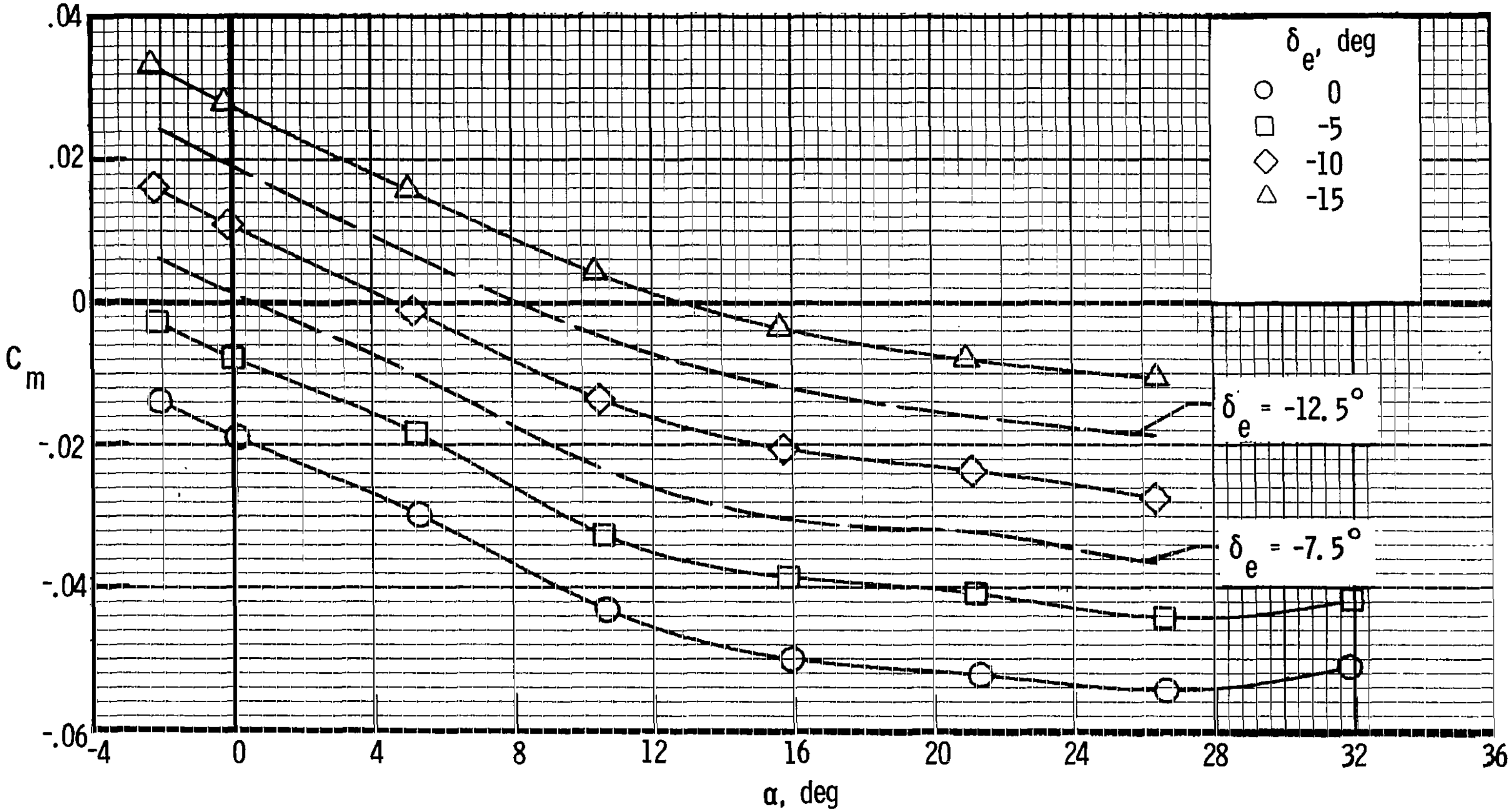

(d) Pitch.

Figure 16.- Continued.

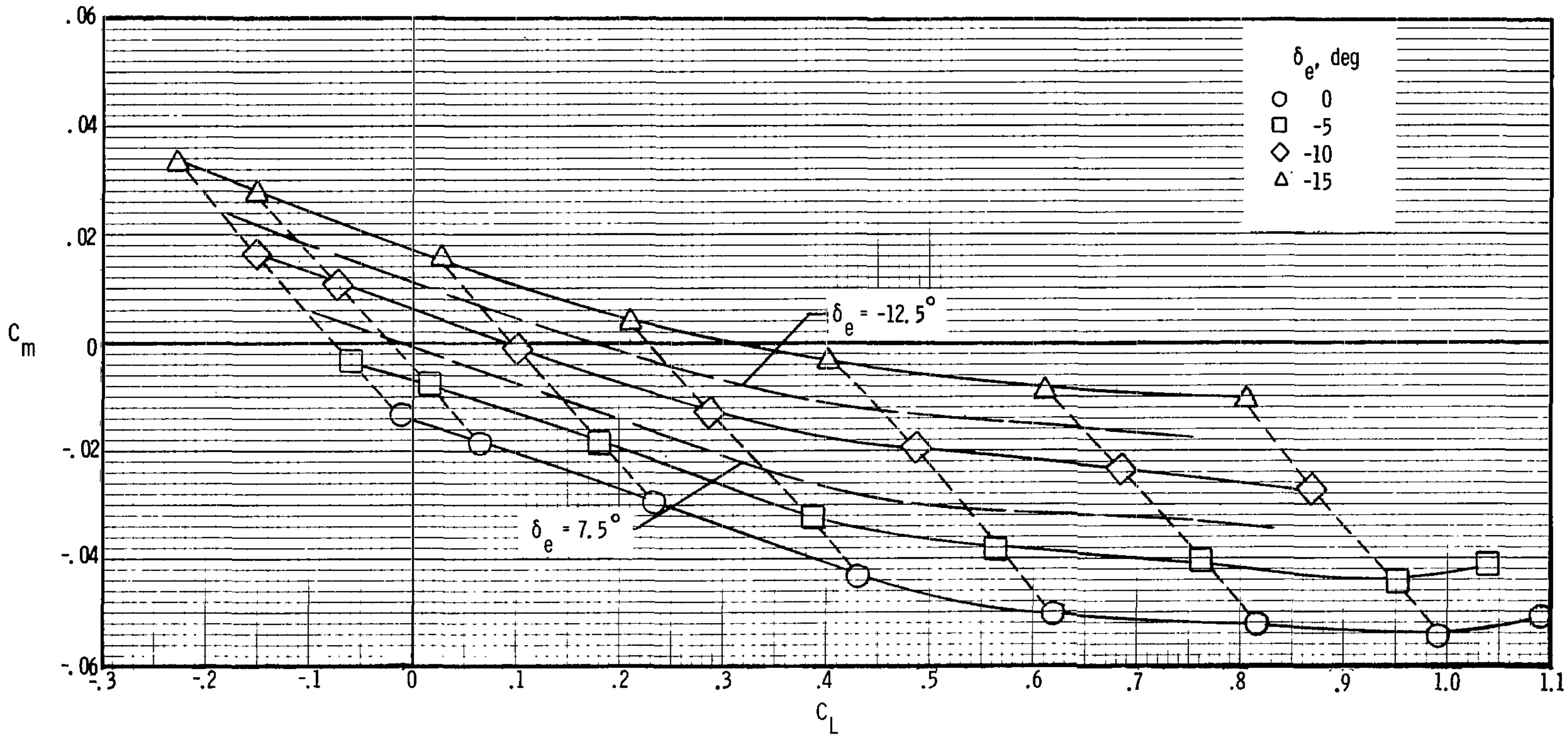

(e) Stability.

Figure 16.- Concluded.

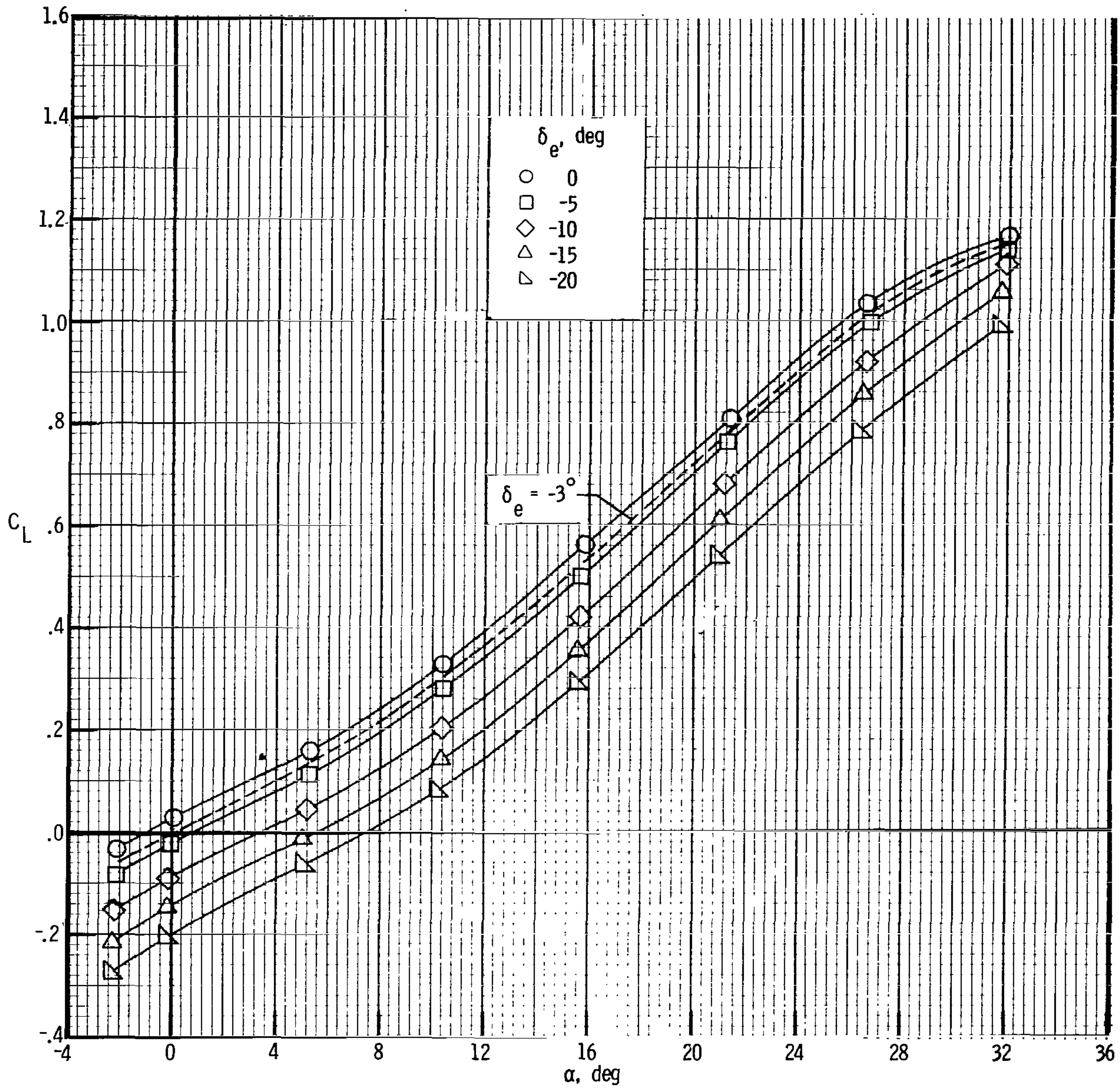

(a) Lift.

Figure 17.- Effect of elevon deflection on longitudinal characteristics of $B_1W_{1f}V_C$.

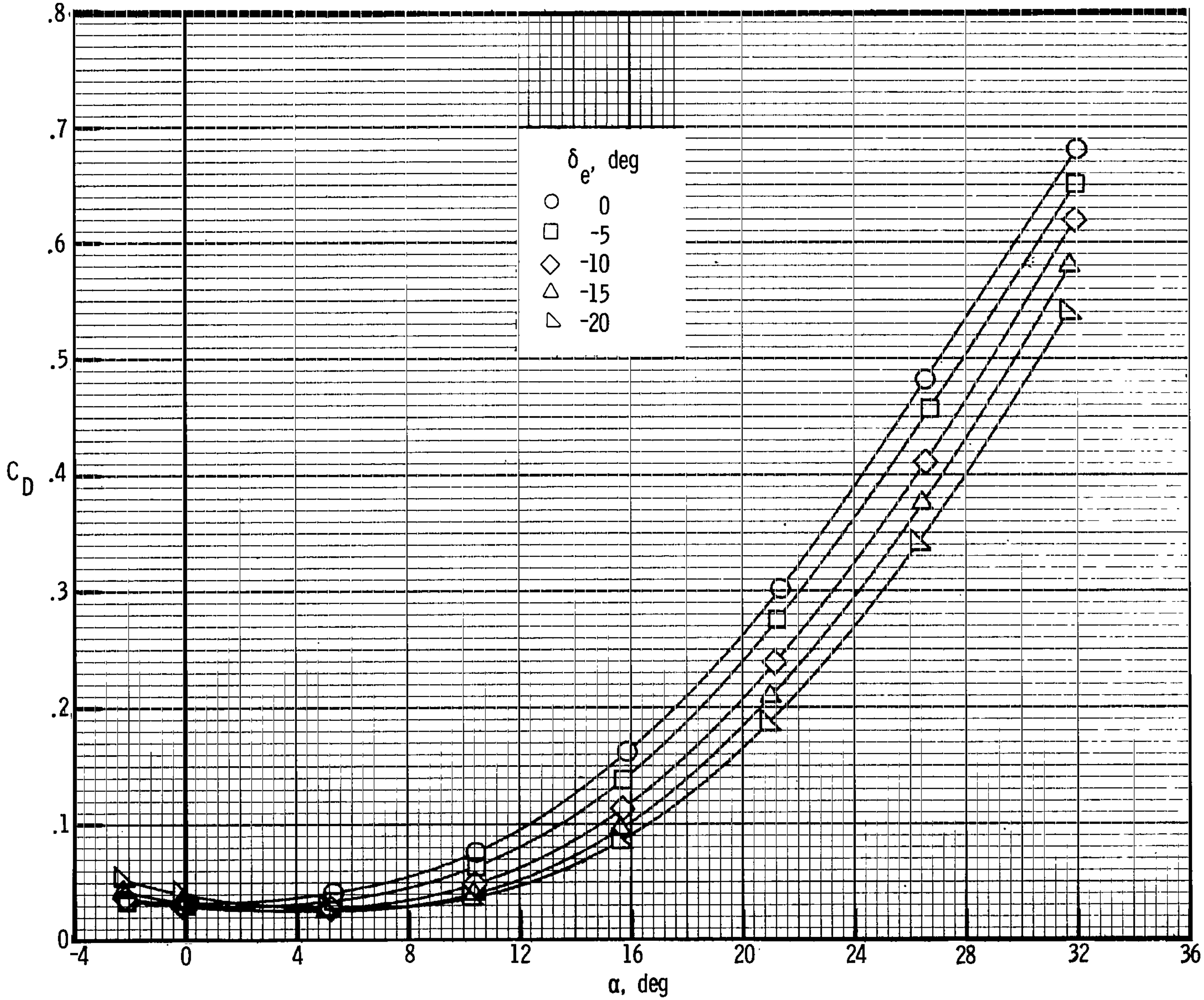

(b) Drag.

Figure 17.- Continued.

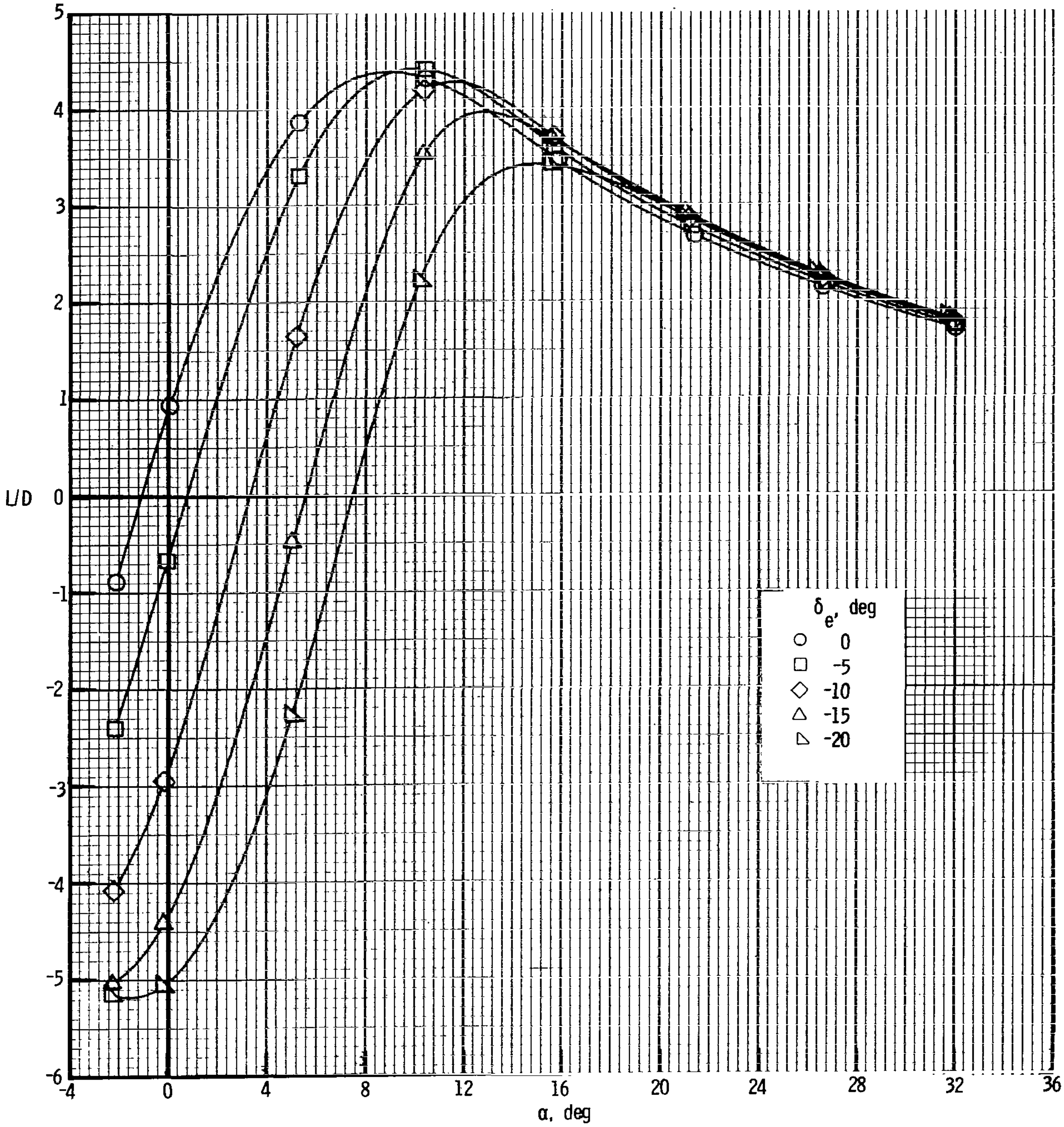

(c) Lift-drag ratio.

Figure 17.- Continued.

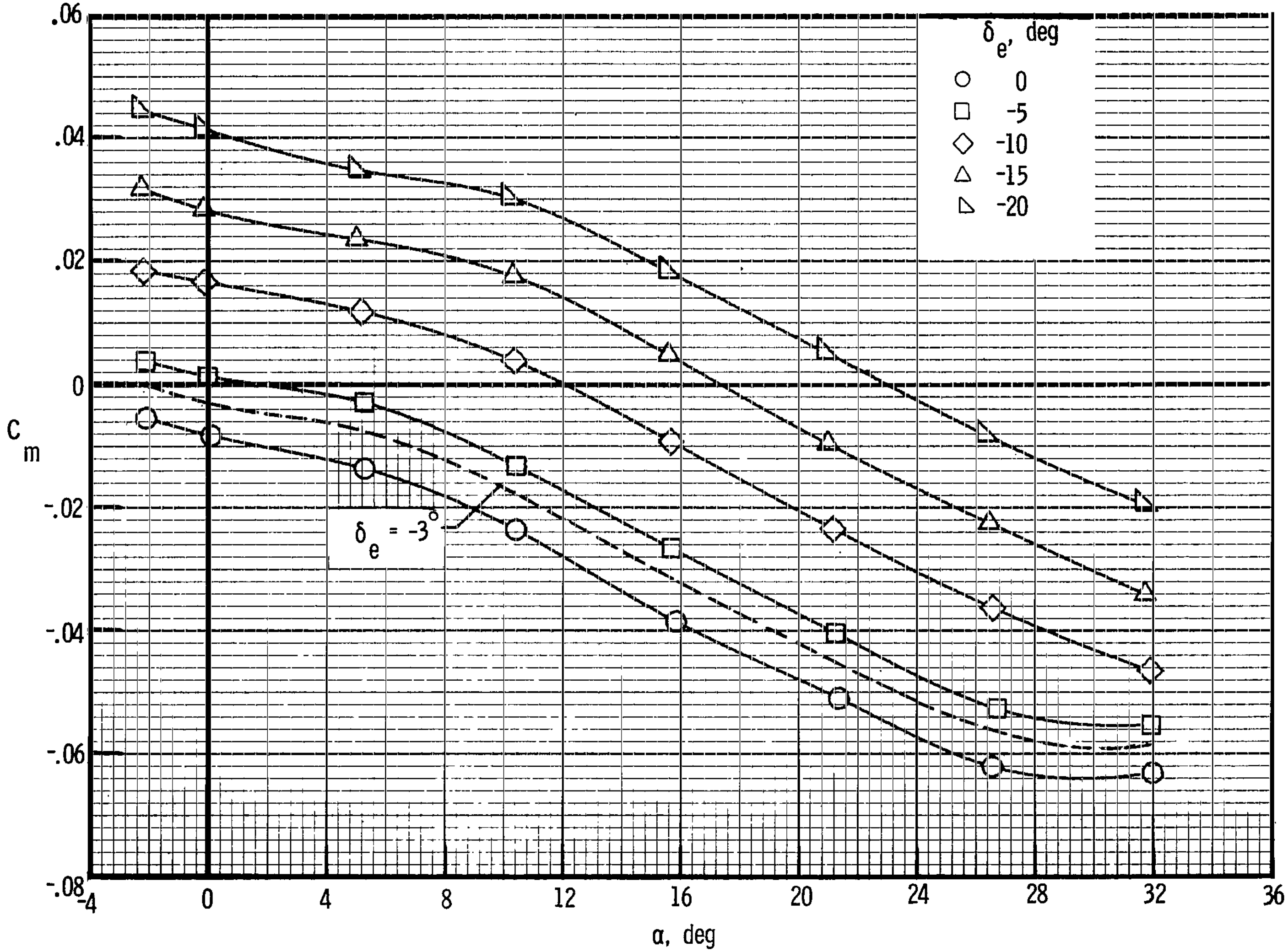

(d) Pitch.

Figure 17.- Continued.

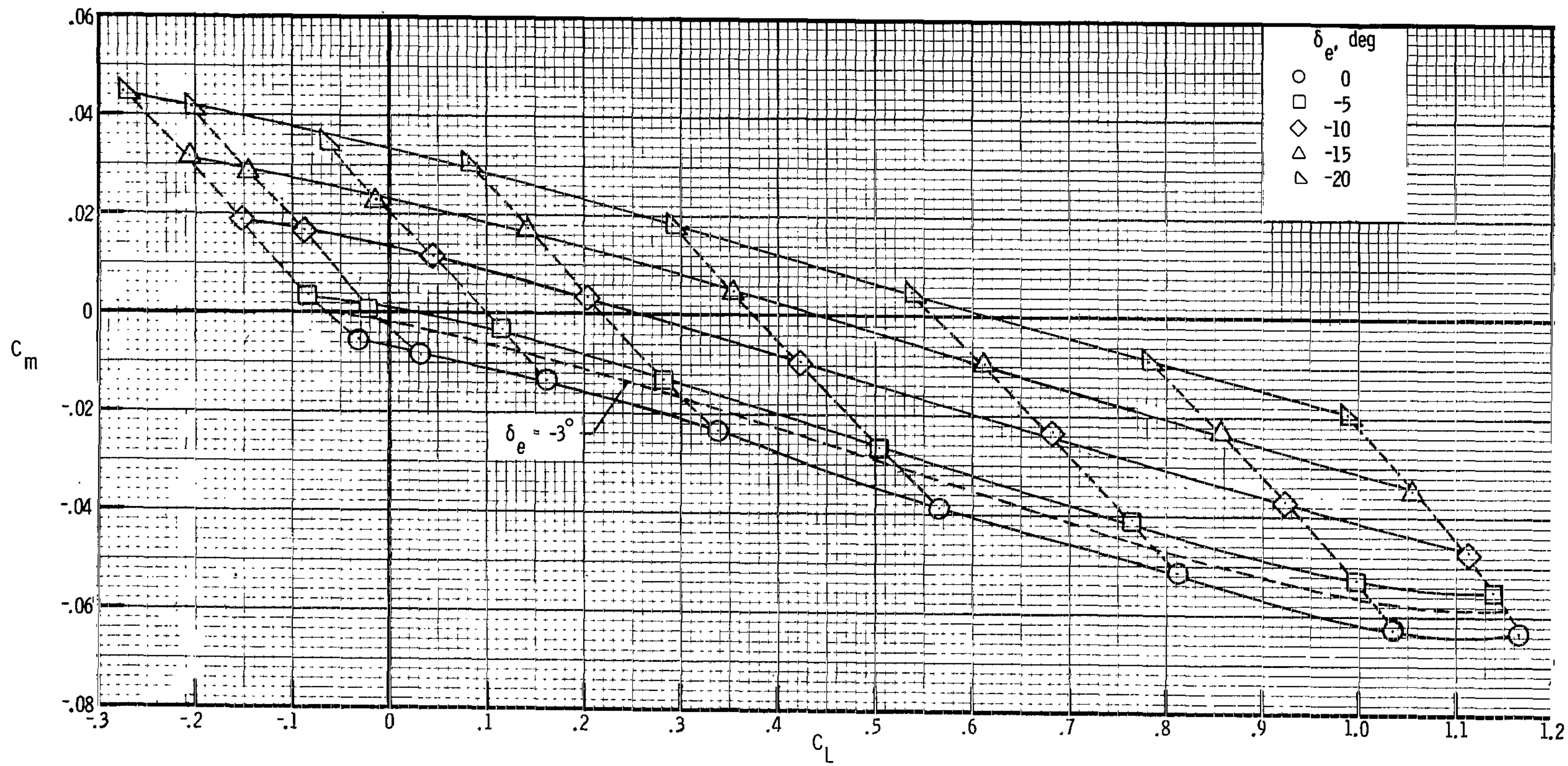

(e) Stability.

Figure 17.- Concluded.

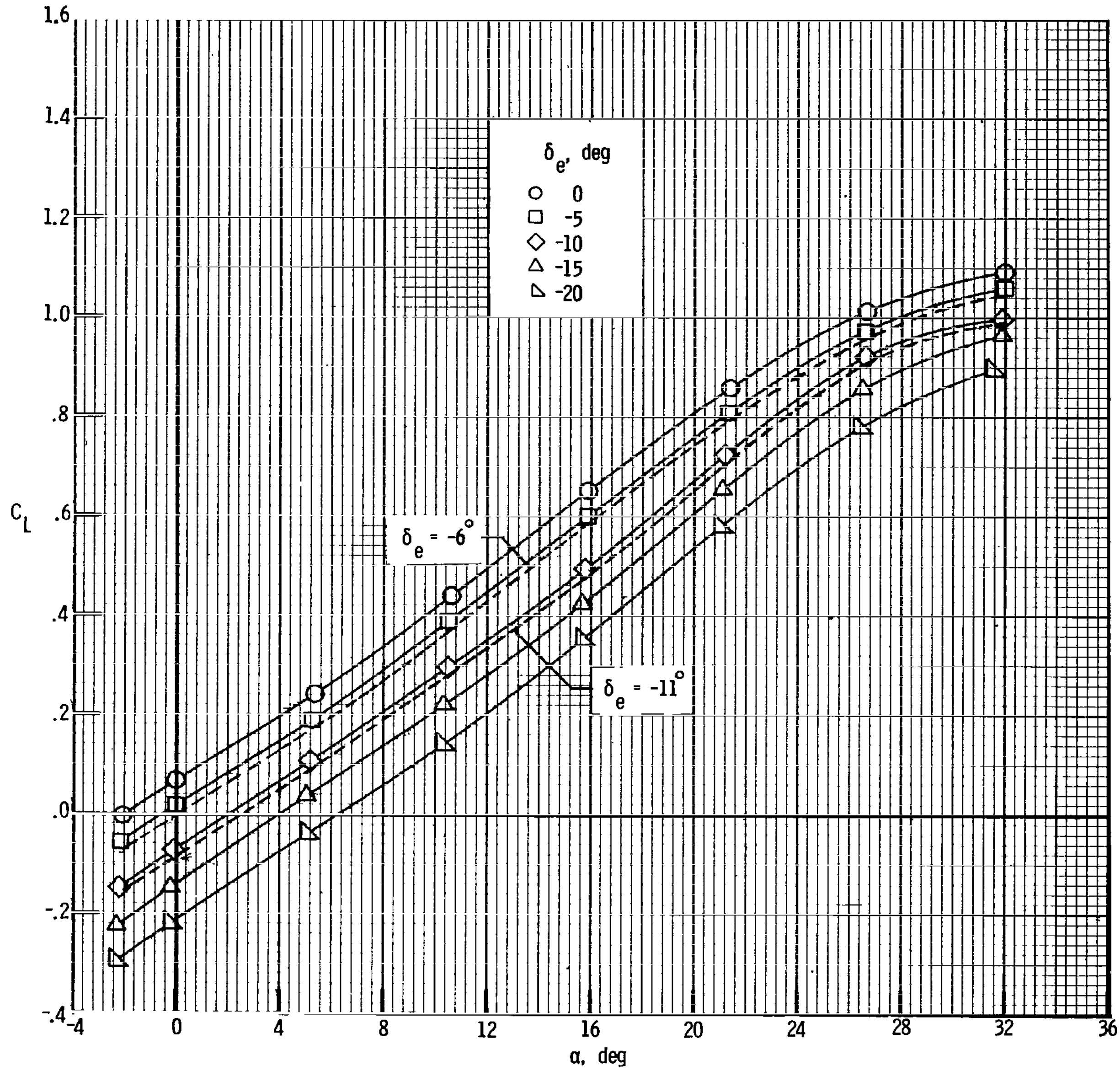

(a) Lift.

Figure 18.- Effect of elevon deflection on longitudinal characteristics of $B_1W_{1f}V_TF_D$.

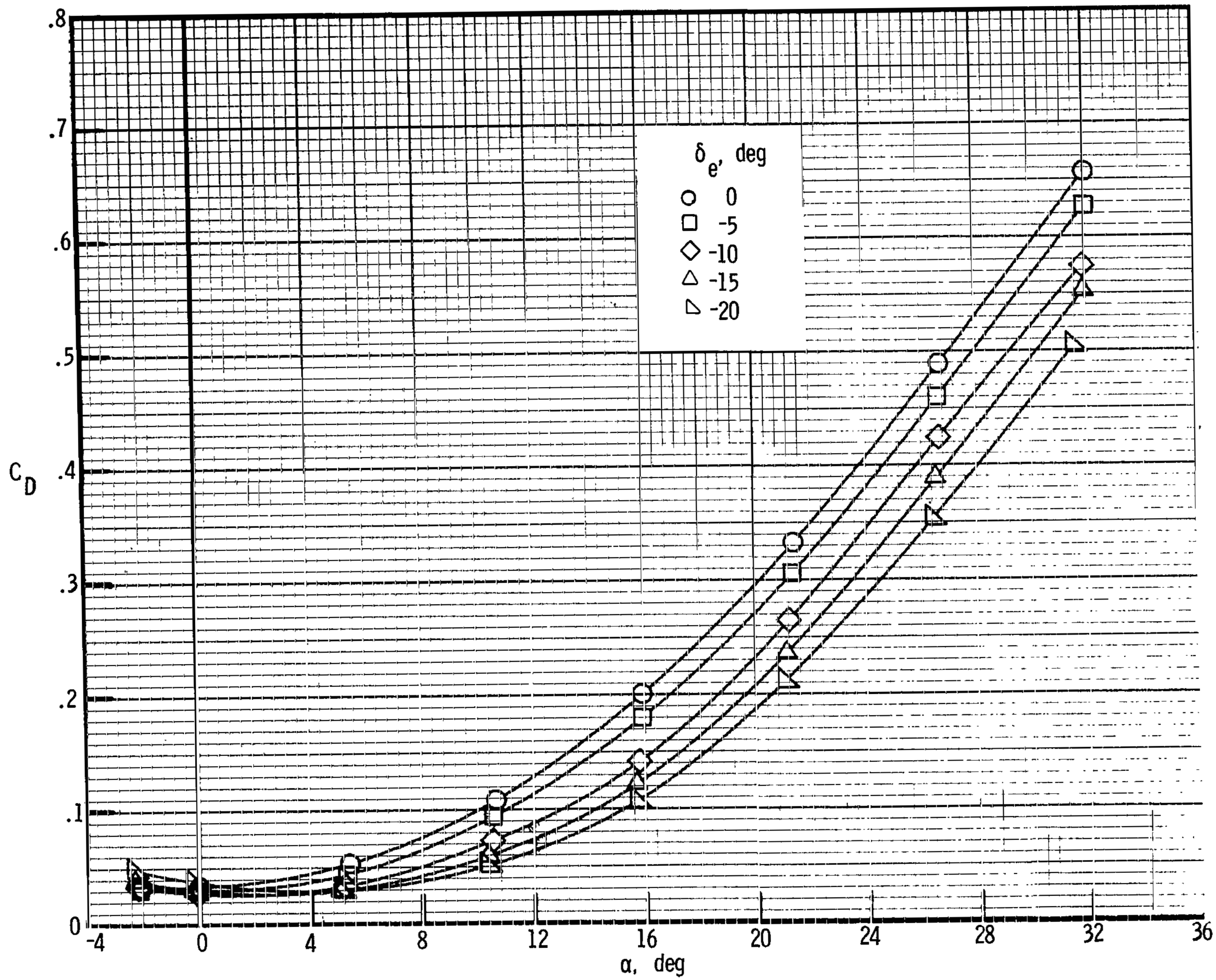

(b) Drag.

Figure 18.- Continued.

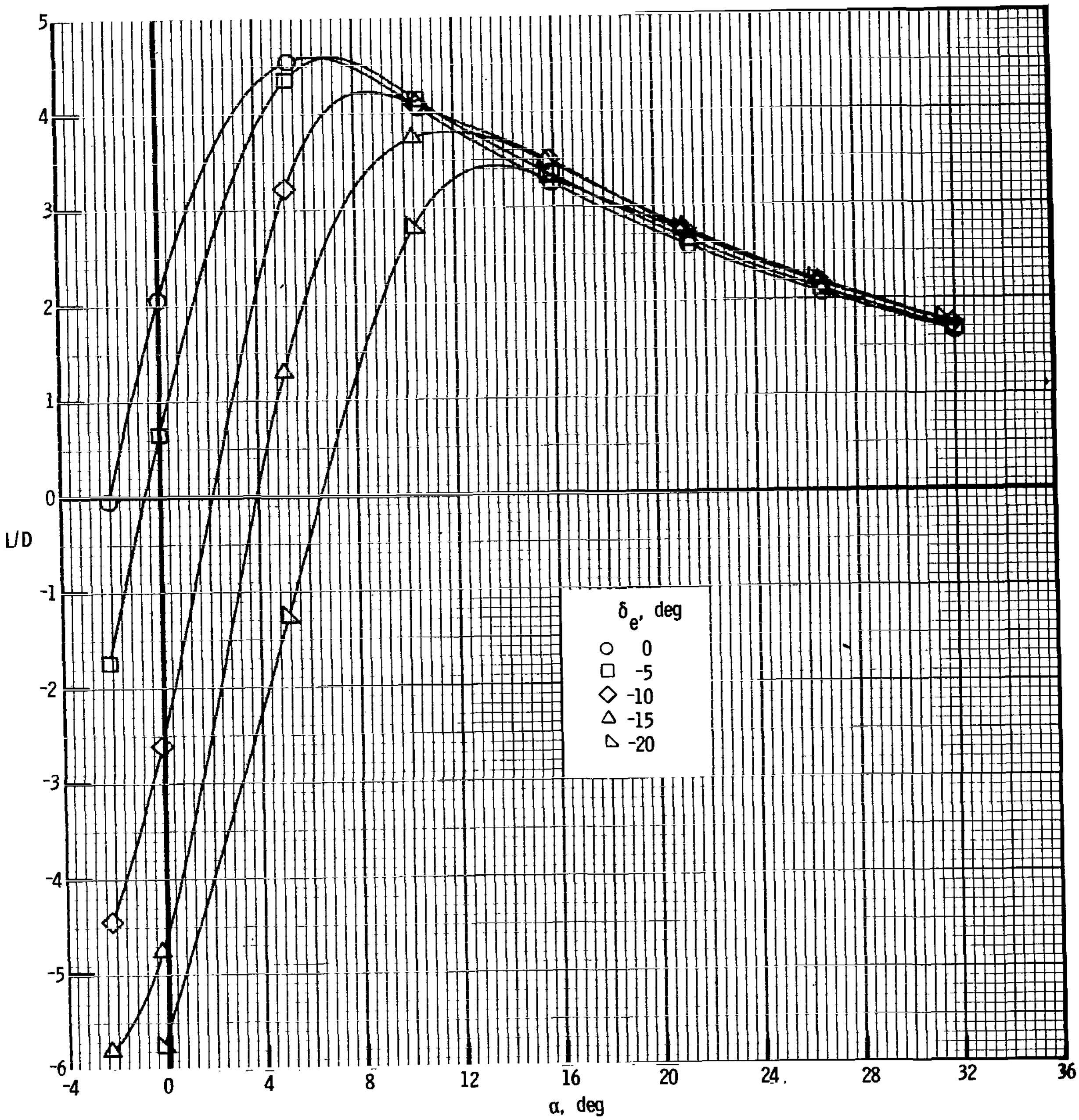

(c) Lift-drag ratio.

Figure 18.- Continued.

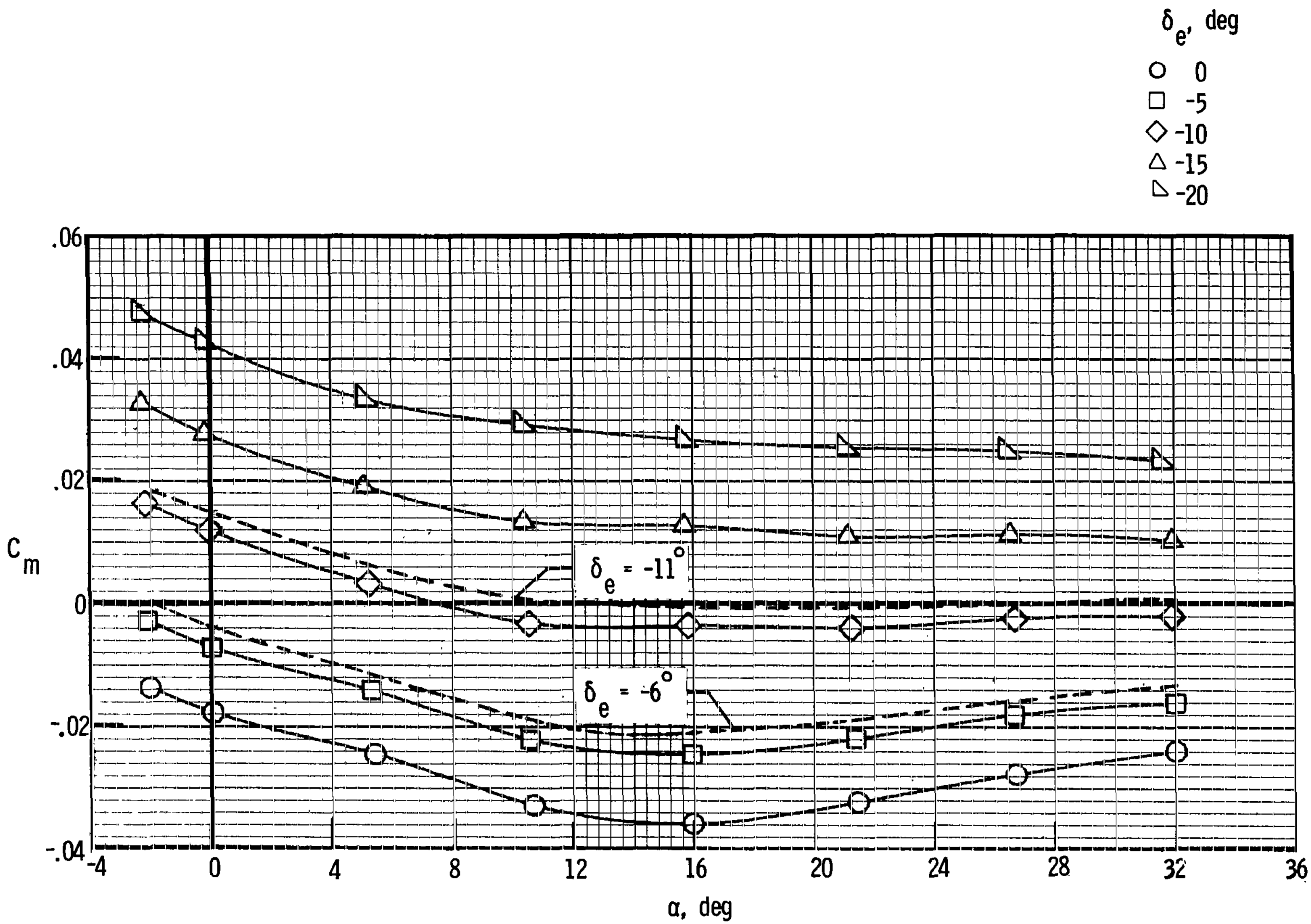

(d) Pitch.

Figure 18.- Continued.

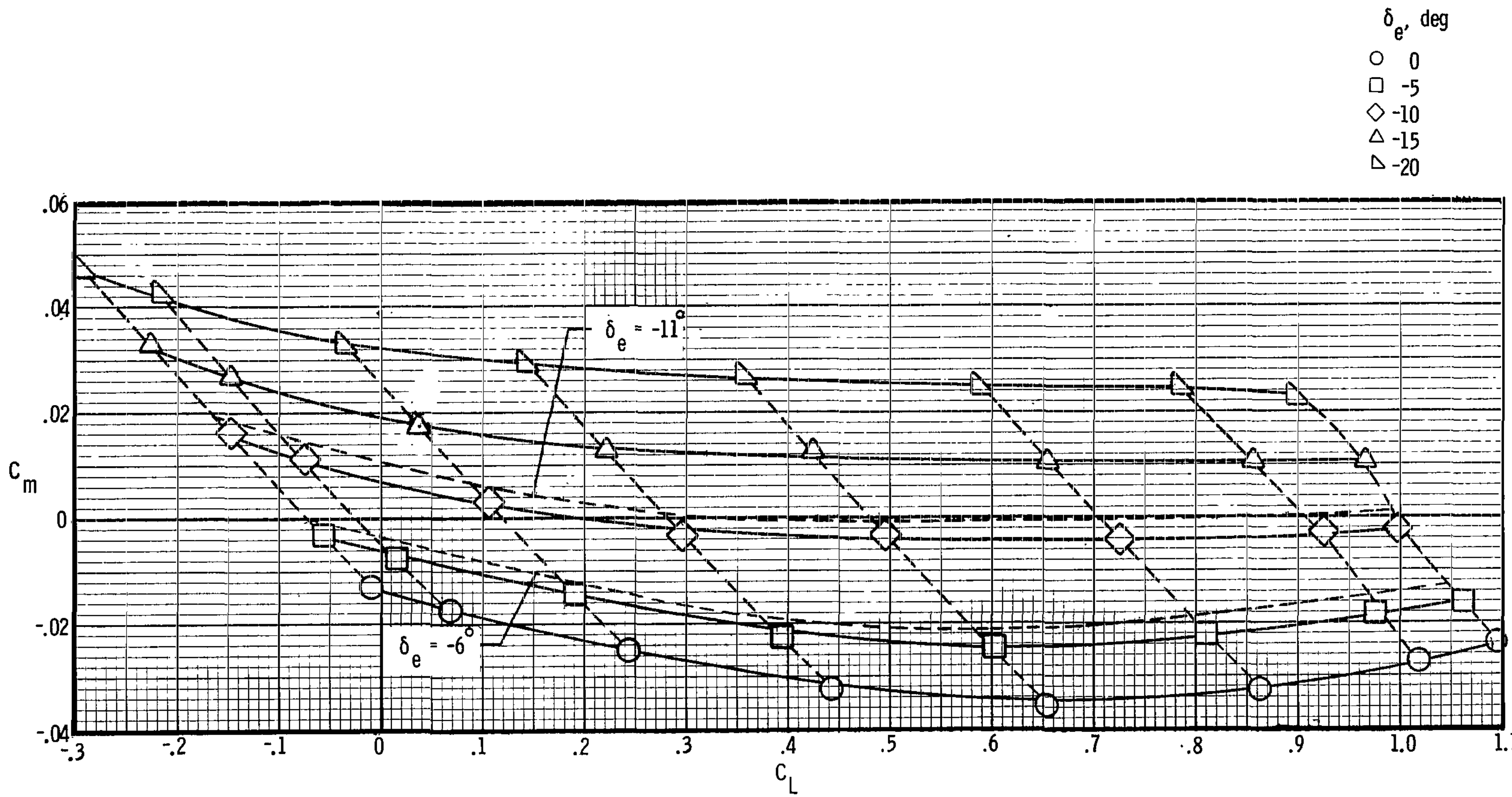

(e) Stability.

Figure 18.- Concluded.

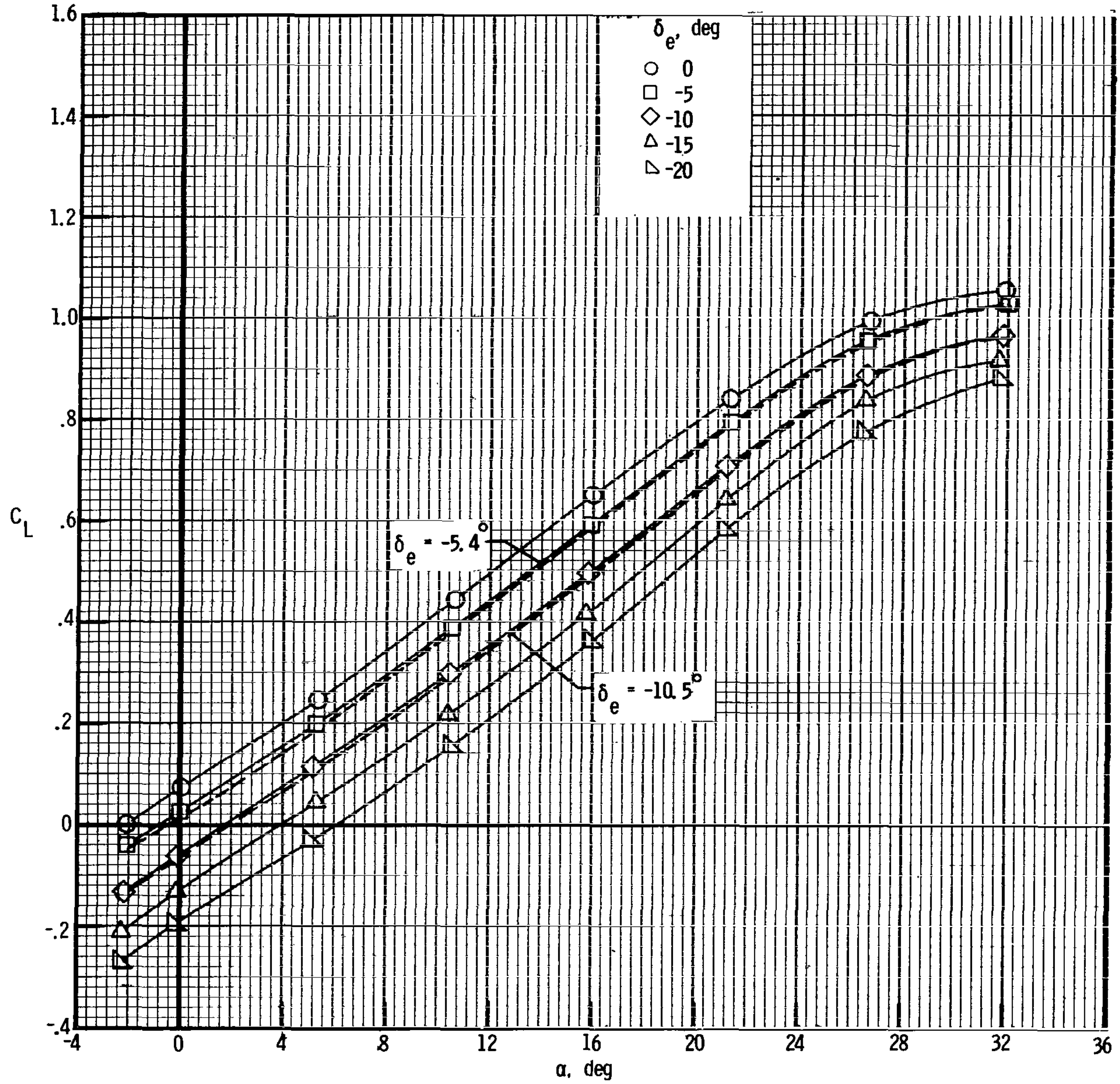

(a) Lift.

Figure 19.- Effect of elevon deflection on longitudinal characteristics of $B_1W_{1f}V_TF_DE$.

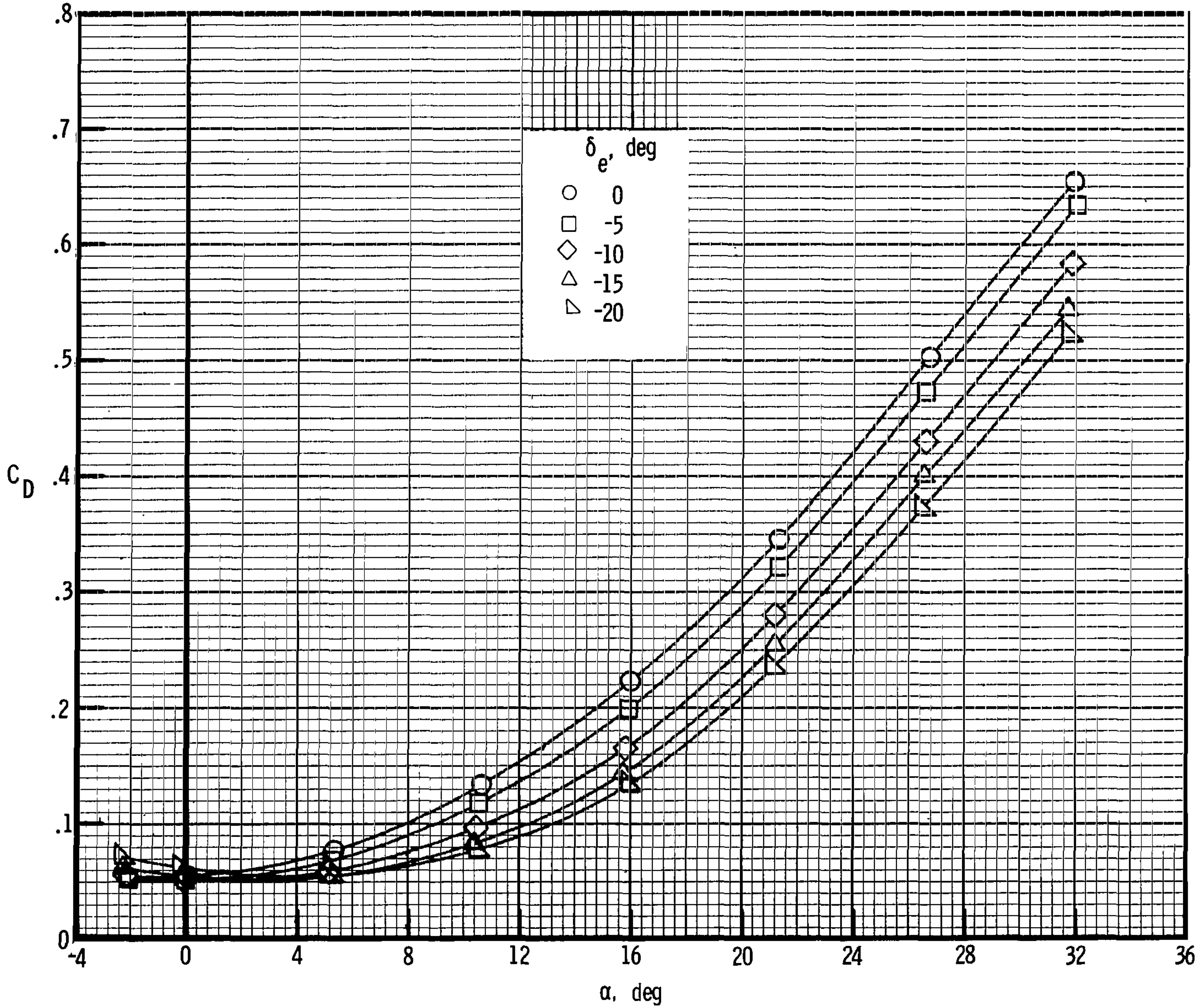

(b) Drag.

Figure 19.- Continued.

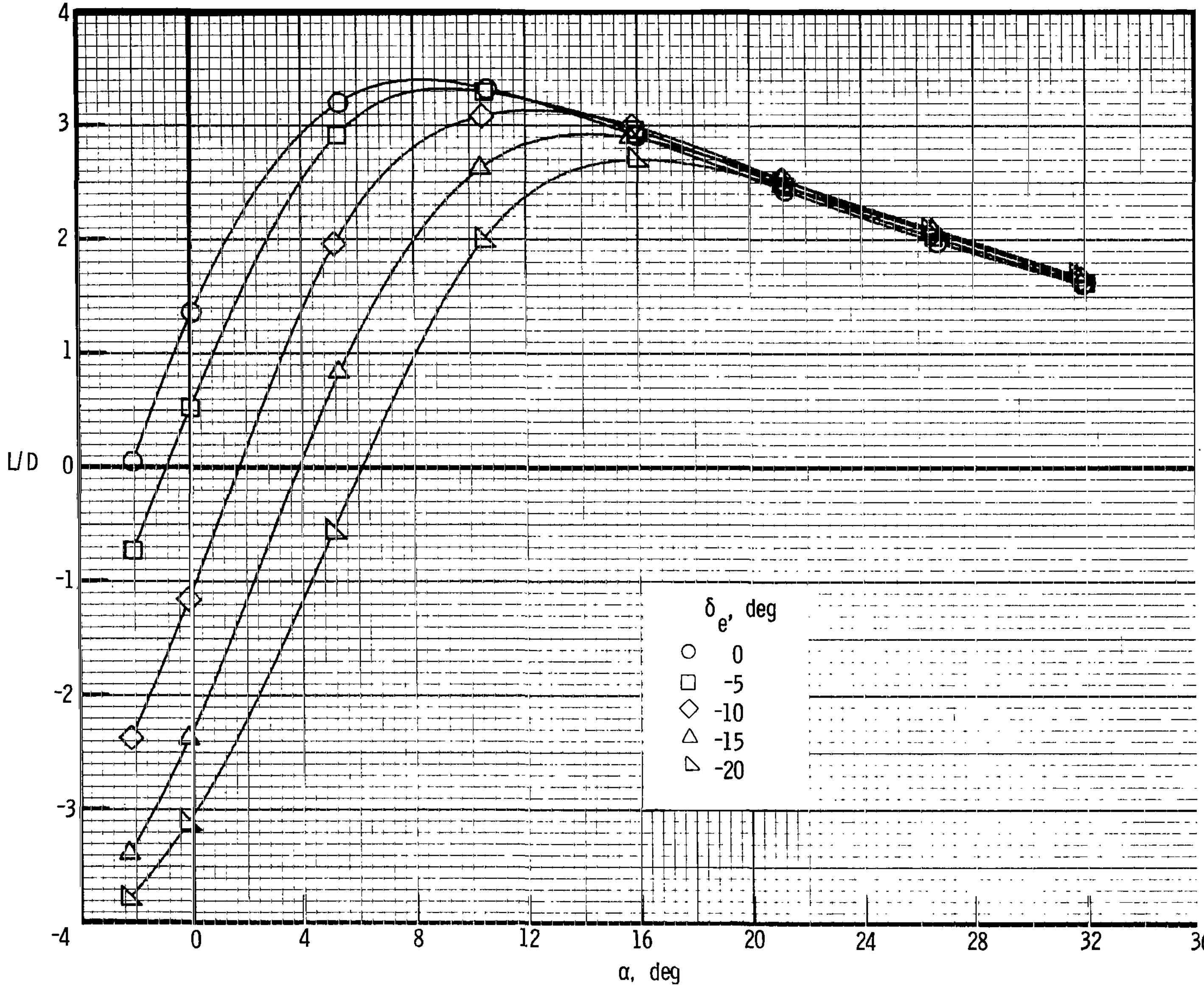

(c) Lift-drag ratio.

Figure 19.- Continued.

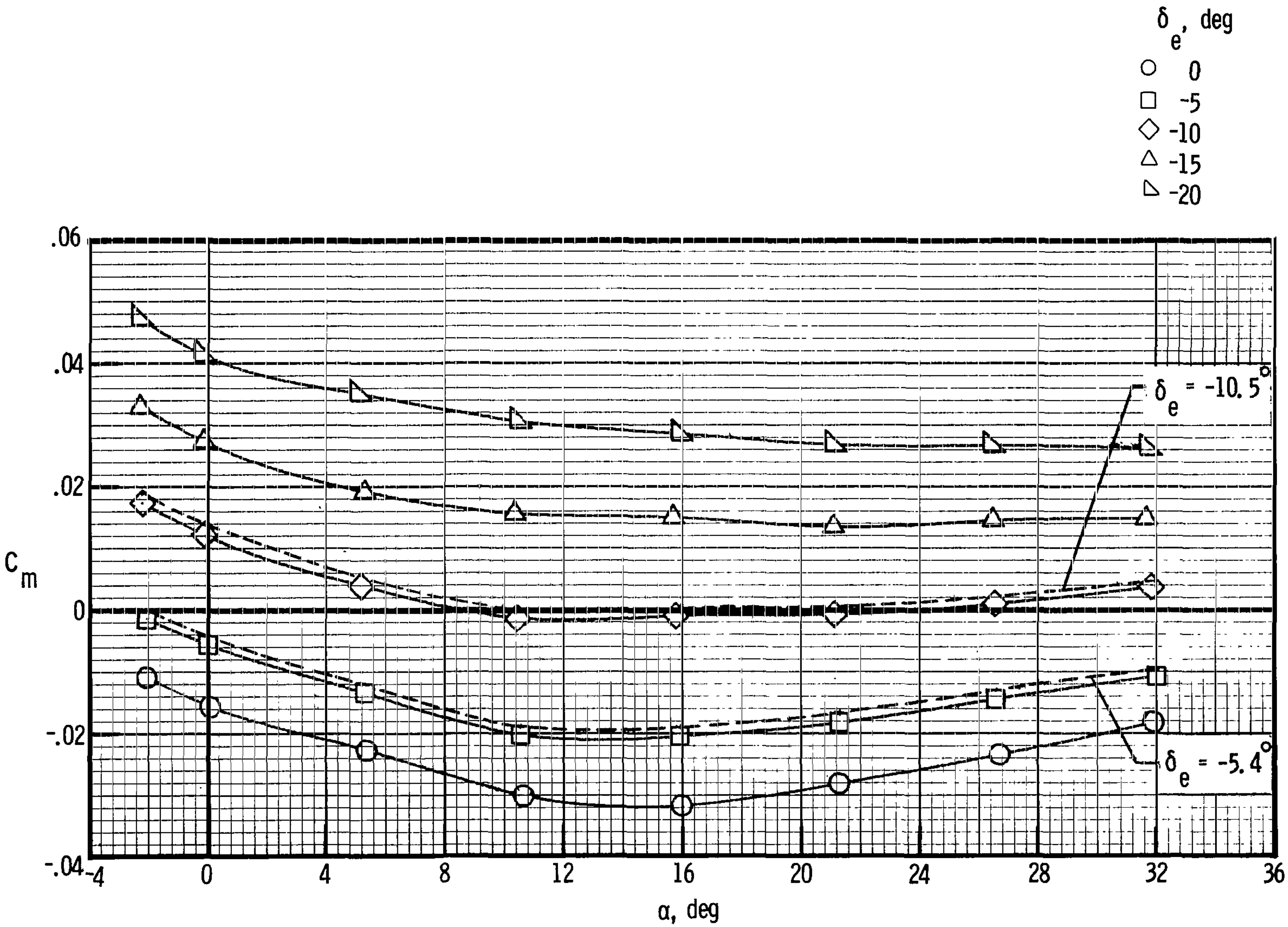

(d) Pitch.

Figure 19.- Continued.

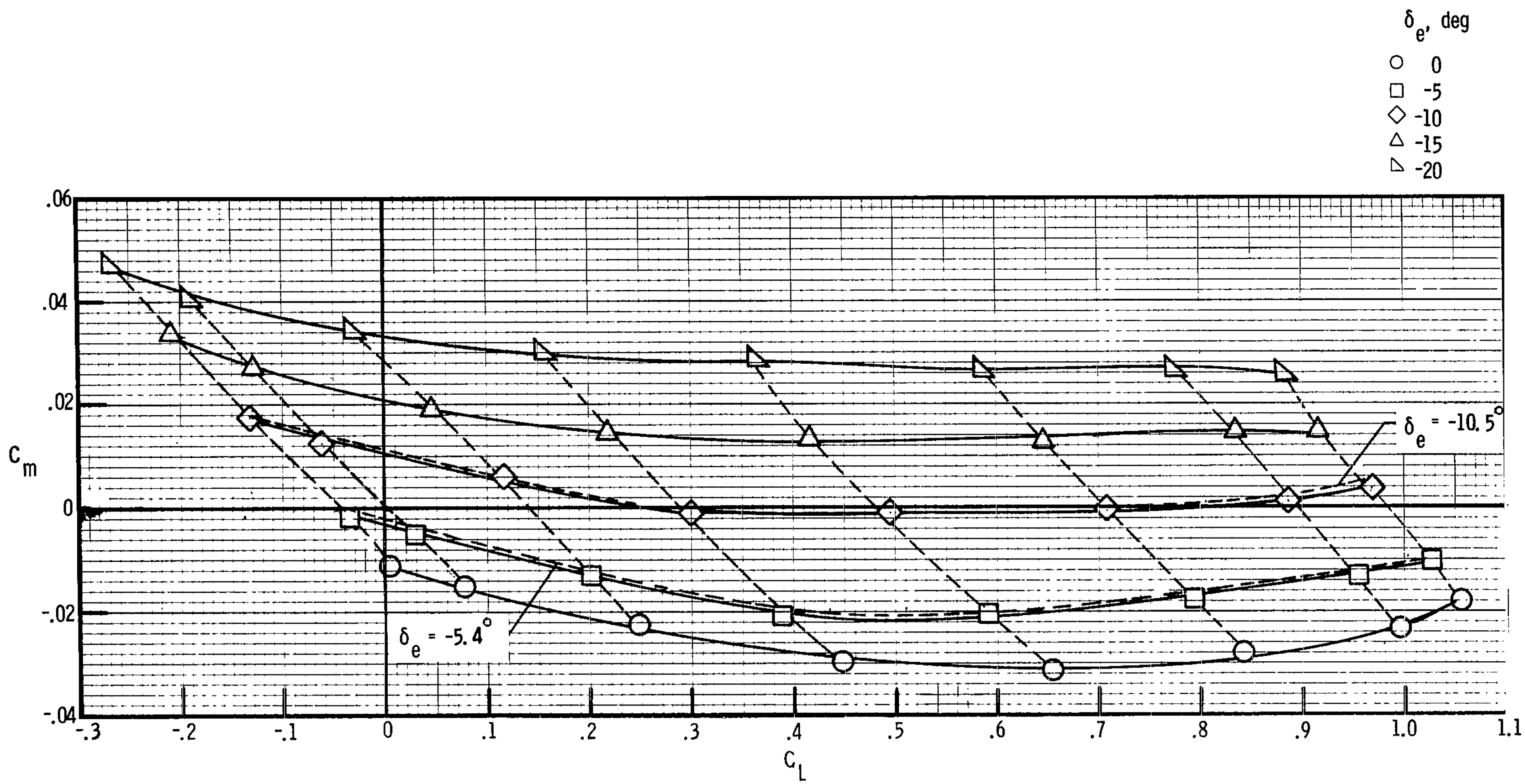

(e) Stability.

Figure 19.- Concluded.

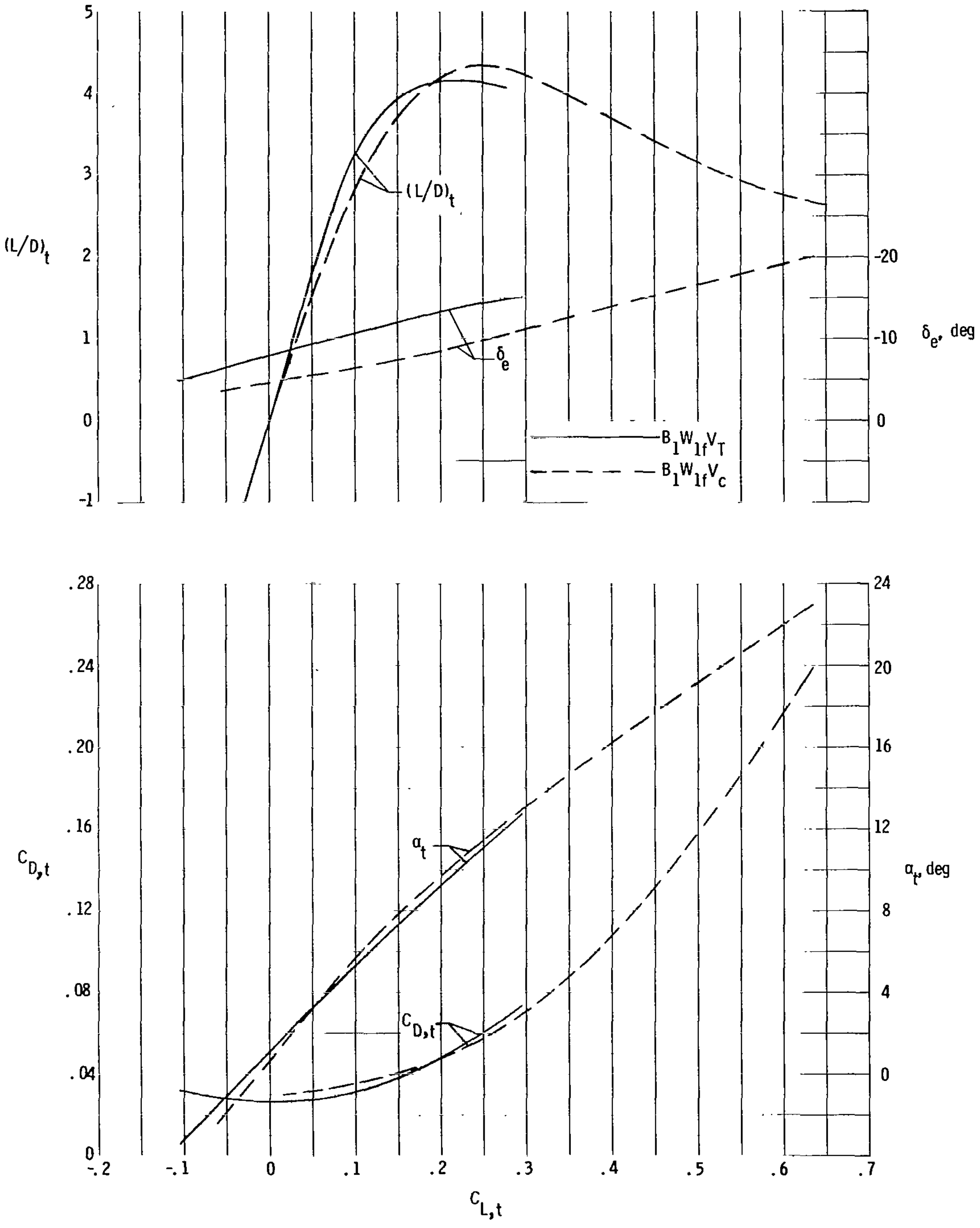

(a) Lift, drag, and lift-drag ratio.

Figure 20.- Longitudinal characteristics at trim of body-wing with tip fin and with center fin components.

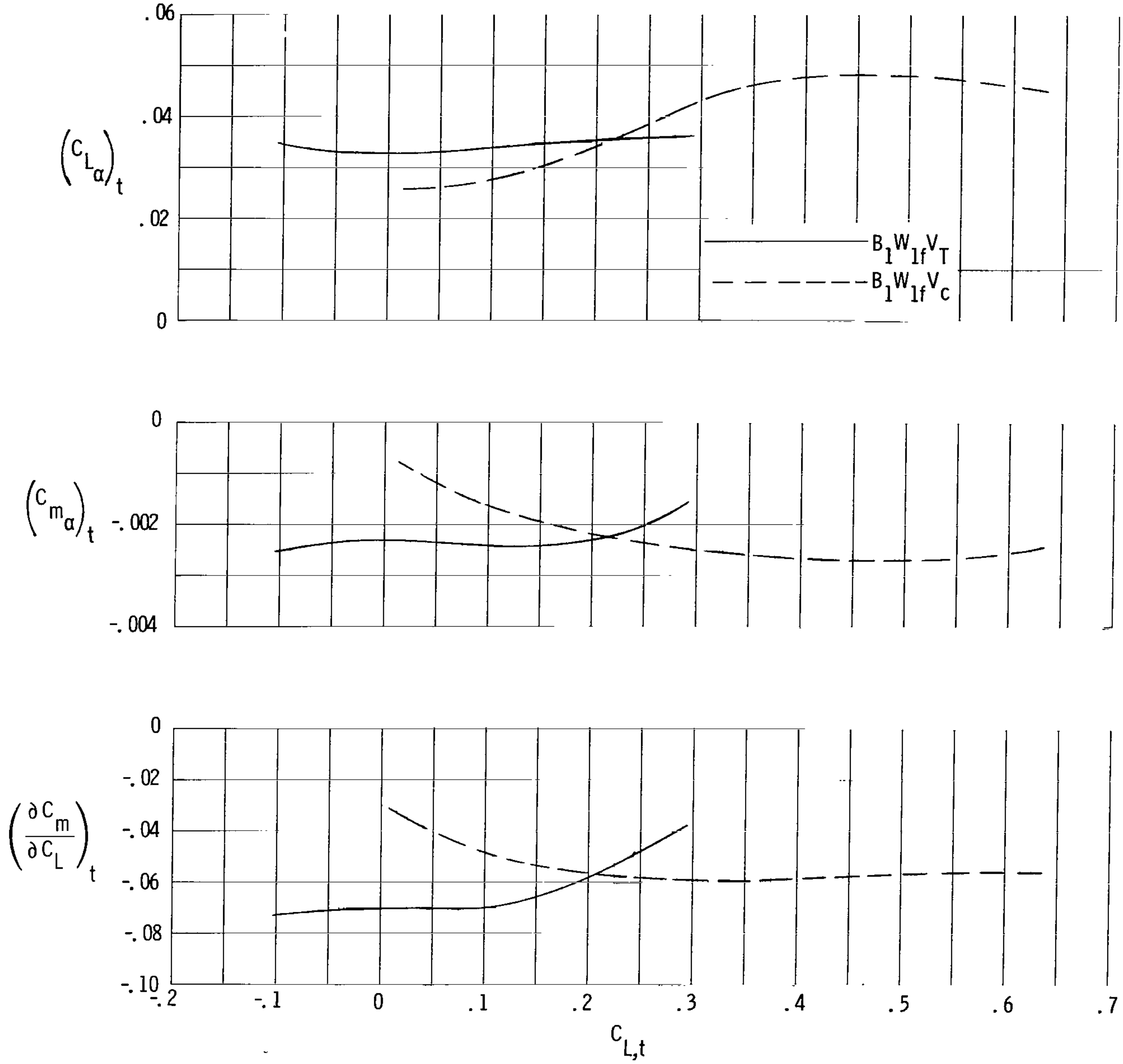

(b) Lift, pitch curve slopes, and longitudinal stability.

Figure 20.- Concluded.

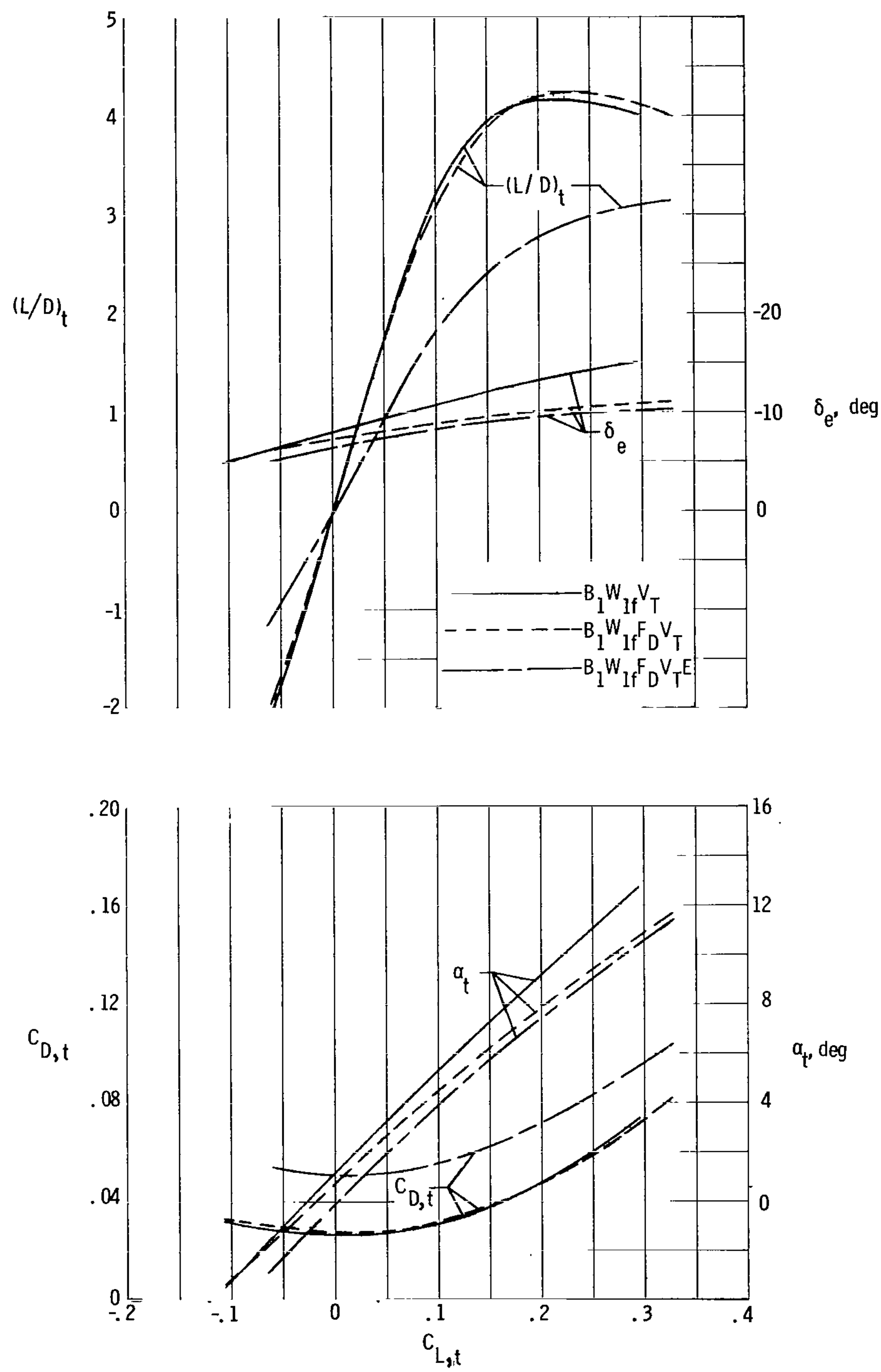

(a) Lift, drag, and lift-drag ratio.

Figure 21.- Longitudinal characteristics at trim of body-wing with tip fin and with forward delta and engine components.

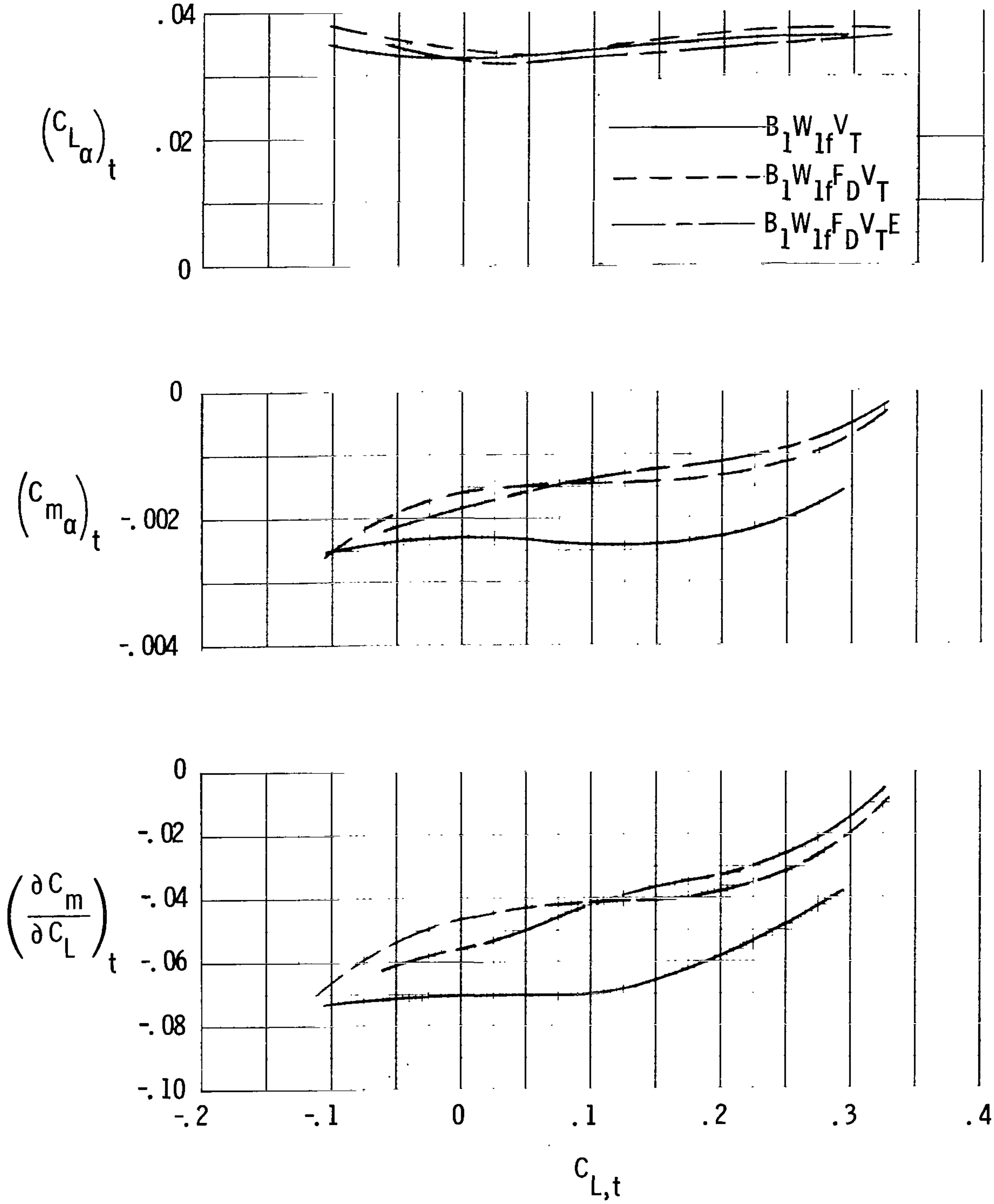

(b) Lift, pitch curve slopes, and longitudinal stability.

Figure 21.- Concluded.

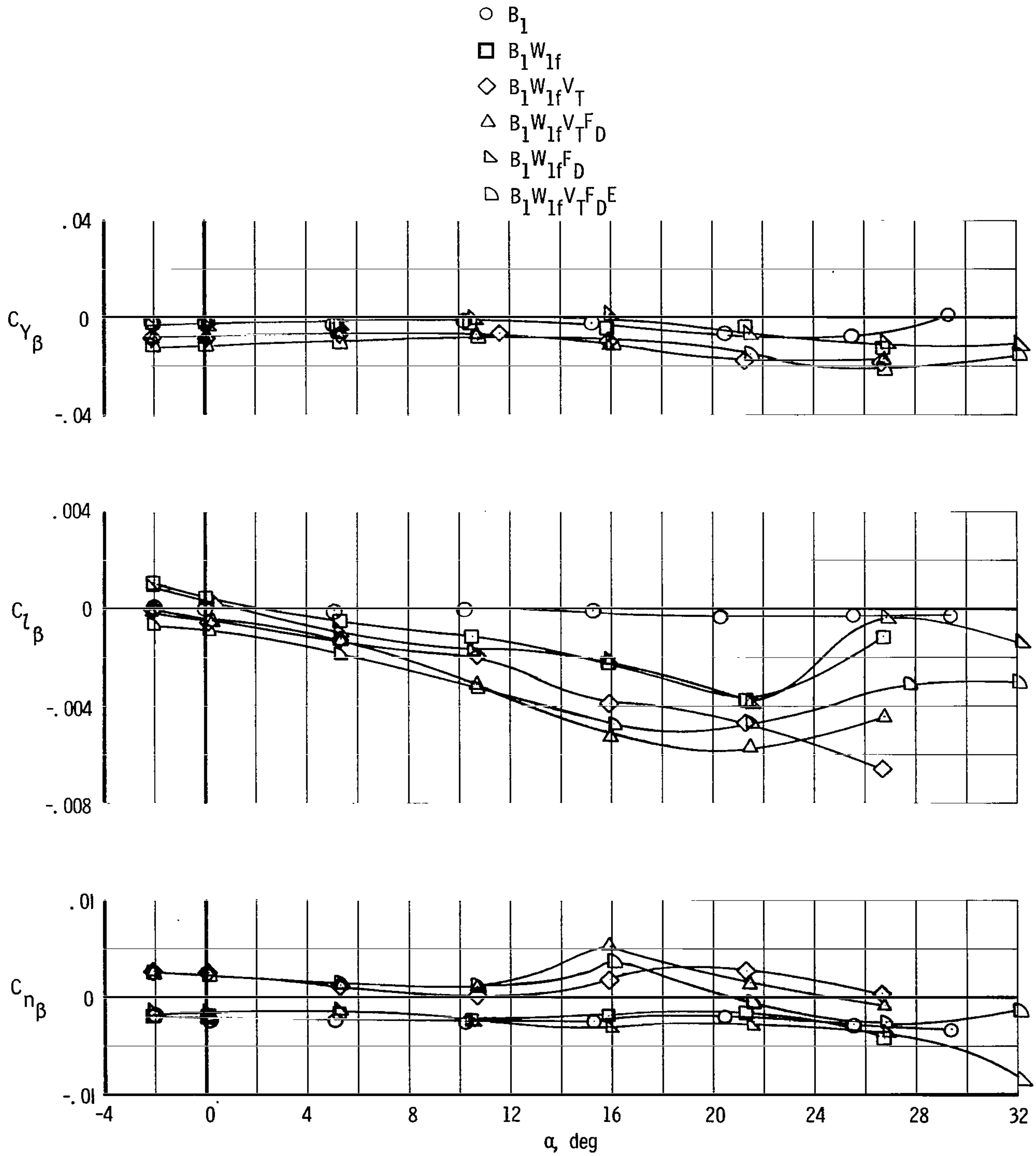

Figure 22.- Variation of lateral and directional stability with component buildup of tip fin configuration for $\delta_e = 0^\circ$.

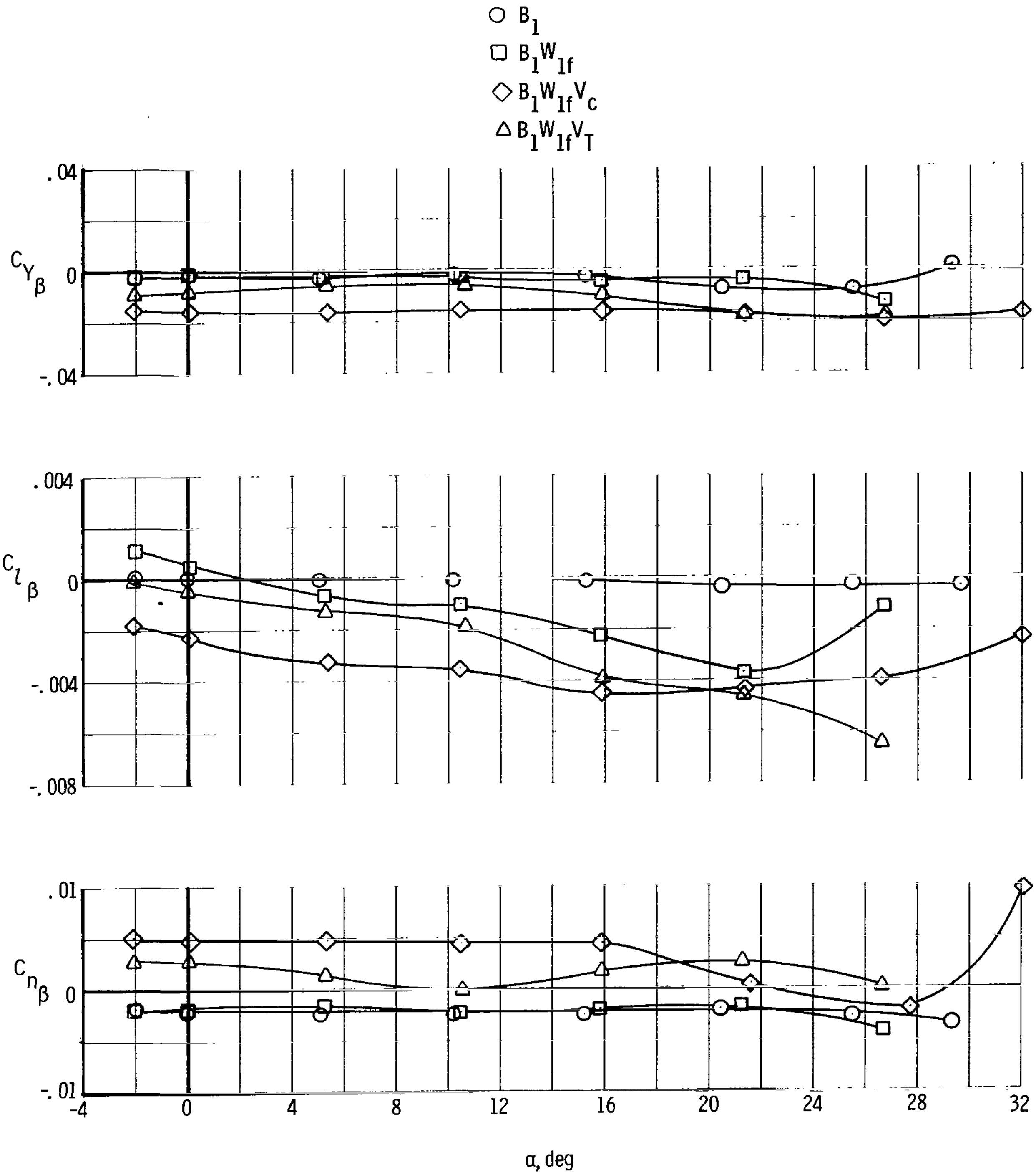

Figure 23.- Comparison of lateral and directional stability parameter for B_1, B_1W_{1f}, $B_1W_{1f}V_c$, and $B_1W_{1f}V_T$ for $\delta_e = 0^\circ$.

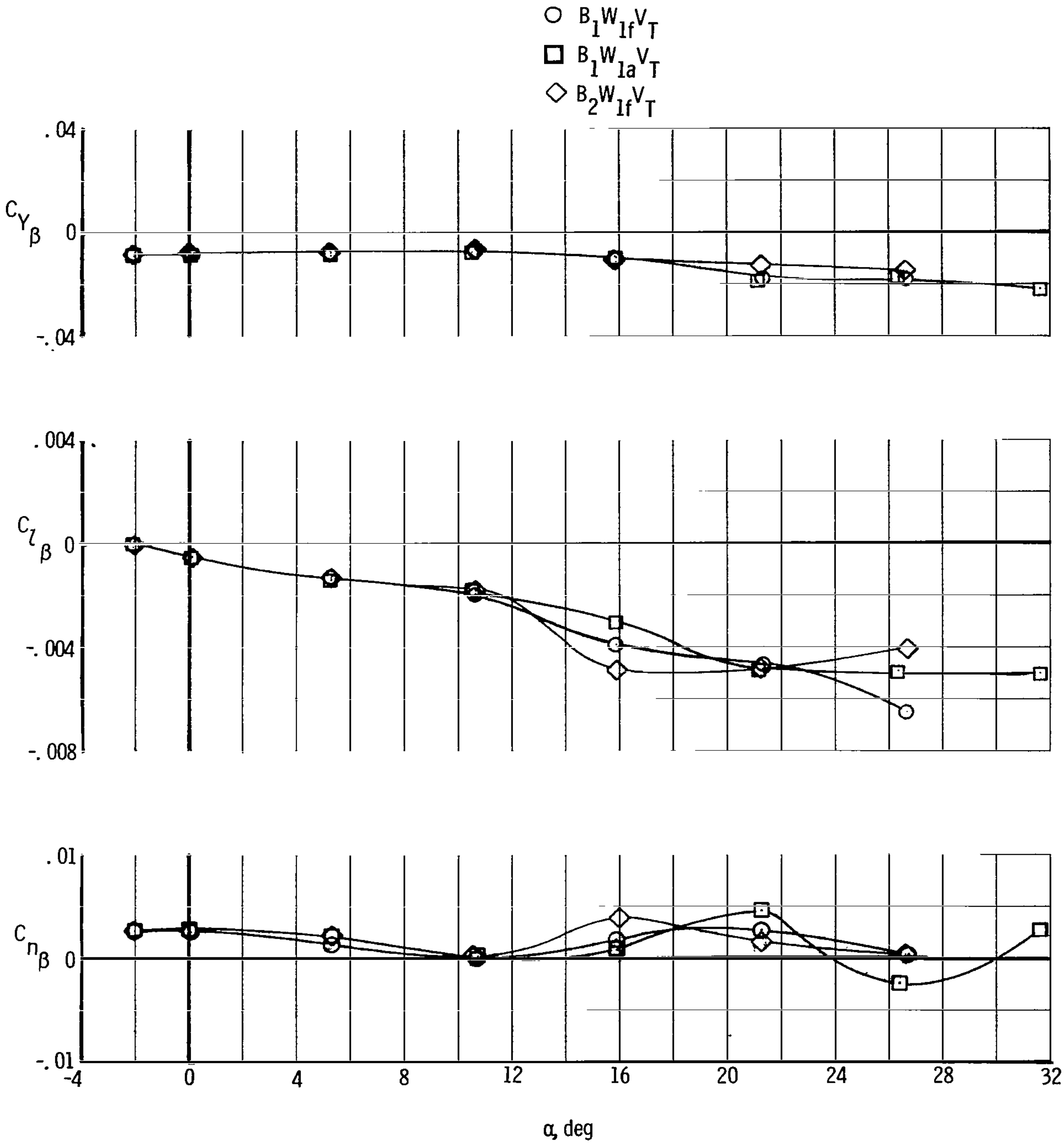

Figure 24.- Comparison of lateral and directional stability of configurations with forward and aft located wing and low and high profile noses for $\delta_e = 0^\circ$.

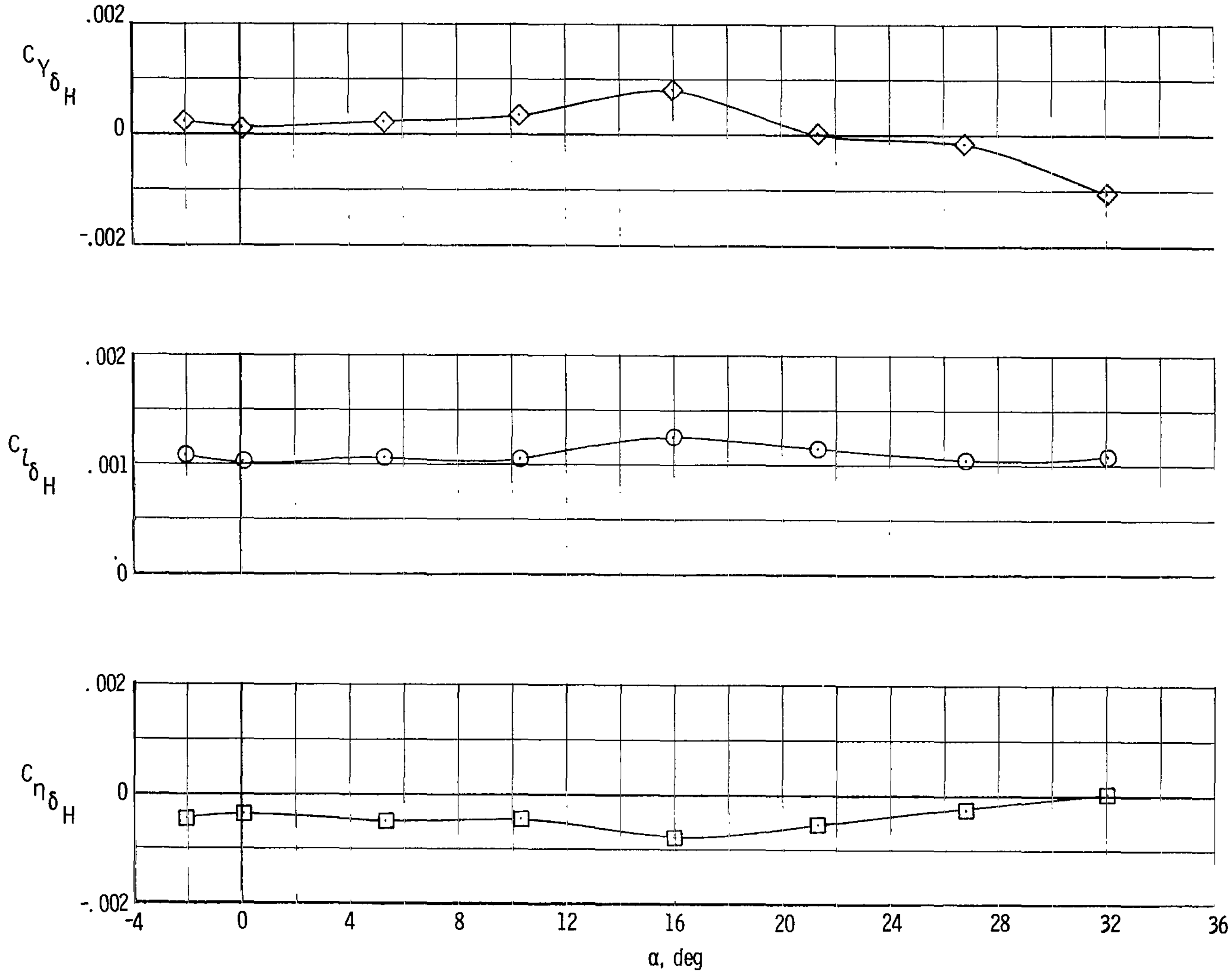

Figure 25.- Roll control of complete model $B_1W_{1f}V_TF_DE$.

1. Report No. NASA TP-1252	2. Government Accession No.	3. Recipient's Catalog No.
4. Title and Subtitle AERODYNAMIC CHARACTERISTICS OF A HYPERSONIC RESEARCH AIRPLANE CONCEPT HAVING A 70° SWEPT DOUBLE-DELTA WING AT MACH NUMBER 0.2		5. Report Date September 1978
		6. Performing Organization Code
7. Author(s) Jim A. Penland, Theodore R. Creel, Jr., and James L. Dillon		8. Performing Organization Report No. L-12215
		10. Work Unit No. 505-11-33-01
9. Performing Organization Name and Address NASA Langley Research Center Hampton, VA 23665		11. Contract or Grant No.
12. Sponsoring Agency Name and Address National Aeronautics and Space Administration Washington, DC 20546		13. Type of Report and Period Covered Technical Paper
		14. Sponsoring Agency Code
15. Supplementary Notes		

16. Abstract

A wind-tunnel investigation of the static longitudinal, lateral, and directional stability characteristics of a hypersonic research airplane concept having a 70° swept double-delta wing was conducted in the Langley low-turbulence pressure tunnel. The configuration variables included wing planform, tip fins, center fin, and scramjet engine modules. The investigation was conducted at a Mach number of 0.2 over a Reynolds number (based on fuselage length) range of 2.26×10^6 to 19.75×10^6 (with a majority of tests at 10.0×10^6). Tests were conducted through an angle-of-attack range from about -2° to 34°, at angles of sideslip of 0° and 5°, and at elevon deflections of 0°, -5°, -10°, -15°, and -20°. The drag coefficient of the integrated scramjet engine appears relatively constant with Reynolds number at the test Mach number of 0.2. Mild pitch-up was exhibited by the models equipped with tip fins. The forward delta, a highly swept forward portion of the wing, was destabilizing. The center fin model had a higher trimmed maximum lift-drag ratio and a wider trim lift and angle-of-attack range than the tip fin model. Both the tip fin models and center fin models exhibited positive dihedral effect and positive directional stability. Roll control was positive for the tip fin model, but yaw due to roll control was unfavorable.

17. Key Words (Suggested by Author(s))	18. Distribution Statement
Hypersonic aircraft Supersonic stability and control Lift Aerodynamics	Unclassified - Unlimited Subject Category 02

19. Security Classif. (of this report)	20. Security Classif. (of this page)	21. No. of Pages	22. Price*
Unclassified	Unclassified	80	$6.00

* For sale by the National Technical Information Service, Springfield, Virginia 22161

NASA-Langley, 1978

National Aeronautics and
Space Administration

Washington, D.C.
20546

Official Business
Penalty for Private Use, $300

THIRD-CLASS BULK RATE

Postage and Fees Paid
National Aeronautics and
Space Administration
NASA-451

U.S.MAIL

4 1 1U,A, 080478 S00903DS
DEPT OF THE AIR FORCE
AF WEAPONS LABORATORY
ATTN: TECHNICAL LIBRARY (SUL)
KIRTLAND AFB NM 87117

NASA

POSTMASTER: If Undeliverable (Section 158
Postal Manual) Do Not Return